Study on Landslide Dam Failure Due to Sliding and Overtopping(Dissertation_全文)

AUTHOR(S):

Awal, Ripendra

Study on Landslide Dam Failure Due to Sliding and Overtopping

By

Ripendra Awal

2008

Abstract

Landslides and debris flows due to heavy rains or earthquakes may block a river flow and create landslide dam naturally. Formation and failure of landslide dam are one of the significant natural hazards in the mountainous area all over the world. Recent predictions of climate change suggest that many part of world will experience a higher frequency of extreme rainfall events and increase in the number and intensity of typhoons, cyclones and hurricanes will produce a rising danger of landslides in future. So, the formation and failure of landslide dams and flash flood events in mountains area will be also increased by global climate change. Landslide dam may cause inundation in the upstream area and potential dam failure may cause downstream flooding. The comparisons of peak discharge for some events of natural dam failure in Nepal indicate that the peak discharge may be many times greater than that triggered by any normal rainfall. Since the failure of landslide dam may be catastrophic to downstream area, the resulting outflow hydrograph has to be predicted in order to determine possible inundation area and other hazards. Prediction of outflow hydrograph plays a vital role in both structural and non-structural countermeasures including evacuation to cope with landslide dam failure. Predicted outflow hydrograph can be used as an upstream boundary condition for subsequent flood routing.

Landslide dam may fail by erosion due to overtopping, abrupt collapse of the dam body or progressive failure. However, in-depth knowledge of the mechanism of the landslide dam failures and measured data are still lacking. Landslide dam failure has been frequently studied as an earthen dam failure despite of their differences in geometry, dimensions and material properties. Very few models are developed for landslide dam failure that can treat the flow as both sediment flow and debris flow. Most of the existing models are applicable to overtopping failure of landslide dam. In this context, an attempt is made to integrate three separate models (i.e. seepage flow model, slope stability model and dam surface erosion and flow model) to predict the outflow hydrograph resulted from failure of landslide dam by overtopping and sudden sliding. The seepage flow model calculates pore water pressure and moisture content inside the dam body. The model of slope stability calculates the factor of safety and the geometry of critical slip surface according to pore water pressure and moisture movement in the dam body. The model of the dam surface erosion and flow calculates dam surface erosion due to overflowing water.

Infiltration process is incorporated in the integrated model although this process is neglected in almost all available models. The model can predict the time at which landslide dam may fail and

also detect failure mode due to either overtopping or sliding based on initial and boundary conditions. Outflow hydrograph is calculated according to failure mode. The model can predict both total discharge and sediment discharge hydrographs. The model is capable of treating all types of flows according to sediment concentration.

Experimental studies are carried out to determine graphical relationship for the prediction of failure mode based on dimensional analysis. Critical channel slope for sediments Mix 1-6 (Silica sand S1 to S6 mixed in equal proportion) and Mix 1-7 (Silica sand S1 to S7 mixed in equal proportion) are derived from flume experiments. For particular discharge and dam height we can determine critical channel slope. If the channel slope is close to the critical channel slope the dam may fail due to instantaneous slip failure. If the channel slope is flatter than critical channel slope, progressive failure may occur. And if it is steeper, then overtopping flow may occur. Set of flume experimental data is used to compare the peak discharge for different failure modes. It is found that progressive failure produced maximum peak discharge comparing with other failure modes.

Infiltration into variable saturated porous media is governed by the Richards' equation. The pressure based Richards' equation descritized by finite differences technique is used in both 2D (Two-dimensional) and 3D (Three-dimensional) seepage flow models. Sudden failure of landslide dam was studied in experimental flume for constant head and steady discharge in the upstream reservoir. A high and constant water level or a gradual rise of water level in the reservoir causes water to penetrate into the dam body, increasing mobilized shear stress and causing dam to fail by sudden collapse after it becomes larger than resisting shear stress. The seepage model is combined with transient slope stability model. The limit equilibrium method is employed to evaluate the transient slope stability. It involves calculating the factor of safety and searching for the critical slip surface that has the lowest factor of safety considering temporal variation of both pore water pressure and moisture content inside the dam body. The numerical procedure used for the identification of critical noncircular slip surface with the minimum factor of safety is based on dynamic programming and the Janbu's simplified method. A 2D analysis is only valid for slopes which are long in the third dimension. However, failure of natural slopes and landslide dams confined in a narrow U- or V-shaped valley occurs in three dimensions. Therefore 3D approach is more appropriate to analyze such stability problems. The 3D slope stability analysis based on dynamic programming and random number generation incorporated with 3D simplified Janbu's method is also used to determine minimum factor of safety and the corresponding critical slip surface for landslide dam in the V-shaped valley. The 3D seepage flow model is coupled with 3D slope stability model so the combined model is capable for

transient slope stability analysis. Numerical simulations and flume experiments are performed to investigate the mechanism of landslide dam failure due to sliding for both 2D and 3D cases. The lateral slope of the flume bed is horizontal for 2D case and is inclined for 3D case. Water content reflectometers (WCRs) are used in the flume experiments to measure the temporal variation of moisture content during seepage process. The shape of the slip surface during sliding of the dam body is measured by analyses of videos taken from the flume sides. Comparisons show that results of numerical simulation and experimental measurement are quite close in terms of movement of moisture in the dam body, predicted critical slip surface and time to failure of the dam body.

Dam surface erosion and flow model is developed for simulation of outflow hydrograph due to landslide dam failure by overtopping. The proposed model is tested for different experimental cases of landslide dam failure for overtopping over full and partial channel width. The model is able to reproduce the resulting hydrograph reasonably. The simulated overtopping time and dam surface erosion at different time steps are also in good agreement with experiments. The simulated breach width depends on inflow and reservoir volume. The incised channel is almost vertical for both simulations and experiments in small inflow discharge and small reservoir volume. In the case of larger inflow discharge and larger reservoir volume, slumping occurred at irregular time steps. The peak discharge is highly influenced by sliding of breached channel bank at crest.

An integrated numerical model is developed by combining seepage flow model, slope stability model and dam surface erosion and flow model for simulation of outflow hydrograph due to landslide dam failure by overtopping and sliding. The main advantage of an integrated model is that it can detect failure mode due to either overtopping or sliding based on initial and boundary conditions. The proposed model is tested for experimental case of landslide dam failure due to overtopping and sliding. The model reproduced reasonably similar hydrograph as that of experiment. The numerical simulation and experimental results of movement of moisture in the dam body, predicted critical slip surface and time to failure of the dam body are also in good agreement.

Key Words: *landslide dam, seepage flow, slope stability, overtopping flow, flood/debris flow hydrograph, integrated model*

Acknowledgements

I would like to thank all people who have helped and inspired me during my doctoral study.

I would like to express my deep and sincere gratitude to my supervisor, Professor Dr. Hajime Nakagawa, Disaster Prevention Research Institute (DPRI), Kyoto University, for his continuous guidance, support and encouragement throughout my study period.

I am deeply grateful to my thesis reviewers, Professor Hideo Sekiguchi and Professor Masaharu Fujita, DPRI, Kyoto University, for their valuable comments and suggestions to refine the thesis.

I am also grateful to other faculty members, Dr. Kenji Kawaike, Dr. Yasuyuki Baba and Dr. Hao Zhang, for their guidance, suggestions in all aspects of my study. My appreciation also goes to Dr. Yasunori Muto and Dr. Tetsuo Ueno for their support in many aspects. I appreciate Dr. Diazo Tsutsumi for providing me experimental apparatus to determine sand parameters. I warmly thank Dr. Rajhari Sharma for his valuable advice, discussions and friendly help.

I am indebted to my all colleagues of River Disaster Prevention System, DPRI, Kyoto University for their kind cooperation and unforgettable friendship. I am especially grateful to Mr. Muhammad Rasheduzzaman, Mr. Hiroshi Teraguchi, Mr. Badri Bhakta Shrestha, Mr. Dong-Keun Lee, Mr. Naoki Ito, Mr. Daizaburo Touchi, Mr. Takaharu Utsumi, and Mr. Yasunori Nanbu.

I thank all the professors and friends in the Research Center for Fluvial and Costal Disaster, Disaster Prevention Research Institute of Kyoto University, who have made my academic experience rich and memorable. I would like to thank Mr. Seiji Fujihara, Mr. Hideo Tagawa and all the staffs in Ujigawa Open Laboratory, Disaster Prevention Research Institute of Kyoto University for their support in routine administrative process and experiment.

I am also greatly indebted to many teachers in the past, Professor Dr. Narendra Man Shakya and Dr. Rghunath Jha (Tribhuvan University, Nepal) for getting me interested in each and every topic of water recourses engineering and coming to Japan.

I gratefully acknowledge the financial support of the Monbukagakusho (Ministry of Education,

Culture, Sports, Science and Technology, Japan).

Lastly, and most importantly, my deepest gratitude go to my parents, Asharam, and Tulshi Devi, my brother Pramod, my sister Sharmila and all other family members for their encouragement and loving support. I am also grateful to my late uncle, Dr. Krishna Prasad Awal, for his continuous encouragement for doctoral study.

Table of Contents

Chapter 1

Introduction

1.1 General

Occurrence of water induced disasters such as floods, landslides, debris flows have been increasing every year due to various factors such as global climate change, environmental and ecological imbalances, increasing population density, urbanization, deforestation, and desertification. Moreover, the number of affected people and the consequent economic losses are also on rise.

Landslides and debris flows due to heavy rains or earthquakes may block a river flow and create landslide dam naturally. Formation and failure of landslide dam are one of the significant natural hazards in the mountainous area all over the world. Landslide dam may cause the inundation of upstream area with high risk of submergence and potential dam failure may cause downstream flooding. In the event of catastrophic failure of landslide dam, resulting outflow hydrograph has to be predicted in order to determine inundation area and hazards in the downstream to provide adequate safety measures. For this reason, landslide damming and failure have been, and continue to be, the subject of numerous studies attempting to define processes, risks and mitigative measures.

The life span of landslide dam ranges from several minutes to several thousand years. When a dam is formed it is very difficult to predict when or whether it will fail. Consequently, understanding how the characteristics of landslide dam influence the peak outflow of resulting dam-break floods are of critical importance for effective hazard management. Managing hazards require an understanding of the temporal and spatial scales on which such phenomena occurs. Many previous works on landslide dam have been mainly descriptive in character, and have produced a multitude of documented case studies and inventories (e.g. Costa and Schuster, 1988; Costa and Schuster, 1991). More recent work is focused on quantitative methods of determining the post-formation development, in particular the controls on dam longevity (Schuster, 2000; Manville, 2001; Ermini and Casagli, 2003; Korup, 2004, 2005).

Landslide dam may fail by erosion due to overtopping, abrupt collapse of the dam body or progressive failure. Although the failure mechanisms of landslide dam are relatively well understood from extensive engineering research on artificial dams, little is known about the actual processes involved in landslide dam failures from few direct observations. The peak discharge produced by abrupt collapse of the dam is very high compared with erosion due to overtopping. However, in-depth knowledge of the mechanism of the dam failures and measured data are still lacking. Landslide dam failure is still frequently modeled as a homogenous earthen dam failure, because the mechanism of breach formation is considered very similar, despite obvious differences in dam geometry and material properties. Most of the existing models are applicable to overtopping failure of landslide dam.

The catastrophic failure of landslide dam may occur shortly after its formation. Rapid forecasting of potential peak discharge is necessary for the management of dam-break flood hazards and to decide appropriate mitigation measures including evacuation. Preliminary peak discharge can be predicted by using empirical regression relationships based on approximate height of dam and volume of dammed lake. Physically based computer models can be used after collecting details data of dam geometry, soil properties, topography and inflow discharge.

This study aims to derive graphical relationship to predict failure modes of landslide dam, behavior of landside dam due to transient seepage flow inside the dam body and prediction of peak discharge caused by landslide dam failure due to overtopping and sliding. This will be achieved through laboratory experiments and numerical simulation of non-cohesive, homogenous landslide dam.

1.2 Formation and failure of landslide dam

Natural dam

Natural dams and the lakes that they impound can form by different geologic processes. Among these processes, stream blockages from landslides, Late Holocene glacial moraines, glaciers, and volcanic activities present the greatest hazards to people and property (Schuster, 2000). The largest known floods of the Quaternary Period had a peak discharge of nearly 20 million m^3/s and resulted from breaches of glacial-age ice dams that blocked large midcontinent drainage systems during ice ages. Most of the other large documented floods are resulted from breaches

of other types of natural dams, including landslide dams, ice dams from smaller glaciers, releases from caldera lakes, and ice-jam floods (O'Connor and Costa, 2004). Those natural dams that fail rapidly and unpredictably pose the greatest threats to human life and infrastructure. Dams in this class include landslide and volcanic dams, which tend to form suddenly and unexpectedly. Rapid analysis of the potential scale of the dam-break flood hazard is an essential step in risk management and mitigation associated with the formation of any natural dam.

Landslide dam

Landslide dam can form in a wide range of physiographic settings, from high alpine debris avalanches to quick-clay failures in wide valley floors. They occur most frequently in active tectonic settings where high mountains border narrow steep valleys and earthquakes are frequent and severe. Landslide dams are formed by various kinds of landslides, ranging from rock falls and rock slides in steep walled, narrow canyons to earth slumps in flat river lowlands (Costa & Schuster, 1988; Schuster, 1995). In a sample of 390 landslide dams, Shuster (1995) found that about 40% were formed by rock and soil slumps and slides, 30% by debris, earth and mud flows, 25% by rock and debris avalanches and less than 10% by sensitive-clay failures and rock and earth falls. The most common mechanisms triggering dam-forming landslides are excessive precipitation (58%), and earthquakes (33%). Landslide dam can be unstable and subject to failure because they have no controlled outlet. The vast majority of dam failures and ensuing floods result from overtopping and incision of the blockage, generally beginning soon after impounded water first reaches the low point of the blockage.

Landslide dams have occurred to heights as great as or greater than the world's largest manmade dam. The highest historic landslide dam is the 600m high earthquake induced Usoi rock-slide dam (Figure 1.1) in southern Tajiskitstan, which impounds 500m deep Lake Sarez on the Murgab River. This dam is nearly twice the height of the largest constructed dam in the world today, the 300-m-high Nurek rockfill dam, also in Tajikistan. The direct and indirect cost due to landslide dam may be very high. The total costs (direct and indirect) of large debris slide at Thistle, Utah (Figure 1.2), were probably on the order of $400 million. Although there were no casualties as a result of the Thistle slide, it ranks as the most economically costly individual landslide in North America, and probably in the world (Schuster and Highland, 2001). Figure 1.3 shows another example of landslide dammed lake caused by Cyclone Bola 1988 in New Zealand.

Figure 1.1 Usoi Dam in Tajikastan,

Usoi Dam in Tajikastan,formed by a landslide in 1911, created 16 km^3 Lake Sarez, the largest lake in the world resulting from a landslide. Five million people live in the valleys downstream of the dam. Even partial breaching of the dam could cause catastrophic flooding. Complete failure of the dam could result in the deadliest natural disaster in human history. (Image courtesy of the Image Science & Analysis Laboratory, NASA Johnson Space Center)

Figure 1.2 The 1983 Thistle landslide, central Utah, U.S.A.

Thistle Lake, which resulted from damming of the Spanish Fork River by debris slide, was later drained as a precautionary measure. (Source: Schuster and Highland, 2001)

Figure 1.3 Cyclone Bola 1988 caused this large landslide in Gisborne, New Zealand, creating a lake. (Photo courtesy: www.sopac.org/tiki/tiki-download_file.php?fileId=842, Noel Trustrum, GNS, NZ)

Failure of landslide dam

There have been at least six historic landslide dam floods with peak discharges greater than 10,000 m^3/s (O'Connor and Costa, 2004). Dam-breach modeling indicates that a flood with a peak discharge of about 540,000 m^3/s, probably the largest flood in recorded history, resulted from breaching of an 1841 rockslide that temporarily blocked the Indus River within the western Himalaya, Pakistan. Similarly, there is stratigraphic evidence of a flood of about 220,000 m^3/s from breaching of a landslide dam across the Columbia River in western Washington about 500 years ago. Most of these large floods were associated with tall blockages of large rivers, including cases where breach depths ranged up to 150 m through landslide dams that were as high as 250 m. The potential peak discharge through a landslide dam increases exponentially with blockage height. Consequently, landscapes that generate large landslides that in turn form tall blockages in confined valleys have the greatest potential for extreme floods.

Landslide dams differ from artificial dams in terms of composition, construction, and geometry. They are typically composed of unconsolidated and poorly sorted material with no engineered features designed to prevent piping, seepage or saturation, or channelled spillways or other

outlets to control overflows. Consequently, they are often prone to rapid failure and breaching. Landslide-dammed lakes may survive for periods ranging from minutes to thousands of years, depending on such factors as volume, size, shape and sorting of the dam and its constituents, and the rates of sediment and water inflow to the lake. According to worldwide statistics (Costa and Schuster, 1988) 27 % of landslide dams (n = 73) fail within one day of formation, 41 % within one week, 56 % within one month, and 85 % within one year. Landslide dam may fail by different failure mode based on material properties of the dam body and stream channel conditions. It may fail by the erosive destruction due to overtopping, abrupt collapse of the dam body or progressive failure (Takahashi, 1991). Landslide dam most commonly fail by overtopping, followed by breaching from erosion by the overtopping water. Based on study of actual landslide dam failure, it seems more than 51% of failure cases were due to overtopping and failure mode of more than 48% cases were unknown (Schuster and Costa, 1986). The majority of failures are caused by the overtopping of water and the associated erosion of the dam body. A few examples are due to piping or sliding collapse of the dam body.

The failure mode of landslide dam is very similar to that observed for artificial earthen dams, generally occurring by overtopping, and infrequently by piping or slope failure (Costa and Schuster, 1988). Overtopping failure is generally caused by water spilling over the dam crest and eroding a channel along the downstream face of the dam. Erosion of the dam crest by the escaping water eventually breaches the dam. Breach growth occurs by both fluvial erosion of the floor of the breach channel via sediment entrainment and slope failures of the breach sidewalls and downstream dam face. The breach may not erode to the base of the dam due to armouring of the outlet channel (Costa and Schuster, 1988). The series of photos (formation of landslide dam, lake filling, overtopping and breached dam) of Mount Adams landslide dam in the Poerua River, New Zealand are shown in Figure 1.4. The dam failed due to overtopping six days after it was formed.

Piping failure occurs when water percolating through the dam causing internal erosion and the development of ‘pipes’ that first appear as springs or seepage’s on the downstream face. The pipes enlarge and erode headwards, increasing the flow rate and eroding a channel on the downstream dam face. Removal of support for the dam crest by the growing pipe usually results in its collapse and the development of an open breach. Piping failure can occur when the lake level is well below the top of the dam. Infiltration rate is one of the major factors which governs failure modes of landslide dam. For the same hydraulic conditions and same shape of dam and

reservoir, if the infiltration rate is small overtopping will occur and if the infiltration rate is very high seepage or progressive failure may occur. When the infiltration rate is very high, seepage which appears on the lower part of the downstream face brings collapse around it and then the collapse proceeds upstream, ending by a large failure at the moment the collapse reaches near the blocked water. Seepage erosion is more likely to occur in landslide dam because they are more heterogeneous than embankment dams and have not undergone the systematic compaction of embankment dams (Schuster and Costa, 1986). Thus, landslide dams are generally more pervious and less resistant to erosion than embankment dams.

A landslide dam with steep upstream & downstream faces and with high pore-water pressure is susceptible to slope failure (Costa and Schuster, 1988). If the infiltration rate of the dam body is intermediate and strength of the dam body is small, instantaneous slip failure may occur. Although abrupt collapse of the dam body is not common, the peak discharge produced by such failure is very high compared with failure due to overtopping. Slope failure is a common subsidiary process in breach growth by piping or overtopping, when vertical erosion and lowering of the base of the breach results in oversteepening of the breach sidewalls. Gravitational failure of the sidewalls then occurs, widening the breach and lowering the sidewall angles. Less commonly, thinning of the dam by erosion on the downstream face results in the hydraulic pressure exerted by the impounded water exceeding the resisting shear and cohesive strength of the dam, allowing it to be effectively ‘pushed over’.

Many examples of landslide dam failure demonstrate that it may fail by different failure modes. Costa and Schuster (1988) have mentioned three cases of landslide dam failure by piping and seepage. The 1945 Cerro Condor-Sencca landslide dam, the 1966 breach of the landslide dam that impounded Lake Yashinkul on the Isfayramsay River in the south-central former U.S.S.R. and the 1906 failure of the landslide dam on Cache Creek in northern California. They also mentioned that one well-documented examples exists in which failure of the downstream slope of a landslide dam may have contributed to over-all failure in the 1945 Cerro Condor-Sencca blockage of the Mantaro River, Peru. The failure of Rio Toro landslide dam in 1992 was due to retrogressive sliding caused by seepage and internal erosion. Post-failure reconnaissance indicated that overtopping did not occur until the dam had already failed by collapse and retrogressive sliding (Mora et al., 1993). Tsatichhu landslide dam in Bhutan also failed by dam-face saturation and progressive seepage (Dunning et al., 2006). Allpacoma Landslide Dam (Figure 1.5) in Bolivia failed by piping and overtopping (Hermanns, 2005).

(a) October 6th 1999: aerial view looking down the side of the mountain to where the slip has dammed the river, which is starting to form a lake.

(b)October 6th 1999: aerial view looking down the Poerua River at lake building up behind landslide debris (from left) building up in the river bed.

(c) October 7th 1999: cross valley view of the landslide and lake

(d) October 12th 1999: Vertical shot of the breach through the dam blocking the Poerua River after Mt Adams landslide

(e) October 7th 1999: close-up of lip of dammed lake and toe of slip before the dam was breached

(f) October 24th 1999: view downriver of the lake draining through the breached dam

Figure1.4 Mt. Adams-Poeura River Landslide, New Zealand (Photo courtesy: John Bainbridge)

Figure 1.5 Natural water-escape tunnel through a landslide dam in Allpacoma valley, La Paz, Bolivia, formed due to piping failure.

Between November 23 and December 13, 2004, wetting of the dam by infiltration was so strong that piping through the dam occurred. This happened when the water level was about 2 m below the dam crest. Piping was slow enough to prevent a dam collapse, and by January 6, 2005, a tunnel about 1.5 m in diameter had eroded through the dam. (Source: Hermanns, 2005)

Overtopping is common in all types of failure modes but the initiation of failure may be different. Some examples of recent landslide dam failure due to seepage and sliding suggest us to rethink about failure modes. Whereas failure mode of many historical dam failure is unknown.

1.3 Significance of landslide dam in Japan and Nepal

1.3.1 Landslide dams in Japan

Japanese islands are part of the island arcs, beneath which the Pacific Plate and the Philippine Sea are subducting. Therefore, the geological history is relatively young and many active volcanoes and earthquakes are dominant. This has led to the occurrence of many landslides in

various regions as the earthquakes and volcanoes together with factors such as heavy rainfall, flooding and tsunami can easily affect the equilibrium of slopes and hills. The Japanese natural environment is very hazardous to human society with potential threats from all kinds of natural disasters. Landslide dams are also common in Japan because of widespread unstable slopes and narrow valleys exist in conjunction with frequent hydrologic, volcanic and seismic landslide triggering events (Swanson et al, 1986). Historical documents and topography have revealed the formation of many landslide dams, some of which broke and caused major damage in Japan (Tabata et al, 2002). Totsugawa disaster in 1889 in Nara Prefecture, 53 natural dams were formed by the landslides induced by a severe rainstorm and about 70% of these dams failed within a day causing a very severe disaster forcing the residents to move from their home village to Hokkaido (Ashida, 1987). Similarly, in the Aritagawa disaster in 1953, 16 deep seated landslides formed natural dams and the majority of them failed during the flood, but two of them at Kongoji and Futagawa were left after the flood and they failed during the flood that occurred two months later (Takei, 1987).

Earthquake-induced slope failures and debris flows often create natural dams with extensive ponded water. Failures of these dams have resulted in catastrophic flooding in downstream areas. Two typical events occurred in central Japan, induced by the 1847 Zenkoji Earthquake (M 7.4) on the Sai River (Ito, 1983) and by the 1858 Hietsu Earthquake (M 7.1) on the Joganji River (Machida, 1966). The latter event yielded a huge amount of sediment totaling 1.3 to 2×10^8 m^3, resulting in tragic flood damage due to the failure of landslide dam. Heavily debris-loaded, devastated river channels also posed serious erosion and flood control problems.

The 2004 Chuetsu earthquake resulted in many landslide dams particularly in the Imo River basin (Mizuyama, 2006). More than 50 landslide dams were formed along the main stream of the Imogawa-River and its tributaries by the landslides triggered by the earthquake. Many of them were naturally overtopped without catastrophic collapse soon after their formation. However, five prominent landslide dams with certain large volumes were formed along the main stream of the Imogawa-River (at the districts of Terano, Nanpei, Naranoki, Higashi-Takezawa and Junidaira). Two of them were critical landslide dams to which emergency operations were to be urgently managed because of their dimensions, namely Higashi-Takezawa landslide dam (Figure 1.6) and Terano landslide dam. In both cases, each landslide has a length of about 300 m and a volume of more than 1 million m^3. Wire-sensors and water level gauges were installed near these landslide dams to monitor the discharge rate of the river and to warn local residents living downstream concerning the dangers of flooding if the dams broke (Kato et

Plane view of the Higashi-Takezawa Landslide

Front view of the Higashi-Takezawa Landslide

Figure 1.6 Higashi-Takezawa landslide dam, Japan - October 2004 (Photo courtesy: Marui and Yoshimatsu, 2007)

al, 2005). A small dam burst on November 4, 2004. Its flood hydrograph was observed, and data was recorded. The flood discharge rate increased sharply for ten minutes and subsided over the next 50 minutes. Although not all possible situations are understood from the data, it did provide valuable data on predicting the peak discharge rate in the case where a landslide dam bursts.

A large landslide caused by Typhoon 14 formed a landslide dam on the Mimi River (Figure 1.7), Miyazaki Prefecture, during the night of September 6, 2005. The recorded rainfall was more than 1000mm in 2 days. The landslide dam was located about 500m downstream of Tsukahara dam. Fortunately, the dam collapsed shortly afterwards and the resulting flood did not cause damage downstream because the flood discharge was small.

Eleven dams were created by landslides triggered by Iwate-Miyagi Inland Earthquake on 14th June 2008. Details of some of the significant landslide dams in Japan can be found in Japanese Ministry of Construction (1987), Costa & Schuster (1991) and Mori (2007).

Figure 1.7 Landslide dam near Tsukahara dam, Mimi River, September 2005 (Photo courtesy: Asia Air Survey Co., Ltd)

1.3.2 Landslide dams in Nepal

Nepal is a mountainous country occupying the central part of the Hindu-Kush Himalayan region. Elevation of Nepal varies from 70m (Terai) to 8,848m (Mount Everest) from mean sea level. Nepal is a highly disaster prone country exposed to various types of natural disasters. High seismicity, steep and unstable slopes, rugged terrain, active geodynamic processes and intense monsoon rains make the Himalaya an active and fragile mountain range. Landslides, debris flows, monsoon floods, landslide dam failures, glacial lake outburst floods (GLOF) are the most common water induced natural disasters in Nepal. Vulnerability to these disasters is compounded by rapid population growth and development of haphazard and unplanned settlements. Different types of water induced hazards in different physiographic regions of Nepal are shown in Figure 1.8. Landslides are the most severe type of natural hazard in Nepal, where the mountains occupy about 83% of the territory. During the monsoon season, water-induced disasters wipe out villages, wash out different infrastructures, and cause damage to agricultural land. Such disasters cause substantial economic losses, human casualties and environment degradation. Earthquake is another triggering factor which causes landslides. The earthquakes of 1934, 1953, 1969, 1980 and 1988 triggered many landslides in Nepal (Dhital, 2002).

Due to the fragile condition of the mountains in Nepal, landslides of different sizes occur every year in mountain areas due to high intensity precipitation. Sediment resulting from mass wasting and landslides is often released into river channels, temporarily damming them. When such a dam is breached peak flood of short duration called *"bishyari"* results. The fact that Nepali language has a word to describe this phenomenon indicates that it has a long natural history (Moench and Dixit, 2004). The flood causes heavy damage along riverbanks, and the impact may continue for several kilometres downstream of the breach. Although landslide dam outburst floods (LDOF) of varying magnitude occur frequently in Nepal, detailed information on such events is still lacking. The list of some of the documented LDOFs (after Khanal, 1996 and Shrestha & Shrestha, 2005) is given in Table 1.1 and their approximate locations are shown in Figure 1.9. However, the actual number of LDOFs is thought to be far more than what is presented, as many LDOFs are not documented due to poor information collection systems, remoteness of the event location and a lack of understanding of the processes involved (Shrestha & Shrestha, 2005).

The outflow hydrograph depends on many factors like inflow discharge, impounded water volume, shape and size of the reservoir formed in the upstream of landslide dam, soil properties of the dam body, failure modes etc. Peak discharge produced by such events may be many times greater than the mean annual maximum instantaneous flood discharge. Figure 1.10 shows the comparison of peak discharge with mean annual maximum instantaneous flood discharge for some events of natural dam failure in Nepal. The recorded data of Burhi Gandaki river shows peak discharge due to LDOF is about 5.79 times greater than the mean annual maximum instantaneous flood discharge (about 18 km downstream). Similar event in Trishuli River, peak discharge is about 1.8 times greater than the mean annual maximum instantaneous flood discharge. One of the GLOF events in Dudh Koshi River, peak discharge is about 2.7 times greater than mean annual maximum instantaneous flood discharge (about 91 km downstream). Figure 1.11 shows the breached landslide dam in Kali Gandaki River near Tatopani Bazar. Failure of landslide dam in the Tinnau River (1981, Figure 1.12) caused flood in the downstream and killed at least two hundred people (Carson, 1985).

Landslide damming is not a recent phenomenon. There are many geological evidences of landslide damming that have occurred 100s to 1000s of years ago. Some examples of massive prehistoric landslide dams (Table 1.2) were failed catastrophic outbursts. However, several of the prehistoric landslide dams were stable and the lakes formed are now filled by sediments.

Formation of temporary (or permanent) lakes due to landslide damming is common phenomenon in mountainous areas of Nepal where there are narrow river channels and steep mountain slopes. Many documented cases illustrate the severity of this phenomenon in terms of loss of life and properties in Nepal.

Table 1.1: Formation and failure of Landslide dam in Nepal

S. No.	Date	Location	River system	Damage	Nature of the event	Reference
1	1926	Niskot Hill/Myagdi Khola, Myagdi	Myagdi	NA	NA	Weidinger and Ibetsberger (2000)
2	1967	Tarebhir/Kashi-gaon, Gorkha	Burhi Gandaki	There was no destruction due to outburst flood but the landslide killed 9 people.	River was dammed for 3 days after the failure of Tarebhir near Kashigaon.	Khanal (1996)
3	2-Aug-68	Tarebhir/Labu-bensi, Gorkha	Burhi Gandaki	One bridge and 24 houses at Arugahat about 10 miles downstream of the damming site were swept away.	Landslide occurred again in Tarebhir. Burhi Gandaki dammed near Lakubesi from 10.30 AM to 2 PM. The water level dropped from normal level of 4 m on August 1 down to 0.99 m on August 2. After the breaching of landslide dam, the water level rose to 14.61 m.	Shanker (1980) and Khanal (1996)
	(Three major landslides occurred at Labu Bensi in 1968. The first landslide on March 5, 1968 completely blocked the river flow and overtopped on 6th March and resulting flood at Arughat Bazar about 1100m^3/s. The second slide occurred on July 17, 1968 and the river was blocked for three hours and resulting peak flood at Arughat Bazar is about 1780m^3/s from the collapsed of the landslide dam. The detail of third landslide is described in the table.)					
4	1970	Tinau/Rupan-dehi	Tinau	92 people swept away by the flood after the breaching of the dam.	Tinau River was blocked.	Khanal (1996)
5	1971	Phalankhu, Rasuwa	Phalankhu	5 people, one house and one water mill were swept away.	Phalankhu Khola was dammed by landslides.	Khanal (1996)
6	1976	Baglung	Myagdi	7 people, 6 animals and 3 bridges swept away.		Khanal (1996)
7	1978	NA	Tinau River	The subsequent over-topping of the dam wiped away Dauretole of Butwal causing heavy damages to life and property.	A landslide caused by 125 mm of downpour falling within a few hours blocked the river.	Dixit (2003)
8	1980	NA	Tamor River	caused shifting of the Kosi River's channel at Chatara necessitating major revision of the intake of the irrigation system being built in the river	NA	Dixit (2003)
9	Sept - 81	North of Butwal, Palpa	Tinau River	The break through of dam formed by landslide resulted in a downstream surge that killed at least two hundred people on the Terai below Butwal.	During a heavy prolonged rainfall, landslide temporarily blocked the Tinau River.	Carson (1985)

Table 1.1: Formation and failure of Landslide dam in Nepal (contd.)

S. No.	Date	Location	River system	Damage	Nature of the event	Reference
10	1982	Phalamesangu, Balephi, Sindhupalchok	Balephi	97 people killed, causing heavy damages to life and property.	The huge landslide of 3km^2 blocked the river near Phalamesangu.	Khanal (1996)
11	1985	Trisuli, Rasuwa	Trisuli	No loss and damage took place.	From steady flow of 350 m^3/s on August 3, 1985, the discharge dropped to 93 m^3/s, 12 hours later it rose within the space of two hours to 2010 m^3/s after which it dropped during 5 hours to normal flow. The ratio of peak flow to mean annual instantaneous	Khanal (1996)
12	1986	Mukut Hill, Tadi, Nuwakot	Ghyangphedi	31 people, 173 animals, 24 houses and 4 bridges were swept away.	Slope of failure of Mukut hill blocked Ghyangphedi Khola.	Khanal (1996)
13	1987	Sunkosi/ Sindhupalchok	Sunkosi	Two gates of Sunkosi hydropower dam damaged completely, water and sand entered into power house, 229 house, 98 people, 309 animals were swept away, Arniko highway in many places was badly damaged.	The peak flood after breaching landslide dam was between 2150-3300 m^3/s which was as high as Glacier lake outburst flood of 1981.	Khanal (1996)
14	1988	Niskot Hill/Myagdi khola, Myagdi	Myagdi	109 people killed, 8 injured and 94 houses were destroyed and 44 animal buried by landslides. Durbang bazaar threatened and evacuated. Discharge was controlled by blasting.	After the failure of Niskot hill, Myagdikhola dammed for 3 hours, discharge was controlled by mobilizing local people.	Khanal (1996)
15	1989	Tarukhola, Bajhang	Tarukhola	16 people and 25 animals killed and 4 houses damaged by the landslide.	Tarukhola was dammed. The discharge was controlled by blasting with the help of Royal Nepal Army.	Khanal (1996)
16	22-Jul-96	Larcha, situated at the 109-km mark of the Arniko Highway, upper Bhotekoshi Valley	Bhairab Kunda Stream	Of the 22 houses in Larcha, 16 were swept away, two were partially damaged and 54 people were killed in a matter of a few minutes.	A combination of rainfall, runoff from cliff faces and stream undercutting triggered failure of the bedrock and colluvium, both on the dip and counterdip slopes, 500 m upstream from the highway. The landslide debris dammed the channel, which was eventually breached and deposited approximately 104,000m^3 of coarse debris.	Adhikari and Koshimizu (2005)

Table 1.1: Formation and failure of Landslide dam in Nepal (contd.)

S. No.	Date	Location	River system	Damage	Nature of the event	Reference
17	26-Sep-98	The landslide originated from Gounpani of Sikha VDC and reached kotesanghu of Bhurung Tatopani VDC at the left bank of the Kaligandaki river.	Kali Gandaki	Tatopani Bazaar and Kotesanghu (southern part of Tatopani Bazar) situated on the right bank of Kaligandaki river were submerged for several hours causing damage to properties and agricultural land worth some NRs. 5 million.	The river was completely blocked for about 8 hours, raising the water level to a height of about 15 meters and forming a lake of about 500 meters length upstream of the Kaligandaki River.	Chhetri and Bhattariai (2001)
18	11-Sep-00	Kakarahawa Khola, Deukhuri Valley	Kakarahawa Khola	Riverbed rose by by 15 m, destroyed an irrigation canal, the river inundated paddy field.	A prolonged rainfall of 3 days and 3 nights caused the landslide about 200 m long, 250 m wide and 120 m high.	Dhital (2002)

Table 1.2 Pre-historic landslide damming and LDOF

S.No.	Landslide	Age	Location	Stability of dam	Life span of lake	Reference
19	Ringmo	30,000 - 40,000 yr	Suli Gad Valley/ Dolpa	Stable due to re-cementation	Still existing after 30,000 - 40,000 yr	Weidinger (2006)
20	Kalopani	Post-glacial	Kaligandaki Valley/Mustang	Stable due to re-cementation	Disappeared within late to postglacial times	Weidinger (2006)
21	Dukur Pokhari	Post-glacial	Marsyandi Valley/Manang	Stable due to re-cementation with sediments	Filled up with alluvions within short period	Weidinger (2006)
22	Latamrang	Post-glacial	Marsyandi Valley/Manang, Neapal	Long time stability due to recementation	Overtopping and piping after < 5000yr	Weidinger (2006)
23	Tal	$\leq$ 1000	Marsyandi Valley	Stable due to cementation with sediments	Filled up with alluvions within $\leq$ 200 yr	Weidinger (2006)
24	Lambagar	Three generations	Tama Koshi Valley/Dolakha	Still Stable	Silted up within short period	Uhlir (1998)
25	Gath-Chaunikharka	Post-glacial	Dudh Koshi Valley/Solukhumbu	Failed by overtopping and erosion	Silted up following a first outbreak after 120yr	Uhlir (1998)
26	Ghatta Khola	Post-glacial	Ghatta Khola Valley/Western Nepal	Stable due to cementaion with sediments	Filled up with alluvions within <=100 yr	Weidinger (2006)

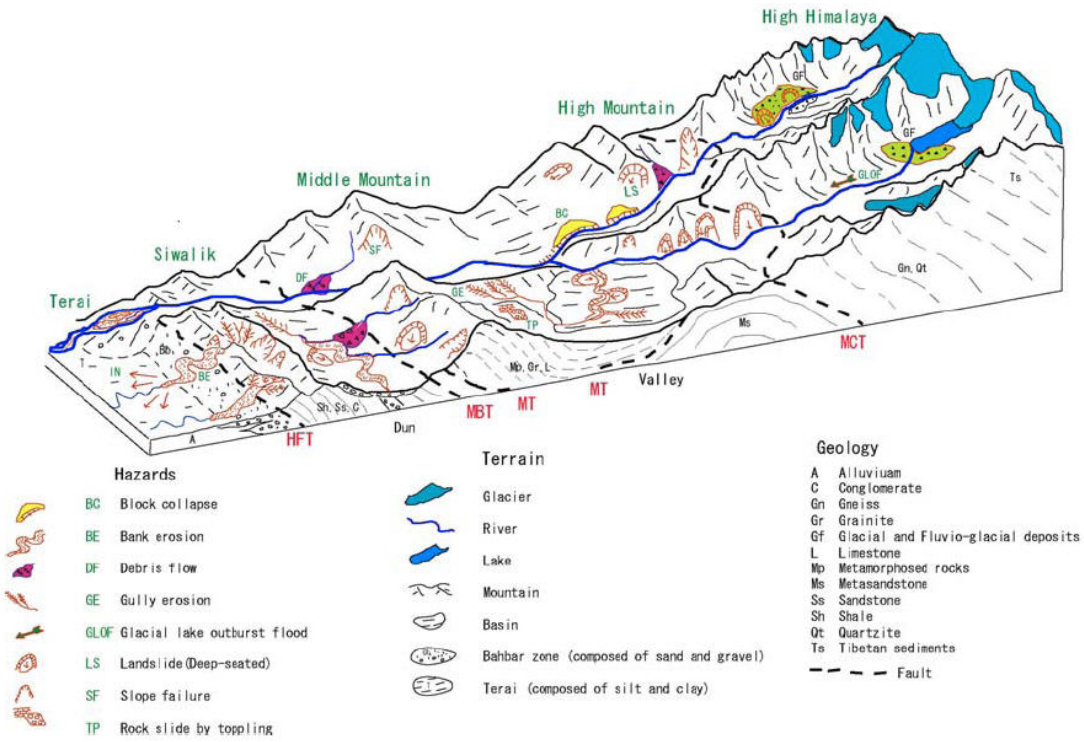

Figure 1.8 Types of water induced hazards in different physiographic regions of Nepal (WECS, 1987)

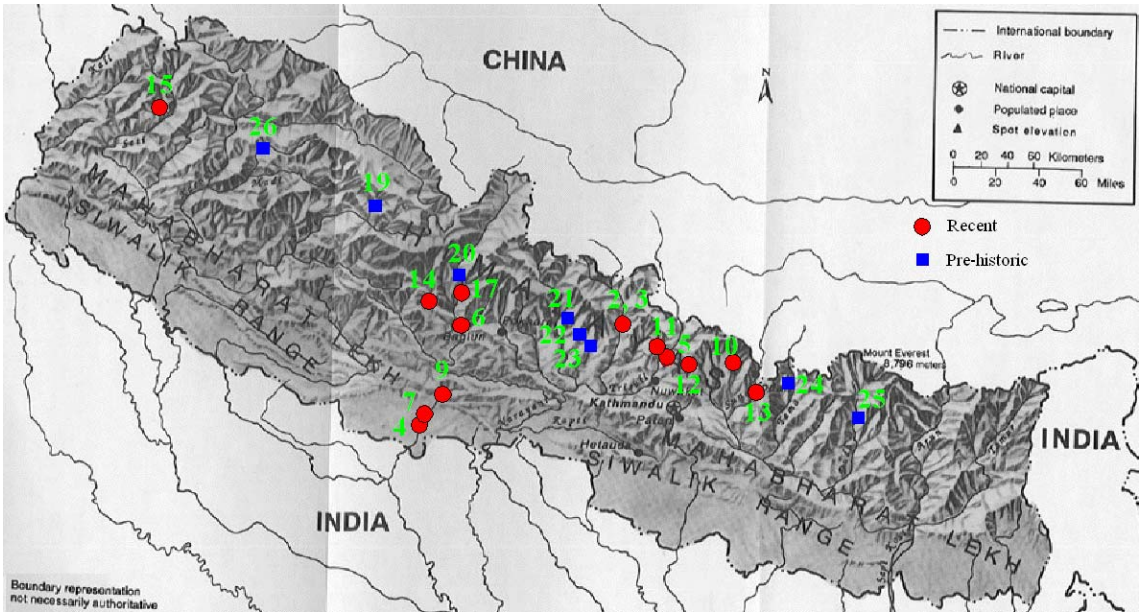

Figure 1.9 Locations of the recent and pre-historic landslide dam in Nepal

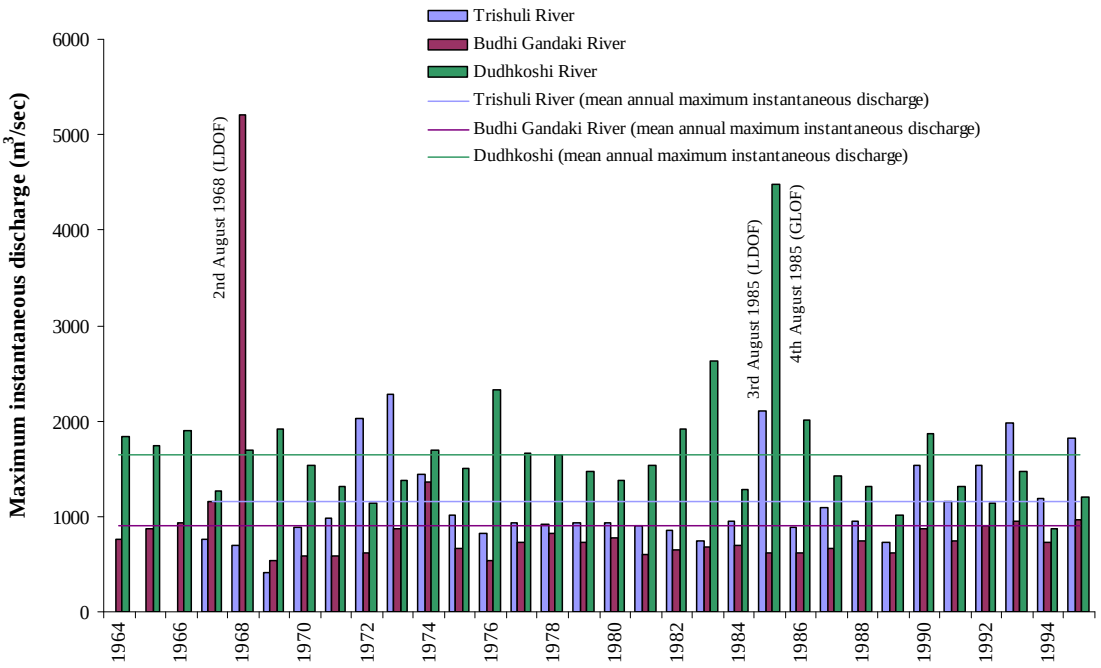

Figure 1.10 Comparison of peak discharge with mean annual maximum instantaneous flood discharge for Landslide dam outburst flood (LDOF) & Glacier Lake Outburst Flood (GLOF) events (Awal et al., 2007)

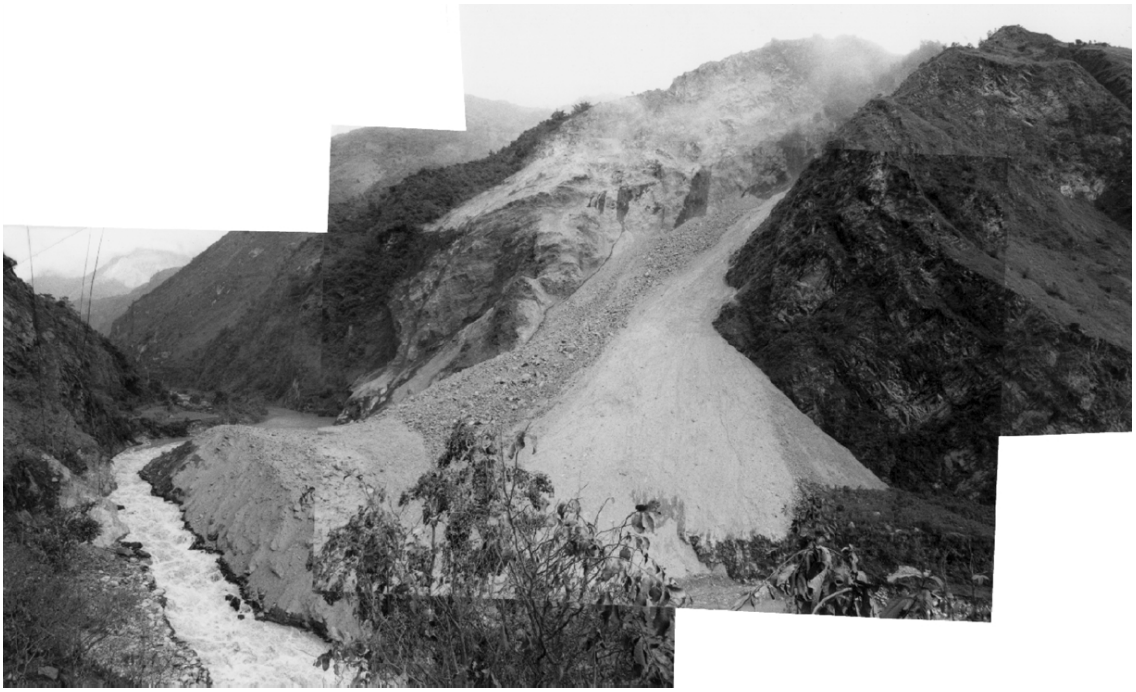

Figure 1.11 Landslide dam in Kali Gandaki river near Tatopani of the Myagdi district, Nepal - September 1998 (Photo courtesy: Peter Christian Ottinger, 2003)

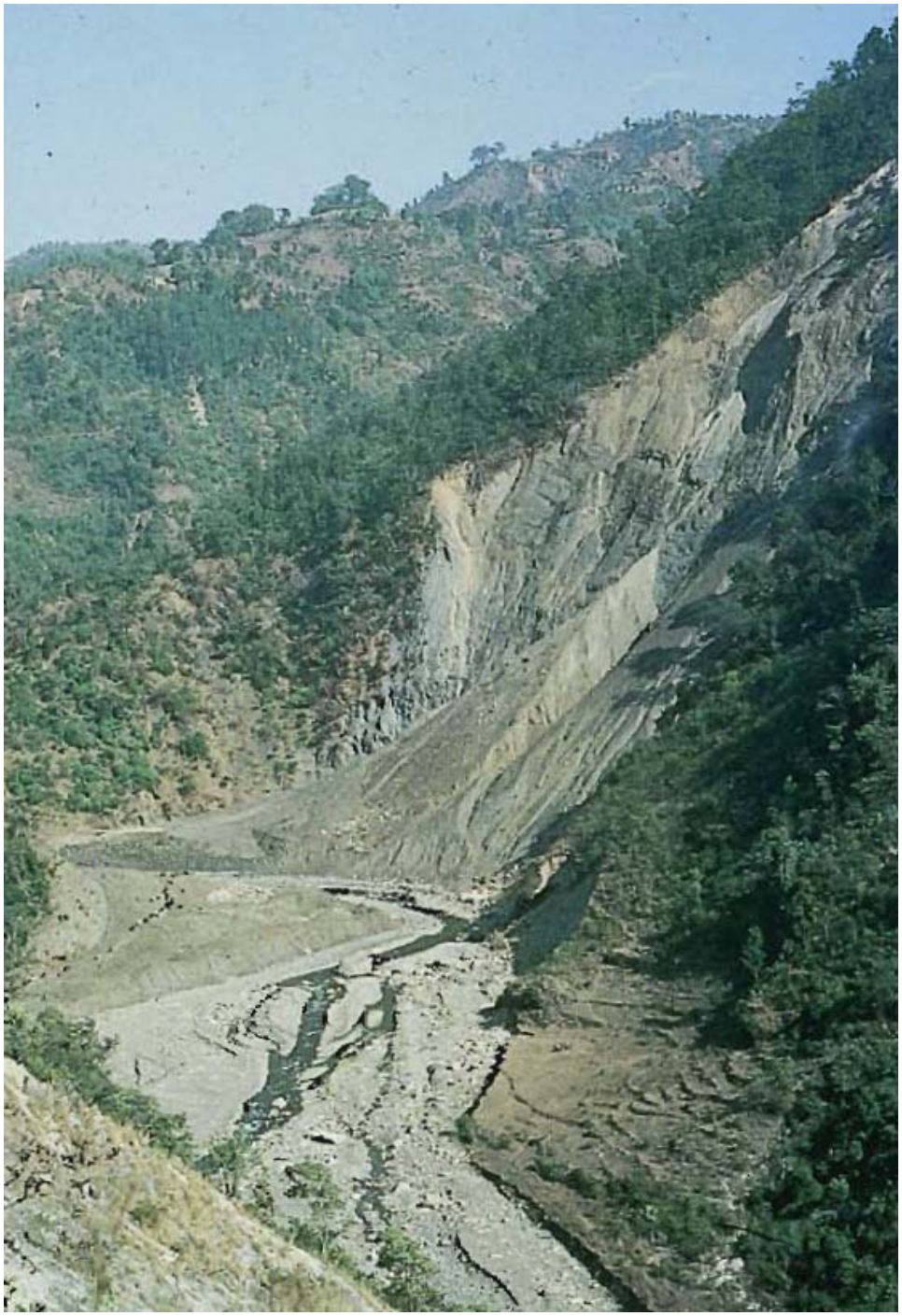

Figure 1.12 Landslide dam in Tinau River north of Butwal, Palpa District.

In Sept. 1981 during a heavy prolonged rainfall, this landslide temporarily blocked the Tinnau River. The break through of this dam resulted in a downstream surge that killed at least two hundred people on the Terai below Butwal. (Carson, 1985)

1.4 Objectives of the research

Flood/debris flow hydrograph will serve as an upstream boundary condition for subsequent flood routing to predict inundation area and hazard in the downstream to provide adequate safety measures. Landslide dam failure is frequently studied as an earthen dam failure. Very few models are developed for landslide dam failure that can treat the flow as both sediment flow and debris flow. Most of the existing models are applicable to overtopping failure of landslide dam. Some model has limitation to represent downstream batter slopes of greater than 1 in 5 (11^o). Infiltration process is neglected in almost all available models. In this context, an attempt has been made to incorporate integration of three separate models to predict the outflow hydrograph resulted from failure of landslide dam by overtopping and sudden sliding. The seepage flow model calculates pore water pressure and moisture content inside the dam body. The model of slope stability calculates the factor of safety and the geometry of critical slip surface according to pore water pressure and moisture movement in the dam body. The model of dam surface erosion and flow calculates dam surface erosion due to overflowing water. The main advantage of an integrated model is that it can predict time at which landslide dam may fail and also detect failure modes due to either overtopping or sliding based on initial and boundary conditions.

The objectives of this thesis can be described as follows:

(1) to review formation and failure of landslide dam with particular emphasis on Nepal.
(2) to determine general criteria for the prediction of failure modes of landslide dam based on flume experiments.
(3) to develop and validate individual models, i.e. model of seepage flow analysis, slope stability and dam surface erosion and flow.
(4) to combine seepage flow model and slope stability model to predict failure of landslide dam by transient slope stability analysis.
(5) to integrate three separate models to predict outflow hydrograph resulted from failure of landslide dam by overtopping and sudden sliding through flume experiments and numerical simulations.
(6) to propose effective hazard management procedure after formation of landslide dam.

1.5 Previous researches: a brief overview

1.5.1 Seepage flow modeling

Many water-related problems relevant to flood risk assessment and management involve variably saturated porous media. Such problems include earthen dams, landslide dams, artificial levees and natural river banks. The condition of seepage in the landslide dam is one of the important factors that affect the safety of the landslide dam. Variably flow models are very useful to study transient seepage flow in the landslide dam. A variety of numerical algorithms are available for solving the differential equations governing the seepage flow.

Several numerical models have been developed for simulating the movement of water in variably saturated porous media. In most applications, the pressure-based form of the variably saturated flow equation is used (Neuman, 1973; Cooley, 1983; Huyakorn et al., 1984, 1986) since the moisture based formulation cannot be used in saturated regions. However numerical solutions of the pressure-based form of Richards' equation are known to have poor mass-balance properties in unsaturated media (Celia et al., 1990; Kirkland, 1991). In the literature, a variety of numerical schemes including finite-difference, integrated finite difference, and finite-element methods have been used to solve variably saturated flow problems (Neuman, 1973; Narasimhan and Witherspoon, 1976; Cooley, 1983; Huyakorn et al., 1984, 1986). Finite-difference approximations have been widely used in several studies solving one-dimensional (vertical), variably saturated flow problems (e.g. Day and Luthin, 1956; Whisler and Watson, 1968; Freeze, 1969; Brandt et al., 1971; Haverkamp et al., 1977; Dane and Mathis, 1981; Haverkamp and Vauclin, 1981). Fewer researchers have used finite differences to solve variably saturated flow problems in higher dimensions (e.g. Rubin, 1968; Cooley, 1971; Freeze, 1971a,b; Kirkland et al, 1992; Clement, 1994). However most of the existing two-dimensional finite-difference solutions to variably saturated flow problems have limitations (Clement, 1994). In particular, finite-difference algorithms offer three major advantages: ease of coding, ease of data input, and more ready public acceptance in comparison with finite-element models (Clement, 1994).

Seepage analyses are an important tool to assess the susceptibility of seepage failure in dams and to study hydraulic conditions for analyzing the stability of dam slopes. Freeze (1971b) and Neuman (1973) are the foremost researchers who considered the variably saturated soil for transient seepage analysis of dams. 2D transient seepage analyses using saturated–unsaturated

seepage theory were conducted to consider initial filling of various reservoirs (Lam et al. 1987; Ng and Small 1995; Chen et al. 2005) and water-level fluctuations in front of dams (Aral and Maslia 1983; Lam et al. 1987).

For dams built in narrow valleys, three-dimensional effects are likely significant and two-dimensional simplifications may not be consistent with field conditions. To consider three-dimensional effects in seepage through dams, Gupta et al. (1986), Xie et al. (2001), and other investigators conducted three-dimensional analyses based on saturated seepage theory. Freeze (1971) presented a three-dimensional analysis of flow through earth dams that included unsaturated soil domains. Chen and Zhang (2006) studied infiltration into rockfill dam using 3D saturated-unsaturated seepage theory. Their study shows that seepage water flows faster and the hydraulic gradients are greater near the abutment boundary in the dam so the 2D analyses will underestimate the risk of seepage failure, particularly near the abutment boundary. Recently, some three-dimensional analyses (Russo et al. 1998; Ng et al., 2001; Zhou et al., 2002, Sharma et al., 2006) were performed to study rainfall infiltration into unsaturated soil slopes. Only limited studies have been reported, that consider three-dimensional reservoir water infiltration into originally unsaturated dams.

1.5.2 Slope stability analysis

Failure of landslide dam may be due to variety of failure mechanisms, including overtopping, seepage/piping and mass movements. The increase in weight of the dam body and pore water pressure due to seepage in the landslide dam are important factors that affect the safety of the landslide dam. After the formation of landslide dam, water flows through the dam body in a transient manner, so the slope stability analysis coupled with transient seepage analysis is useful to study stability of landslide dam.

A wide variety of analytical procedures have been developed over the years for slope stability analyses. They include limit equilibrium methods and finite element methods. In recent years finite element methods have been developed for slope stability analyses but limiting equilibrium methods are still widely used. One of the major advantages of limiting equilibrium methods is that a single numerical value is calculated to give an indication of the safety against failure of the slope under consideration. This value is often called the ‘‘factor of safety’’. The factor of safety simplifies the interpretation of the analysis results as only one number has to be evaluated. Factor of safety for a specified slip surface can be calculated by different methods. Extensive

studies have been undertaken in this area, and a variety of generalized safety factor formulations are now available, including those of Bishop (1955), Morgenstern and Price (1965) , Spencer (1967), Janbu (1973), Sharma (1973), Fredlund et al. (1980), and others. These methods differ in how well the conditions of equilibrium are satisfied and how the interslice forces are included in the solution. They can be divided into simple, complex and rigorous methods. For simple methods, the effects of interslice forces are neglected, whereas in complex methods, the interslice forces are included in the formulation. Methods where all conditions of static equilibrium are satisfied are named rigorous methods. The various slice methods also differ with respect to the failure surface shape which can be analyzed. For many of the methods, only a failure surface in the form of a circular arc is allowed. There are, however, an increasing number of methods where the failure surface could be non-circular or even partly composed of straight lines. The bases and performance characteristics of the various analytical procedures were examined by Fredlund (1984) in a state-of-the-art review. Several comprehensive reviews of slope stability analysis have appeared recently (e.g. Duncan, 1992, 1996(a), (b); Morgenstern, 1992).

The evaluation of slope stability by the limit equilibrium method involves calculating the factor of safety for a given sliding surface and searching for the critical slip surface that has the lowest factor of safety. When the potential slip surface can be considered circular in shape, the factor of safety may be obtained by widely used methods such as that proposed by Bishop (1955). The analysis of stability for non circular slip surfaces can be performed by any of commonly used methods such as the simplified or generalized Janbu method (Janbu et al. 1956; Janbu 1973), the Morgenstern–Price method (1965), and the Spencer method (1967, 1973). However determination of a non circular critical slip surface is much more complex than that of a circular critical slip surface. Many attempts have been made to locate the position of critical slip surface by using general noncircular slip surface theory coupled with different non-linear programming methods. Baker (1980) combined the Spencer method with dynamic programming, Celestino and Duncan (1981) combined the Spencer method with the alternating variable method, Naguen (1985) used simplex method to Bishop method, Arai and Tagyo (1985) used the conjugate gradient method, Yamagami and Ueta (1986) coupled the Janbu's simplified method with dynamic programming involving Baker's ideas, Yamagami and Ueta (1988) performed a comparative study by combining several optimization methods with the Morgenstern-Price method. These nonlinear programming methods appeared to be reasonably efficient in locating a general-shaped critical slip surface for examples reported in the references. The random search

method has been occasionally used in determining critical slip surfaces (Boutrup and Lovell, 1980; Greco, 1996; Husein Malkawi, 2001). Though effective in some cases, this method can only be considered as an ad hoc method due to its poor theoretical background (Zhu, 2001). Several researchers attempted to apply variational calculus to the determination of the position of the critical slip surface (Castillo and Revilla, 1977; Revilla and Castillo, 1977; Ramamurthy et al., 1977). This method is mathematically complex and limited to very simple slopes.

A two-dimensional analysis is only valid for slopes which are long in the third dimension. For shorter slopes, the failure surface will probably be bowl-shaped and the three-dimensional effects cannot always be neglected. Failure of natural and man made slopes occurs in three dimensions, such as an embankment confined in a narrow U- or V-shaped valley, a trench of limited extent, a corner defined by the intersection of two embankments, a mining crater or a coal heap, predictions based on a 2D analysis might be grossly idealized and economically not justified. In practice, limit equilibrium approaches of columns are commonly used for 3D stability analyses of slopes. 3D slope stability analysis using the method of columns was first made by Hovland (1977). The 3D method proposed by Chen and Chameau (1983) can be considered partly as an extension of the assumptions associated with the ordinary method, and partly as an extension of the assumptions associated with Spencer's (1967) method. Ugai (1988) and Ugai and Hosobori (1988) extended the simplified Janbu method and Spencer method in 2D problems to three-dimensions. Huger et al. (1989) used a 3D method that was an extension of the assumptions in Bishop's (1954) simplified and Janbu's simplified 2D methods. A generalized limit equilibrium method for 3D analysis was developed by Lam and Fredlund (1993). Their 3D method can be considered partly as an extension of the 2D Moregenstern and Price method (1965).

Searching for the 3-D critical slip surface can be classified into two major groups. The first assumes a slip surface to have a particular shape, i.e. extended circular arc (Baligh and Azzouz, 1975), a log spiral surface (Giger and Krizek, 1975), a cylindrical surface (Ugai, 1985), a surface of revolution (Gens et al., 1988), or an ellipsoidal surface (Xiang, 1988), and the second is valid for an arbitrary slip surface. When the analysis of slope stability is carried out by the first group of methods, slip surfaces can be expressed analytically and the critical slip surface can be found easily through simple numerical computations. Based on the methods that are valid for slip surfaces of arbitrary shape, however, it is quite difficult to search for the critical slip surface because possible slip surfaces exist infinitely. 3-D slope stability analysis using method

of random generation of surfaces was presented by Thomaz and Lovell (1988) and Yamagami et al. (1991).

Yamagami and Jiang (1997) developed an effective method based on dynamic programming and the method of Random Number Generation to search for the 3D critical slip surface of a general slope using 3-D simplified Janbu method proposed by Ugai et al (1988). The search scheme presented by Yamagami and Jiang (1997) was also applied to determine sliding direction in 3D slope stability analysis (Jiang and Yamagami, 1999) and to locate 3D critical slip surfaces based on a nonlinear strength envelop (Jiang et al. 2003). Jiang and Yamagami (2004) used more rigorous method of columns, i.e. Spencer method, satisfying both force and momentum equilibrium is incorporated into dynamic programming to locate 3D critical slip surface for a general slope.

Many researchers used different slope stability analysis method combined with hydrological model to analyse slope stability of natural slope. Wilkinson et al. (2000, 2002) used a combined hydrology and stability model by incorporating an automated non-circular search technique into the Janbu's method of stability. Tsutsumi et al. (2007) used combined hydrology and stability model to analyse deep-seated landslide triggered by the Typhoon in Taketa City, Oita Prefecture. Some researchers focused on transient stability analysis of a collapsible dam using dynamic programming combined with finite element stress fields (e.g. Pereira et al., 1996; Brito et al., 2004) and very few studies analyzed transient slope stability of embankments (e.g. Staiano et al., 2001, Gitirana and Freduland, 2003).

1.5.3 Overtopping erosion modeling and outflow hydrograph prediction

The dominant failure mode for landslide dams, embankment dams and flood defense embankments is by overtopping. Piping, slope instability and foundations failures may also occur. At present, many models are being developed, using different approaches to simulate breach formation process. The majority of the models consider breaching through an embankment dam, rather than through a landside dam. The process of breach through a landslide dam is different from that through an embankment dam. When a landslide dam is overtopped, there commonly is much more sediment and debris to erode before a full breach develops than is the case for embankment dam. Landslide dams thus fail more slowly than

constructed dams of the same height or volume, and flood peak discharges are less (Costa, 1985). However, landslide dam failure is still frequently studied as an earthen dam failure, because the mechanism of breach formation is considered very similar, despite of different geometry, dimensions and material properties. Brief review of existing models to predict breach formation through embankment dams and flood embankments and some specific models developed for landslide dam failure is discussed in this section.

Embankment dams and flood embankments breaching

A number of numerical techniques have been developed to predict peak discharge of dam-break flood, time-to-peak, and final breach dimensions. Many empirical formulations have already been developed for predicting dam breach characteristics and peak outflows based on hydraulic and geometrical properties of dams and reservoirs. Kirkpatirick (1977), Hagen (1982), MacDonald & Langridge-Monopolis (1984), Costa (1985), Forehilich (1995), Evans (1996), Walder & O'Connor (1997), Broich (1998) developed regression equations to determine peak discharge. All of these methods, except Walder and O'Connor, are straight forward regression relations that predict peak outflow as a function of various dam and/or reservoir parameters, with the relations developed from analyses of case study data from real dam failures. Wahl (2004) presented a quantitative analysis of the uncertainty associated with these various methods, and concluded wide bands of uncertainty within the processes. Empirical relations are generally used as a guideline in dam breach analysis rather than as a basis for flood forecasting purposes. Characteristic analysis recognizes that the geometry and size of the breach as well as the lake play an important role in a dambreak and that breaches are typically trapezoidal and two to four times wider than they are deep (Johnson and Illes 1976; Walder and O'Connor 1997). These relationships have been reduced to empirical equations (e.g., MacDonald and Langridge-Monopolis, 1984; Froehlich, 1987).

In the last forty years, particularly since the 1980's, many mathematical models have been developed for the simulation of breach growth in embankments. Some models ignore the mechanisms of erosion by lumping every possible factor into two principal parameters: final shape and breach formation time (Fread, 1988a; U.S. Army Corps of Engineers, 1981). Other physically based embankment breach models use principles of hydraulics, theory of sediment transport and soil mechanics to simulate the breach growth process and the breach outflow hydrograph. This category includes models, e.g. Ponce and Tsivoglou (1981), Fread (1988b), Singh and Scarlatos (1988), Bechteler and Broich (1991), Visser (1998), and Wang and Bowles

(2006). Physically based models are more complicated in structure and possess the potential to model in more detail and more accurately the embankment breaching process, although they are restricted by the degree of understanding of the embankment breaching mechanism (Zhu, 2006).

Summary of the most recently developed breach models can be found in Singh (1996), Wahl (1988), Morris (2000) and Zhu (2006). Among these models, Cristofano (1965), Ponce and Tsivoglou (1981), Giuseppetti and Molinaro (1989), Havnø et al. (1989), Wetmore and Fread (1983), Singh and Scarlatos (1988), Peviani (1999), Tingsanchali and Chinnarasri (2001), Coleman et al. (2002), and Wang and Bowles (2006) deal with earth dam breaching due to overtopping; Renard and Rupro study only piping failure of earth dams; and Brown and Rogers (1981), Fread (1988a), Fread (1988b), Bechteler and Broich (1991), Loukola and Huokuna (1998) and Mohamed et al. (2002) take both overflowing and piping into account. Fread (1988a), Singh and Scarlatos (1988), Peviani (1999) and Mohamed et al. (2002) also contain the breach side-slope stability analysis. Almost all the models describe the breach flow with broad-crested weir formula when dam overflowing is concerned.

There are no existing breach models that can reliably predict breach formation through embankments. Discharge prediction may be within an order of magnitude, whilst the time of breach formation is even worse. Prediction of breach formation time due to a piping failure is not yet possible. Existing breach models should be used with caution and as an indicative tool only. There is a clear need to develop more reliable predictive tools that are based on a combination of soil mechanics and hydraulic theory (Morris, M.W. & Hassan, M., 2002).

Various experiments on the breaching of embankments have been conducted during the last several decades. These experiments include both large-scale tests in the field and small-scale tests in the laboratory. The former includes, e.g. Pan and Loukola (1993), Visser et al. (1991 and 1996), Meadowcroft et al. (1996), Hahn et al. (2000) and Höeg et al. (2004). The small-scale tests in the laboratory include numerous flume and wave basin experiments, which can be found in e.g. Powledge and Dodge (1985), Fujita and Tamura (1987), De Looff et al. (1997), Visser (1998), Tingsanchali and Chinnarasi (2001), Coleman et al. (2002), Rozov (2003), Mohamed et al. (2004), Zhu et al. (2006), Ito (2007). Nevertheless, the breach formation and development in embankments is such a complicated process with various influencing factors involved in, such as profile and structure of embankment, type of foundation (erodible or non-erodible), type of material (cohesive or non-cohesive), causes of failure (overtopping, piping, slope sliding, etc.).

Despite the many experiments conducted and the insight gained, our understanding of the embankment breaching mechanism is still unsatisfactory.

Landslide dam breaching

When a landslide dam is overtopped, there commonly is much more sediment and debris to erode before a full breach develops than is the case for embankment dam. Landslide dam thus fail more slowly than constructed dams of the same height or volume, and flood peak discharges are less (Costa, 1985). Therefore, modeling the failures of landslide dam requires some modifications to conventional dam-break flood models developed for failure of constructed dams (Glazyrin and Reyzvikh, 1968; Ponce and Tsivoglou, 1981). Although, landslide dam failure is frequently studied as an earthen dam failure, very few models are developed for landslide dam failure that can treat the flow as both sediment flow and debris flow. If the concentration of sediment is above 10%, non-newtonian viscous flow has to be taken into account. During surface erosion of landslide dam, sediment concentration increased more than 10%, so the model to predict the flood/debris flow hydrograph due to landslide dam failure should be capable to treat all types of flow based on sediment concentration.

Different available tools for analyzing landslide dam failures and their resulting outflow hydrograph can be grouped in four categories:

1. Empirical regression equations

The most basic of these are empirical regression equations that relate the observed peak discharge to some measure of the impounded water volume: depth, volume or some combination thereof (Costa, 1985; Costa and Schuster 1988; Walder and O'Connor 1997) and regression equations that relate experimental peak discharge to some measure of impounded water volume: depth, torrent bed gradient and inflow discharge (Tabata et al., 2001). Despite the limitations of the regression equations, they do provide useful information on general trends in the peak discharge at the dam breach for landslide dam failure floods.

2. Dimensional analysis

Walder and O'Connor (1997) used dimensional analysis to evaluate the relative effects of breach growth rate, lake volume, and hypsometry (i.e. a measure of the three-dimensional shape of the lake – the relationship between lake surface area and lake surface elevation) on peak

discharge. They ignored tailwater effects and assumed that the fundamental physical mechanisms are the same for all dambreak flood events.

3. Parametric models

Parametric models derive discharge hydrographs by assuming a final breach size, geometry, and development time, and calculating instantaneous outflows through the evolving breach using standard hydraulic weir flow equations (e.g., Manville 2001). DAMBREAK and OUTFLOW3 are the examples of parametric models which can be used for both landslide dam failure and embankment dam. The DAMBRK model is a dam break flood routing model (one dimensional Saint- Venant equations) developed by Fread in 1977 with the latest version released in 1988. The failure duration and the final shape and dimensions of the breach are required as input for the model. The breach is initiated at the dam crest and grows at a linear rate over the failure duration to the ultimate breach dimensions. The OUTFLOW3 was developed by Manville (2001). Three alternate broad crested weir equations are used to generate different values for the instantaneous peak discharge through a trapezoidal breach that would occur if the breach attained its final size instantaneously when the reservoir was at the dam crest. However this condition is unrealistic due to lake draw down, the technique constrains the potential upper maximum discharge likely during a dam break flood (Wishart, 2007).

4. Physically based models

Physically based models relate erosion by the escaping water to the development of the breach. Breach erosion rate is linked to discharge by a sediment transport equation. However some models are applicable to debris flow. Some of the physically based models used/developed or applicable for landslide dam failure are BREACH, Takahashi and Kuang (1988), Takahashi and Nakagawa (1994), Mizuyama (2006), Cencetti et al. (2006) and Satofuka et al. (2007). These models require detailed information on dam geometry and dimensions, geotechnical properties of dam material, lake volume and geometry, which may be poorly known for landslide dams.

BREACH was developed by Fread in 1984 and later revised in 1988. The model is capable of simulating dam failure due to either overtopping or piping. This model couples the breach outflow with the sediment transport capacity of the unsteady uniform flow along the erosional channel cut through the dam, using the Meyer-Peter-Muller sediment transport relation modified by Smart (1984) for steep channels. Breach channel growth depends on the dimensions of the dam and the grain size, sorting, density, friction angle, and cohesive strength of the dam

material, and is calculated iteratively. The model is most sensitive to the internal friction angle and cohesive strength of the dam materials. The model is also tested for landslide-formed dams. However the inability of this model to represent batter slopes of greater than 1 in 5 (11^{o}) is a significant limitation (Davies, 2007).

Takahashi and Kuang (1988) derived relationship for the shape and length of the landslide dam in a narrow channel with the width and the total volume of the landslide. They also developed the separate 1-D model to predict the debris flow hydrograph due to failure of landslide dam by overtopping and sudden sliding.

Takahashi and Nakagawa (1994) developed 2-D model to predict flood/debris flow hydrograph due to collapse of a natural dam by overtopping. Lateral erosion velocity as a function of the shear stress on the side wall was used to model channel enlargement during overtopping.

Mizuyama (2006) conducted flume experiments and used 1-D two layer model which is applicable to immature debris flow and debris flow to predict outburst discharge. The simulated result indicated that the shape of the landslide dam and the inflow rate are the major parameters determining peak discharge.

Cencetti et al. (2006) implemented Schoklitsch formula as an alternative to Smart equation in BREACH model. The bed load transport formula used in BREACH (Meyer-Peter & Muller, modified by Smart), is based on experiments performed in a flume with the grain size distribution ratio D90/D30 lesser than 10. Such a methodology makes this equation not much suitable to describe the sediment transport peculiar to a landslide body having a very low sorting. However, because the landslide deposits may often have a strongly bimodal grain-size frequency curve, the percentile D50 can sometimes correspond to one of the grain-size classes which are really present to a lesser degree. To consider this phenomenon, the BREACH programme was implemented with a new procedure that calculates two granulometric curves, one for each mode of the original distribution, and evaluates transport of the landslide material separately.

Satofuka et al. (2007) proposed a one-dimensional model for river bed variation and flood runoff which is composed of two-layer model for immature debris flow and bank erosion model. The model was applied to study Nonoo landslide dam formed by the typhoon 0514 heavy

rainfall in Miyazaki prefecture. Similar model was used by Mori (2007) to predict outflow hydrograph from failure of landslide dam.

1.6 Outlines of the dissertation

This research investigates the applicability of integrated model developed to predict outflow hydrograph due to landslide dam failure by overtopping and sliding. To communicate the findings, the dissertation is organized in seven chapters.

Chapter 1 backgrounds the formation and failure of landslide dam. Particular emphasis is given to the objectives of study and brief overview of previous study.

Chapter 2 outlines the experimental studies. Descriptions of the instruments used in the laboratory experiments are provided. Different dam structures are tested under different inflow and flume slopes. The criteria to determine failure modes of landslide dam are also presented based on experiments.

Chapter 3 backgrounds seepage flow models. Verification of model results with different experiments are presented for both 2D and 3D cases.

Chapter 4 backgrounds the slope stability models. Identification of critical slip surface and time to failure based on dynamic programming are verified with experimental data for both 2D and 3D cases.

Chapter 5 backgrounds the overtopping and dam breach modelling. Verification of model with different cases of overtopping from full channel width and partial channel width is presented.

Chapter 6 presents the overview of integrated model to predict flood/debris flow hydrograph. Results are presented in the form of moisture profile at different location of dam body, sliding surface, longitudinal profile and outflow hydrographs. The effective hazard management after formation of landslide dam is also presented.

Chapter 7 summarises the main conclusions based on the present study with recommendations for future efforts needed in the study of landslide dam.

Chapter 2

Experimental Studies

2.1 Introduction

The experimental studies were focused on observation of failure modes, measurement of moisture profile inside the dam body, observation of slope failure due to transient seepage flow, measurement of outflow hydrograph both sediment and total discharge for the validation of individual models and integrated model. Basic principle and methods of measurement of some of the major apparatus used in the experiment are discussed in this section. Many experiments were done to observe failure modes of landslide dam in different channel slopes and inflow discharge.

2.2 Experimental set-up and measurement apparatus

2.2.1 Laboratory flume

A rectangular flume of length 5m, width 20cm and depth 21cm was used. The slope of the flume could be changed from horizontal to inclination of 20 degree or more. The schematic diagram of the flume including instrumentation and data acquisition system is shown in Figure 2.1. Details of flume used for the validation of three-dimensional seepage flow model and slope stability model are discussed in Chapter 3.

Dam body was prepared in the lower part of the flume allowing sufficient space for upstream reservoir. To measure the movement of the dam slope during sliding, red colored sediment strip was placed in the dam body at the face of the flume wall. A fixed inflow discharge was supplied from upstream part of the flume. The arrangement to measure outflow hydrograph both sediment and total discharge at the channel outlet was achieved by employing container to trap sediment and servo type water gauge in the downstream tank. The submerged weight of sediment trapped in the container was measured with the help of load cell at fixed time interval. Holes were drilled in the sidewall of the flume for the insertion of Water Content Reflectometers (WCRs) at the interval of 20cm longitudinal distance. A digital video camera

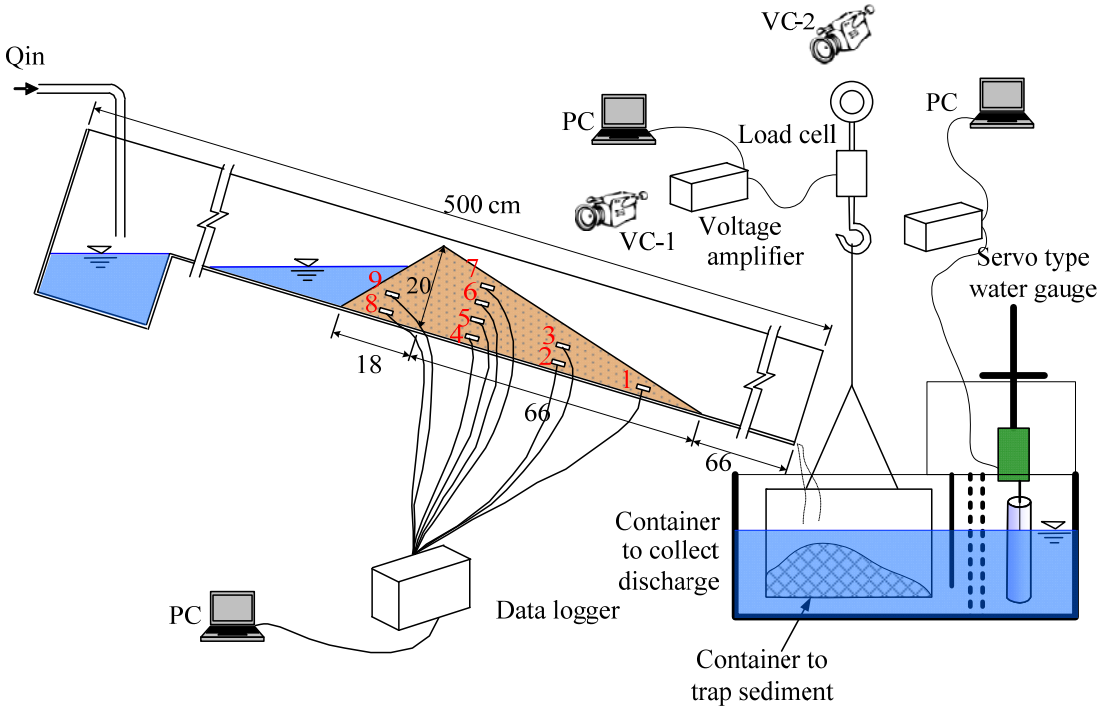

Figure 2.1 Experimental setup

was placed in the side of the flume to capture the shape of slip surface due to sudden sliding and transformation of the dam body with time due to surface erosion. Video camera was also placed in the front side of the flume to capture the failure mechanism of dam.

2.2.2 Multi-fold pF meter

The water retentivity of the soil can be expressed by a variety of factors including the volumetric water content and the pF value. The matrix potential (pF value) of a soil sample and its volumetric water content are correlated by a characteristic curve depending on the texture of the soil and this curve is called a "moisture retention curve". DIK-3423 Multi-Fold pF Meter (Figure 2.2) was used for measuring the moisture retention curve of a soil sample. It can set up to 24 pieces of sampling tubes in the sample chamber. Any optional pF value can be set with the automatic pressure controller. This controller can set an accurate and stable pressure without taking the influence of atmospheric pressure. A specified pressure is applied to a soil sample and the weight of the soil at equilibrium is measured to determine the volumetric water content corresponding to the matrix potential; this procedure is repeated at various pressures to construct a moisture retention curve for the soil sample. For each magnitude of the air pressure applied, the moisture content of the soil sample is determined by calculating the difference between the

DIK-3421-11 Sample chamber DIK-9221 Automatic pressure controller

Figure 2.2 Multi-fold pF meter

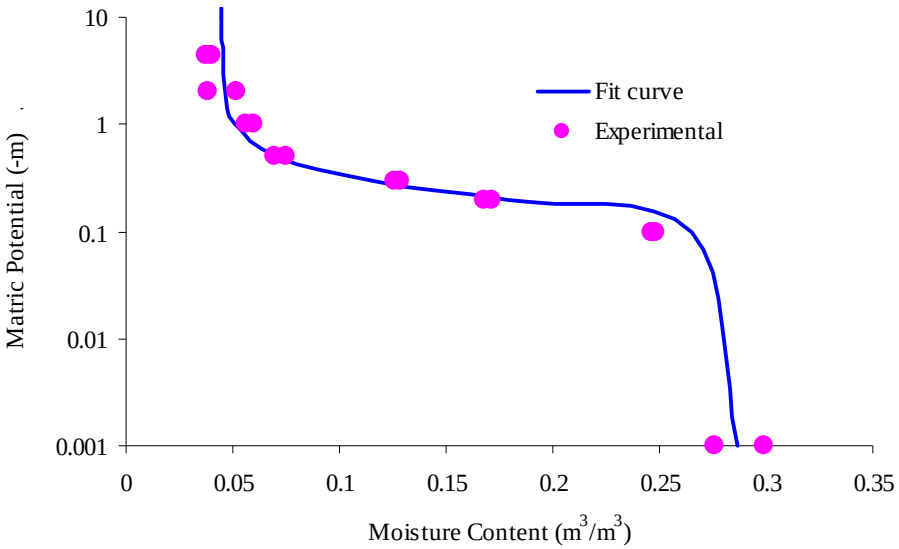

Figure 2.3 $\theta - h$ relationship curve for sand mix 1-7

weight of the measured soil sample and that of the same soil sample in a dry state. The determined moisture content corresponds to the applied air pressure, hence, the moisture potential at the time of measurement, thus providing a moisture content corresponding to a

given pF value.

Two types of sediment mixes; Mix 1-6 and Mix 1-7 were used in the study. Typical $\theta - h$ relationship curve for sand mix 1-7 is shown in Figure 2.3. van Genuchten parameters (including θ_r) were estimated by non-linear regression analysis of soil moisture retention data obtained by pF meter experiments for different sediment mix which are shown in Table 2.1.

2.2.3 Water content reflectometer

The volumetric water content of soil can be determined from the measurement of its dielectric constant. A typical method that relies upon the electric pulse approach is TDR (time-domain reflectometry) which determines the dielectric constant of the soil from the propagation time of electric pulses. According to the principle of measurement by TDR, water has a relative dielectric constant of 81 which is by far greater than the values for soil solids (mica 3-6) and air (1) and the empirical correlation established between the apparent relative dielectric constant of the soil and its water content is utilized to measure the volumetric soil water content. Specific means of measurement comprises inserting two parallel electrodes into the soil, applying microwaves to the electrodes and measuring the propagation time of the interfering reflected wave.

The water content reflectometer (Figure 2.4), CS 616 manufactured by Campell Scientific, Inc. was used in the experiment to measure moisture profile inside the dam body. The two stainless steel rods of the WCR has spacing of 32mm, diameter of 3.2mm and length of 20cm (originally 30cm). WCR (CS 616) employs TDR principles for measuring volumetric soil water content. The travel time of signal on the probe rods depends on the dielectric permittivity of the material surrounding the rods and the dielectric permittivity depends on the water content. The probe output period ranges from about 14 microseconds with rods in air to about 42 microseconds with the rods completely immersed in typical tap water. The amount of soil organic matter and some clays can alter the response of the WCR (Campbell Scientific, Inc, 2004). The method used for probe insertion can affect the accuracy of the measurement. The probe rods inserted in a manner that generates air voids around the rods and nonparallelness of probe rods affects the measured value of water content.

A calibration equation is used to convert the period to the volumetric water content. Campbell

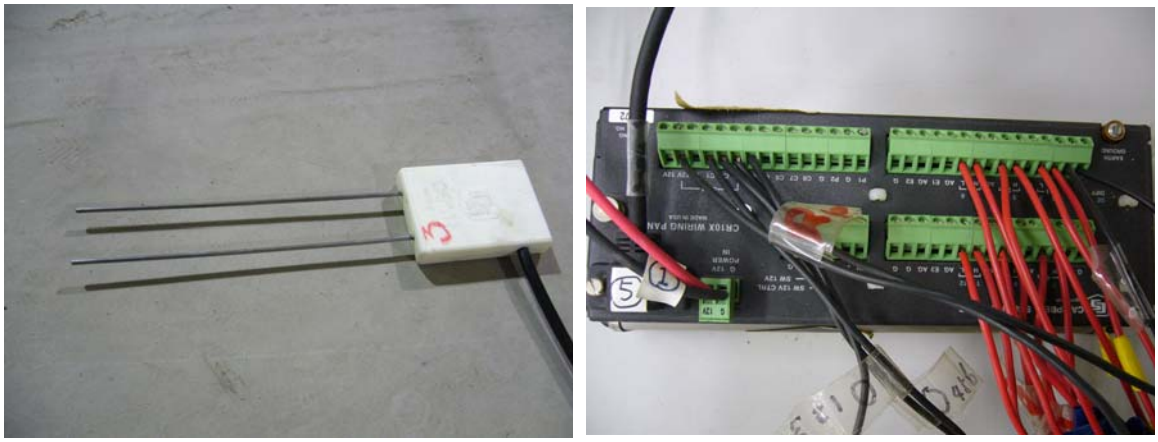

CS 616 Water content reflectometer (WCR) Data logger

Figure 2.4 Water content reflectometer and data logger

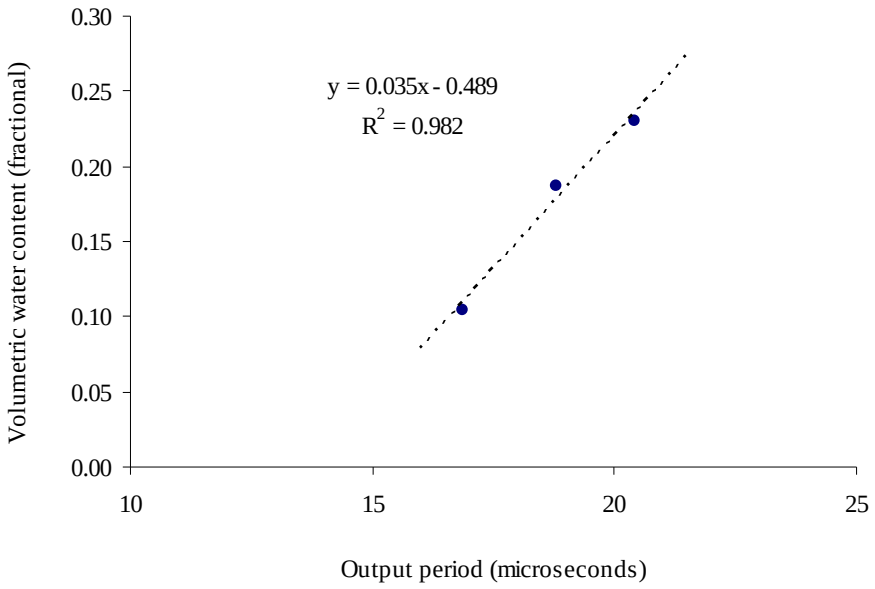

Figure 2.5 Typical calibration curve for WCR

Scientific, Inc. has suggested using quadratic or linear equation to describe probe output response to changing water content. The calibration coefficients were derived from a curve fit of independently determined volumetric water content and probe output period (microseconds). Typical calibration curve for WCR is shown in Figure 2.5.

2.2.4 Load cell

Load cells are measuring device that produces an output signal proportional to the applied weight or force. Tension load cells are used for measuring the pulling apart or positive force along a single axis. The information that load cell monitor is then signaled to a recorder or other computerized data collection system.

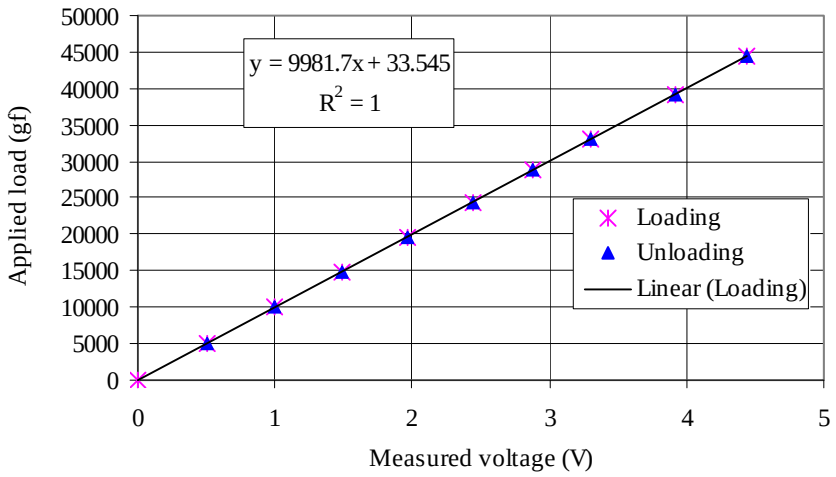

Figure 2.6 Calibration curve of load cell

Load cell Amplifier

Figure 2.7 Load cell and voltage amplifier

Load cell, model KYOWA LT-50KG, was used to measure tension loads with an accuracy as high as 1/2000. It was used by attaching a ball joint, rotating attachment, hook and shackle. Amplifier, KYOWA DPM-612B, was used to measure the output voltage. Calibration curve was produced by the comparison of the load cell outputs against standard test loads before measurement. The calibration curve of load cell is shown in Figure 2.6. Load cell and Amplifier used in the experiment is shown in Figure 2.7. The temporal change of submerged weight of trapped sediment in the container was measured by using load cell to determine sediment discharge.

2.2.5 Servo-type water level gauge

Discharge at the downstream end of the flume was measured by using water tank with servo-type water level gauge. Detector, KENEK NST-10 was used to measure water level. The maximum measurable water level of detector was ± 50mm. Main body, KENEK NS-101 was used to measure output voltage. The detector and main body of servo type water level gauge is shown in Figure 2.8. Calibration curve was produced by the comparison of output voltage against known height of water level before measurement in all experiments.

Detector, KENEK NST-10

Main body, KENEK NS-101

Figure 2.8 Servo-type water level gauge

2.3 Dam body construction

Triangular dam was prepared on the rigid bed of flume by placing mixed sand on the flume. The upstream and downstream faces of landslide dam are slightly shallower than the angle of repose of the sand mixture. The sediment placed in the flume was leveled and compacted in every thickness of approximately 5cm by using timber plate. The final shape of the dam body according to flume slope was prepared by removing extra sediment and smoothing the surface of the dam. In the case of experiment to measure water content, WCR was inserted before giving final shape of the dam because part of dam body may settle during insertion of WCR. To measure the movement of dam slope during sliding, red colored sediment strip was placed at the face of the flume wall before preparation of the dam body.

2.3.1 Dam geometry

Takahashi and Kuang (1988) define the shape of landslide dam based on amount of available landslide material. When the volume of landslide mass is large it will form a triangular dam with upstream and downstream slope angles almost equal to the angle of repose, otherwise it will become trapezoidal, however formation and shape of landslide dam depends on number of factors such as landslide velocity, riverbed width, river water discharge, grain size and texture of the blockage material etc.

The shape and size of landslide dam, grain size distribution, degree of compaction and moisture content of landslide dam material depend on the site condition and the process that have triggered dam forming landslides. However for simplicity, in these experiments, triangular dams of homogeneous material with uniform compaction and uniform initial moisture content were used. The upstream and downstream slopes of the landslide dams are slightly smaller than the angle of repose of the sand mixture. The height of the dam was 20cm and the longitudinal base length was different according to channel slope. The shape of dam for channel slope 17^{o} is shown in Figure 2.1. The details of shape and size of the dam body used in experiments for 3D cases are discussed in Chapter 3.

2.3.2 Sediment properties

Silica sand S1, S2, S3, S4, S5, S6 and S7 are mixed in equal portion to make the mixed

sediment for dam body in sediment type “Mix 1-7” and S1 to S6 are used in “Mix 1-6”. The grain size distributions of sediment mixture are shown in Figure 2.9. van Genuchten parameters i.e. α and η (including θ_r) were estimated by non-linear regression analysis of soil moisture retention data obtained by pF meter experiment. Some other parameters of mixed sand are listed in Table 2.1.

Table 2.1 Different parameters of the sediment considered

Sediment type	Mix 1-6	Mix 1-7
Saturated moisture content, θ_s (-)	0.325	0.287
Residual moisture content, θ_r (-)	0.038	0.045
α	9.60	5.50
η	2.74	3.20
Specific gravity, *Gs*	2.65	2.65
Mean grain size, D_{50} (mm)	1.15	1.00
Angle of repose, ϕ (degree)	34	34

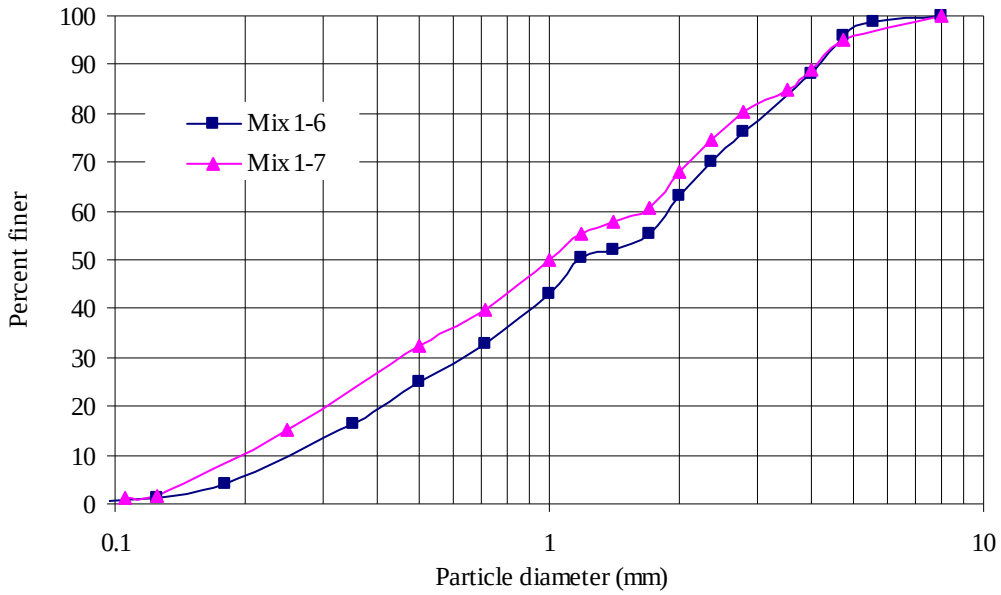

Figure 2.9 Grain size distribution of different sediment mixes

2.4 Experiment conditions

The slope of the flume, size and material properties of the dam body, inflow discharge is

different according to purpose of experiments. The main purposes of experiments are as follows:

- to predict failure modes (e.g. overtopping, progressive, instantaneous slip failure)
- to measure moisture profile in the dam body (2D and 3D cases).
- to observe slope failure of landslide dam in longitudinal section (2D and 3D cases).
- to measure outflow hydrograph (sediment and total discharge) and dam surface erosion due to overtopping from full channel width.
- to measure outflow hydrograph (sediment and total discharge) and dam surface erosion due to overtopping from partial channel width.
- to measure outflow hydrograph (sediment and total discharge) and dam surface erosion due to sudden sliding and overtopping.

The experimental procedures and conditions will be briefly described for each experiment in corresponding chapters.

2.5 Criteria to determine different failure modes

2.5.1 Introduction

Process of failure of landslide dam can be classified into three types; overtopping, abrupt collapse of the dam body (instantaneous slip failure) and progressive failure. Infiltration rate is one of the factors which govern failure modes. When the infiltration rate is small, overtopping results. When the infiltration rate is very large, seepage which appears on the lower part of the downstream face brings collapse around it and then the collapse proceeds upstream. Large failure occurs at the moment the collapse reaches near the blocked water. When infiltration rate is intermediate, water levels both upstream and inside the dam body rise simultaneously and a large scale slippage can result (Takahashi and Kuang, 1988). For similar hydraulic condition peak discharge produced by failure of landslide dam depends on failure modes. Potential disaster in the downstream largely depends on magnitude of peak discharge so this study attempted to derive graphical relationship to predict failure modes by flume experiments.

Very few studies attempted to predict failure modes of landslide dam and some research was focused on prediction of behavior of landslide dam. Takahashi and Kuang (1988) described infiltration rate and strength of the dam body are the main factors which determine failure modes. Canuti et al. (1998) and Casagli and Ermini (1999) used blockage index (BI) to

determine the landslide dam either stable or unstable based on database of cases collected in Northern Apennines. Ermini and Casagli (2003) used geomorpholoigical dimensionless blockage index (DBI) to predict the behavior of landslide dam based on 84 events inventoried worldwide. Liao and Chou (2003) studied the debris flow generated by seepage failure of landslide dam and attempted to determine threshold lines of landslide dam failure for different grains (0.58mm, 1.48mm, and 7.85mm). Weidinger (2006) proposed a diagram which correlates the grain, boulder and block size of landslide material and the stability of a dam (life span of the dammed lake). The analysis of twenty case studies from India, Nepal and China shows that the greater the average diameter of the components, the longer the life of the dam and the lake.

Mechanism of landslide dam failure is different according to failure modes and peak discharge

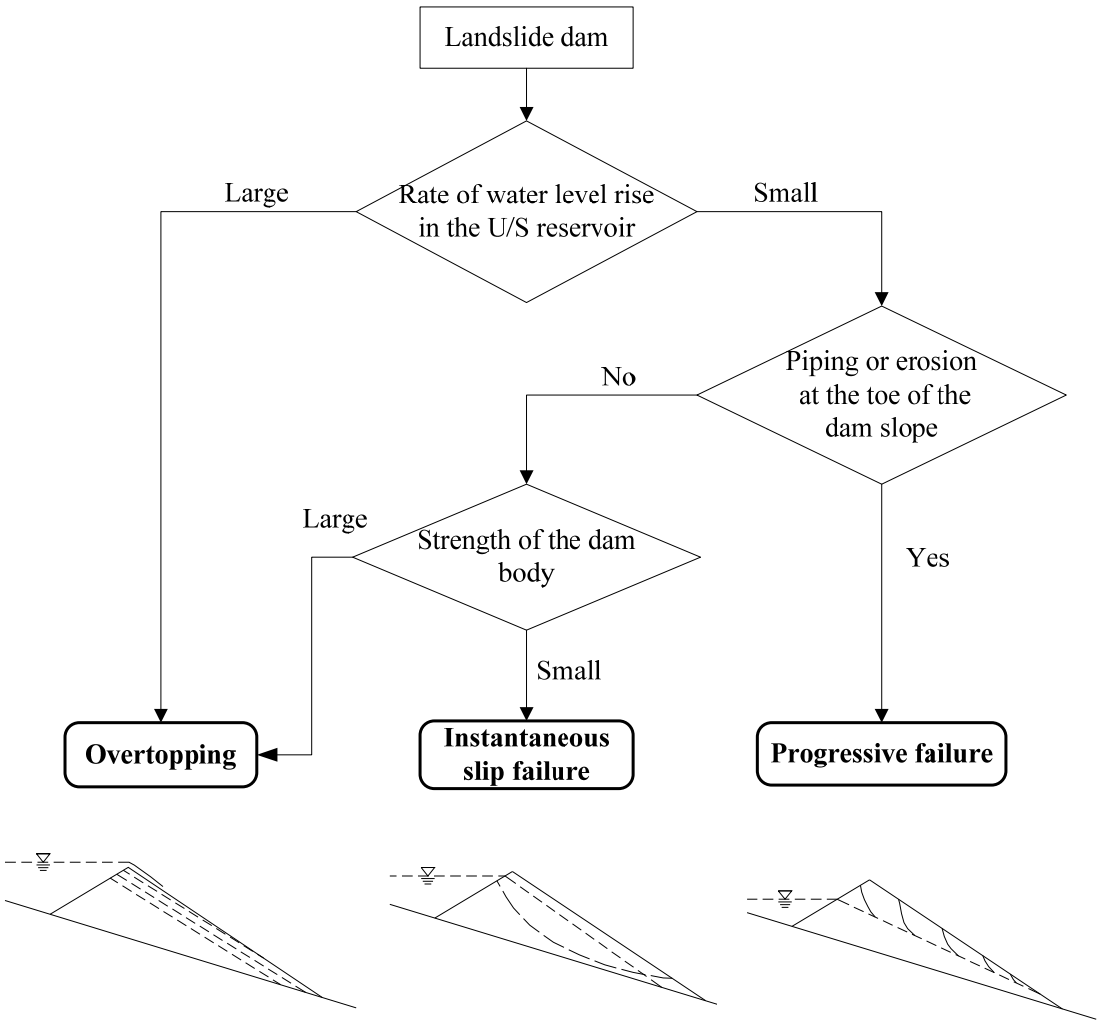

Figure 2.10 Failure modes of landslide dam (Modified from Takahashi & Kuang, 1988)

produced by landslide dam failure also depends on failure modes. Individual models (dam surface erosion by overtopping, instantaneous slip failure and progressive failure) can be easily combined if we can predict the failure mode in the beginning. Experimental data will serve for the validation of Process Based Model (model which can identify failure mode based on different initial and boundary conditions). From series of experimental studies in the laboratory flume at different angles, it becomes clear that the failure modes are highly influenced by rate of water level rise in the upstream reservoir. Based on this, the failure modes may be overtopping, instantaneous slip failure or progressive failure as shown in Figure 2.10.

2.5.2 Dimensional analysis

The rate of water level rise in the upstream reservoir depends on many factors. The level in the reservoir at any time depends on, flow condition (q_{in}), dam size (α, H), characteristics of landslide dam ($\phi, K_s, \theta_s, \theta_i, d$), reservoir volume ($\alpha$, H) and fluid properties. The upstream and downstream faces of landslide dam are slightly shallower than the angle of repose of the sand mixture in all cases of experiments. So the size of the dam body and upstream reservoir depends on height of the dam and flume slope. Landslide dam in the actual field may have some cohesive strength. However in this study sediment mix without cohesive strength was used. The measured internal friction angles (ϕ) for both sediment mixes were about 34^o, so, ϕ is taken as constant. These parameters are neglected in the set of parameters of Equation 2.1. Attempts were made to develop a relationship among the different parameters using dimensional analysis technique (Buckingham Pi theorem). Buckingham Pi theorem provides a method for computing sets of dimensionless parameters from the given variables, even if the form of the equation is still unknown. Different failure modes of landslide dam depend on rate of rise of water level in the upstream reservoir. The water level in the reservoir at any time may express as:

$$h = f(t, q_{in,} H, L, K_s, \theta_s, \theta_i, d, \alpha) \tag{2.1}$$

where, h is the water level in the reservoir, t is the time after the formation of landslide dam, q_{in} is the inflow rate per unit width, H is the height of the landslide dam, L is the length of landslide dam, K_s is the saturated hydraulic conductivity, θ_s is the saturated moisture content, θ_i is the initial moisture content, d is the mean diameter of sediment and α is the slope of flume.

Applying Buckingham Pi Theorem, above equation in dimensionless form can be expressed as

$$\frac{h}{H} = f\left(\frac{tK_s}{H}, \frac{q_{in}}{HK_s}, \frac{L}{H}, \frac{d}{H}, \theta_s, \theta_i, \alpha\right) \quad (2.2)$$

According to Equation 2.2, the main factors which govern water level in the upstream reservoir are the time period after the formation of landslide dam, unit discharge, material properties, geometry of the dam body and the flume slope. Therefore, experiments are carried out for two sediment mixes in different channel slopes, dam geometries and discharges. For particular sediment mix, if we use the same initial moisture content, d, θ_s and θ_i can be consider as constant. As already mentioned, the failure mode of landslide dam is influenced by rate of water level rise in the upstream reservoir. However, it is difficult to relate rate of water level rise with failure modes. Thus, relationship between dimensionless parameters is used to derive condition for different failure modes.

2.5.3 Laboratory experiments

The experimental setup as shown in Figure 2.1 was used. The slope of the flume could be changed from horizontal to inclination of 20 degree or more. Mixed silica sand “Mix 1-6” and “Mix 1-7” were used to prepare dam body. Triangular shaped dam was prepared on the rigid bed of the flume by placing mixed sand on the flume. The sizes of dam body for different flume slopes are shown in Table 2.2 and 2.3. The sediment placed in the flume was leveled and compacted in every thickness of approximately 5cm by using timber plate. The final shape of the dam body according to flume slope was prepared by removing extra sediment and smoothing the surface of the dam. To measure the movement of dam slope during sliding, red colored sediment strip was placed at the face of the flume wall before preparation of the dam body. The summary of experiments for sediments “Mix 1-7” and “Mix 1-6” are shown in Table 2.2 and 2.3 respectively.

2.5.4 Condition for different failure modes

The condition for different failure modes of landslide dam are experimentally studied using an inclined flume with slope varying from 13^o to 20^o. As already explained, landslide dam may fail by overtopping, abrupt sliding collapse and progressive failure. However overtopping is common in all types of failure modes although initiation may be different. Following relationships between dimensionless parameters of Equation 2.2 are derived from series of experiments (Figure 2.11 and Figure 2.12) which can be used for particular sediment mix:

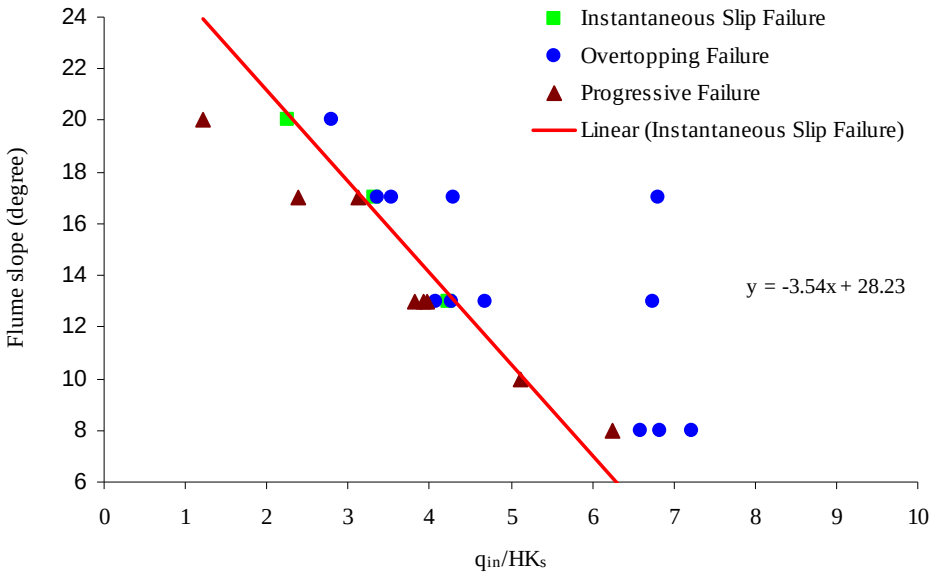

Figure 2.11 Graphical relationship to predict failure modes (Sediment Mix 1-7)

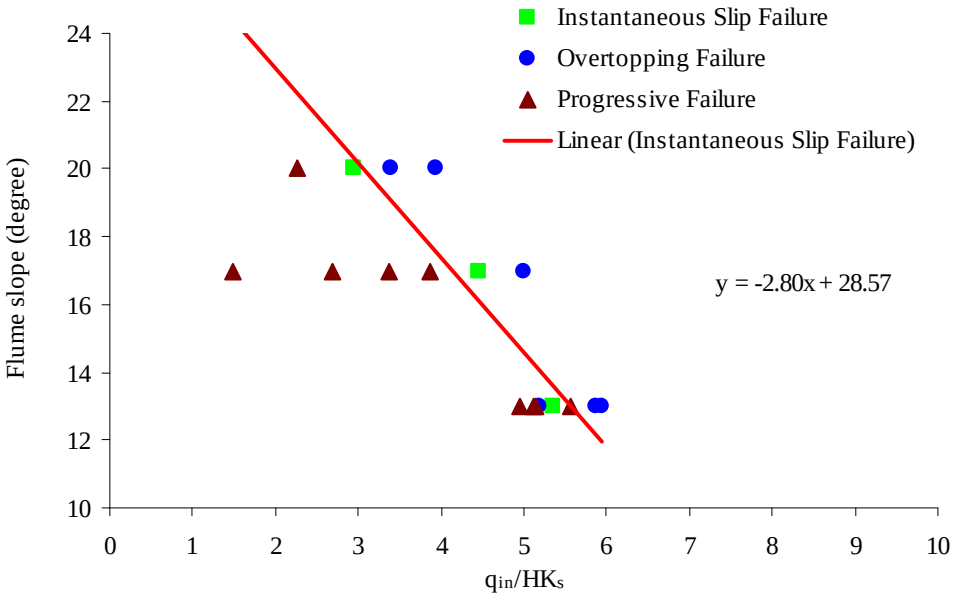

Figure 2.12 Graphical relationship to predict failure modes (Sediment Mix 1-6)

For sediment, Mix 1-7

$$\alpha_{cr} = 28.23 - 3.54\left(\frac{q_{in}}{HK_s}\right) \tag{2.3}$$

For sediment, Mix 1-6

$$\alpha_{cr} = 28.57 - 2.80\left(\frac{q_{in}}{HK_s}\right) \tag{2.4}$$

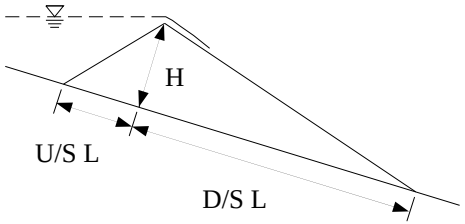

Table 2.2 Summary of Experiments (Sediment Mix: 1-7)

										Failure mode (Value represents the flume slope)			
S.No.	Expt. Ref.	Flume slope	Q (cm3/s)	H (cm)	U/S L (cm)	D/S L (cm)	L (cm)	K_s (cm/s)	q_{in}/HK_s	Instantaneous Slip Failure	Overtopping Failure	Progressive Failure	Remarks
1	B6	17	23.97	20	18	66	84	0.018	3.32917	17			Sliding and overtopping
2	B39	13	30.39	20	20	52.5	72.5	0.018	4.22083	13			Sliding
3	B53	20	16.25	20	16	82	98	0.018	2.25694	20			Sliding and overtopping
4	B4	17	30.89	20	18	66	84	0.018	4.29028		17		Overtopping making channel in the left side
5	B22	17	25.51	20	18	66	84	0.018	3.54306		17		Overtopping making channel in the right side
6	B24	17	17.19	20	18	66	84	0.018	2.38750			17	Progressive failure followed by overtopping
7	B31	13	26.43	18	18	48	66	0.018	4.07911		13		Overtopping making channel in the right side
8	B32	13	26.06	19	18	51	69	0.018	3.81065			13	Two sliding followed by overtopping
9	B33	13	29.18	19	18	51	69	0.018	4.26592		13		Overtopping making channel in the right side
10	B34	13	27.11	19	18	51	69	0.018	3.96335			13	Two sliding followed by overtopping
11	B38	13	28.20	20	20	52.5	72.5	0.018	3.91638			13	Two sliding followed by overtopping
12	B45	13	33.73	20	20	52.5	72.5	0.018	4.68433		13		Overtopping making channel in the right side
13	B47	8	44.27	18	22.5	37.5	60	0.018	6.83172		8		Small sliding in the lower part and Overtopping
14	B48	8	51.98	20	24	42	66	0.018	7.22004		8		Overtopping making channel in the two sides
15	B49	8	44.97	20	24	42	66	0.018	6.24533			8	Sliding in the lower part and Overtopping
16	B50	8	47.49	20	24	42	66	0.018	6.59583		8		Overtopping making channel in the right side
17	B51	10	36.84	20	22	46	68	0.018	5.11678			10	Seepage - progressive failure
18	B52	13	48.65	20	22	46	68	0.018	6.75694		13		Overtopping making channel in the right side
19	B58	20	20.20	20	18	82	100	0.018	2.80556		20		Overtopping making channel in right side
20	B59	20	8.81	20	18	82	100	0.018	1.22361			20	Progressive failure followed by overtopping
21	B60	17	24.26	20	18	66	84	0.018	3.36944		17		Overtopping making channel in the left side
22	B61	17	22.43	20	18	66	84	0.018	3.11528			17	Two sliding followed by overtopping
23	C	17	49.00	20	18	66	84	0.018	6.80556		17		Overtopping

Table 2.3 Summary of Experiments (Sediment Mix: 1-6)

S.No.	Expt. Ref.	Flume slope	Q (cm3/s)	H (cm)	U/S L (cm)	D/S L (cm)	L (cm)	K_s (cm/s)	q_{in}/HK_s	Failure mode (Value represents the flume slope)			Remarks
										Instantaneous Slip Failure	Overtopping Failure	Progressive Failure	
1	B28	17	57.44	20	18	66	84	0.032	4.45963	17			Sliding
2	B40	13	68.89	20	20	52.5	72.5	0.032	5.34860	13			Sliding and overtopping
3	B56	20	37.83	20	16	82	98	0.032	2.93711	20			Sliding and overtopping
4	B16	17	34.60	20	18	66	84	0.032	2.68634			17	Seepage - progressive failure
5	B19	17	19.26	20	18	66	84	0.032	1.49534			17	Seepage - progressive failure
6	B26	17	43.32	20	18	66	84	0.032	3.36335			17	Progressive failure followed by overtopping
7	B27	17	49.92	20	18	66	84	0.032	3.87578			17	Two sliding followed by overtopping
8	B29	17	64.49	20	18	66	84	0.032	5.00699		17		Overtopping making channel in the two sides
9	B35	13	72.60	19	18	51	69	0.032	5.93367		13		Overtopping making channel in the right side
10	B36	13	60.56	19	18	51	69	0.032	4.94940			13	Progressive failure followed by overtopping
11	B37	13	63.47	19	18	51	69	0.032	5.18744		13		Overtopping making channel in the right side
12	B41	13	66.35	20	20	52.5	72.5	0.032	5.15104			13	Two sliding followed by overtopping
13	B42	13	65.90	20	20	52.5	72.5	0.032	5.11644			13	Two sliding followed by overtopping
14	B43	13	71.63	20	20	52.5	72.5	0.032	5.56172			13	Two sliding followed by overtopping
15	B44	13	75.76	20	20	52.5	72.5	0.032	5.88161		13		Overtopping making channel in the right side
16	B54	20	50.71	20	18	82	100	0.032	3.93747		20		Overtopping making channel in the both sides
17	B55	20	43.71	20	18	82	100	0.032	3.39349		20		Overtopping making channel in the left side
18	B57	20	29.10	20	18	82	100	0.032	2.25939			20	Progressive failure followed by overtopping

Relationship for critical channel slope (α_{cr}) is proposed as shown in Equation 2.3 and 2.4 for sediment Mix 1-7 and Mix 1-6. Flume slope close to this angle may cause instantaneous slip failure and progressive failure will occur if the flume slope is less than critical channel slope. Overtopping will occur if the flume slope is steeper than critical channel slope. Collapse of crest at once before appearance of sliding in the downstream is considered as instantaneous slip failure. Whereas, collapse of crest after sliding partly in the down stream is taken as progressive failure, so some points are very close to line of critical channel slope.

2.5.5 Some constraints

Infiltration inside the dam body is one of the factors which affect the rate of water level rise in the upstream reservoir. In each and every experiment effort was made to follow same procedure to prepare dam body and tried to mix the sediments uniformly. However it is difficult to mix sediment uniformly and difficult to achieve same degree of compaction which affects the failure mode when channel slope for particular discharge and hydraulic conductivity is very close to the critical channel slope. The variation of hydraulic conductivity is discussed in following section.

Hydraulic conductivity:

Both saturated hydraulic conductivity and unsaturated hydraulic conductivity are related to the degree of resistance from soil particles when water flows in pores. These resistances are affected by characteristics of the permeable material as well as viscosity of water. The permeability of a soil can be estimated by the following equation (USACE, 1984):

$$K = d^2 \frac{\gamma}{\mu} \frac{e^3}{(1+e)} C_s \tag{2.5}$$

where, K is the hydraulic conductivity, d is the effective particle diameter, μ is the viscosity of water, e is the void ratio and C_s is the shape factor.

Equation 2.5 indicates that the hydraulic conductivity is inversely proportional to the viscosity of water which varies considerably with temperature. The void ratio has also substantial influence on hydraulic conductivity. From loosest to densest condition, permeability may vary 1 to 20 times. The narrower the range of particle sizes, the less the permeability is influenced by density.

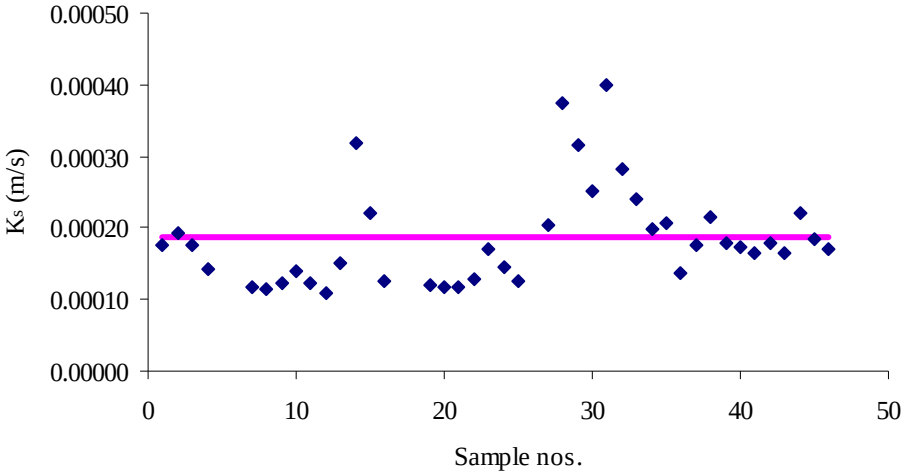

Figure 2.13 Measured saturated hydraulic conductivity (Sediment Mix 1-7)

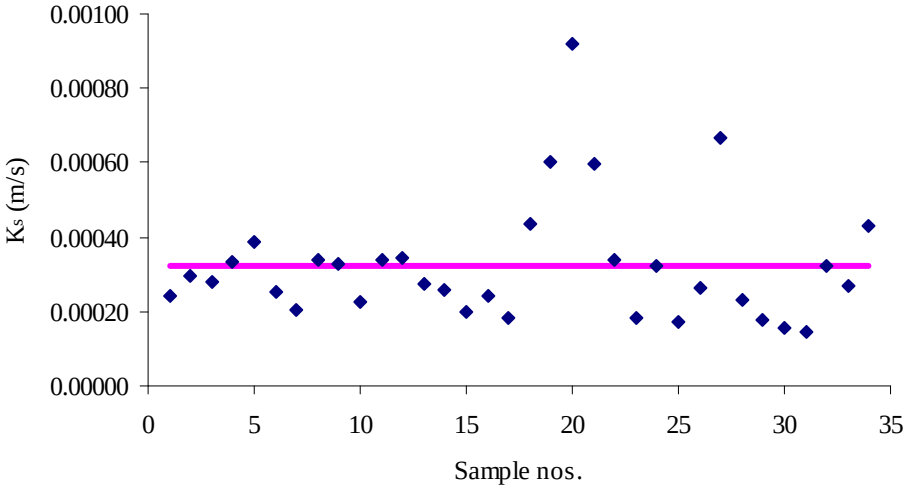

Figure 2.14 Measured saturated hydraulic conductivity (Sediment Mix 1-6)

The measured saturated hydraulic conductivity of sediment mix for different samples is not constant. The average of samples was considered in this analysis. The range of measured saturated hydraulic conductivity for both sediment mixes are shown in Figures 2.13 and 2.14.

2.5.6 Comparison of peak discharge for different failure modes

Set of flume experimental data was used to compare the peak discharge for different failure modes. From Figures 2.15, 2.16 and 2.17, it is clear that peak discharge produced by progressive failure is highest among different failure mode in all cases of channel slope. In progressive

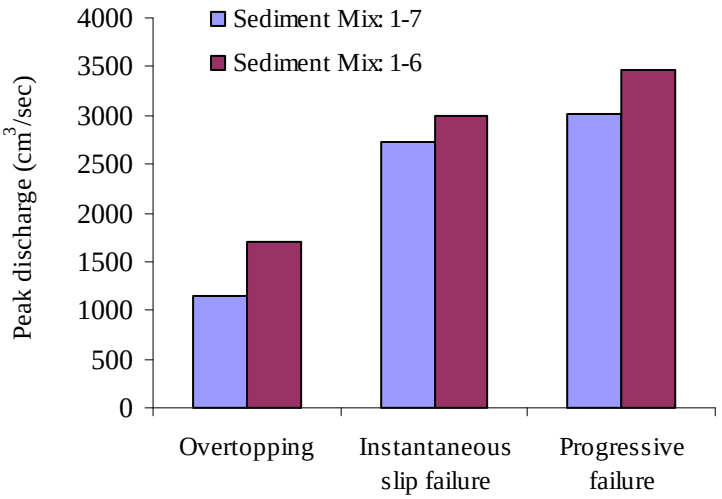

Figure 2.15 Comparison of peak discharge for different failure modes (Channel slope = 13^{o})

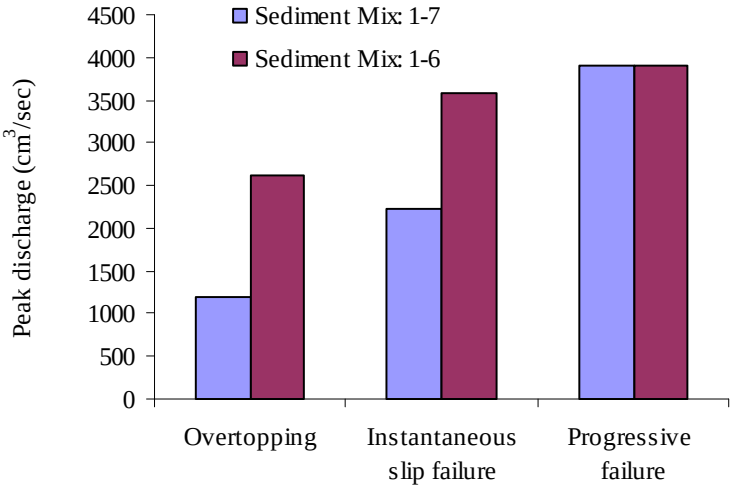

Figure 2.16 Comparison of peak discharge for different failure modes (Channel slope = 17^{o})

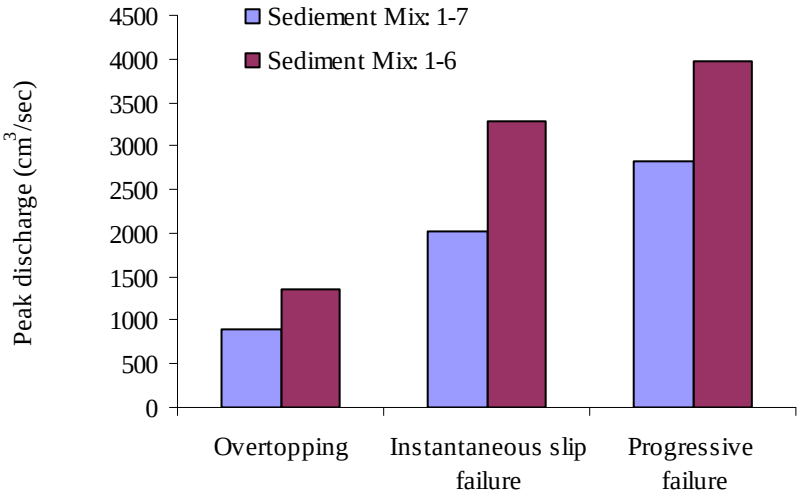

Figure 2.17 Comparison of peak discharge for different failure modes (Channel slope = 20^{o})

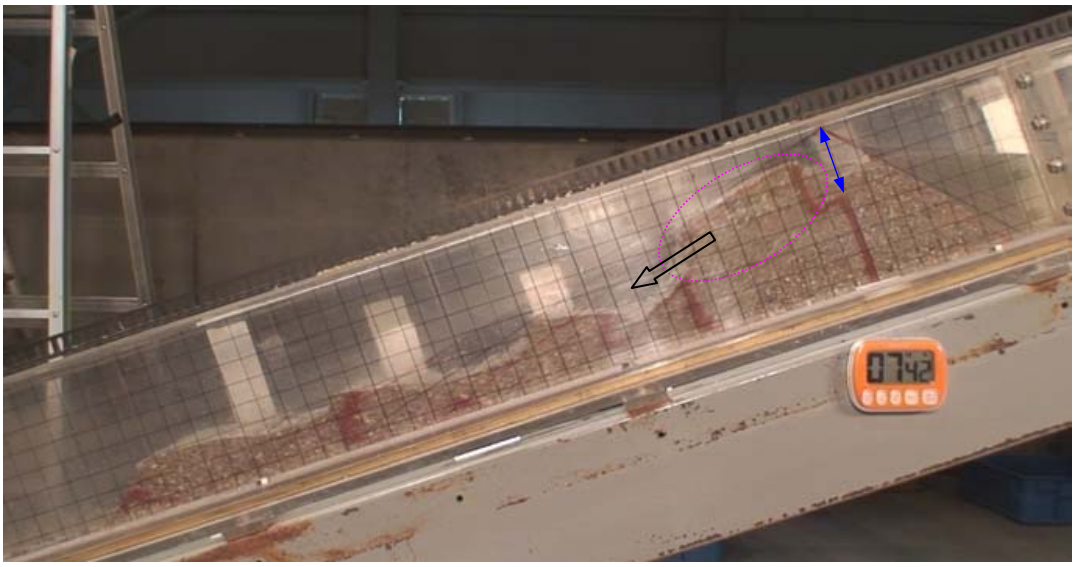

Figure 2.18 Progressive failure

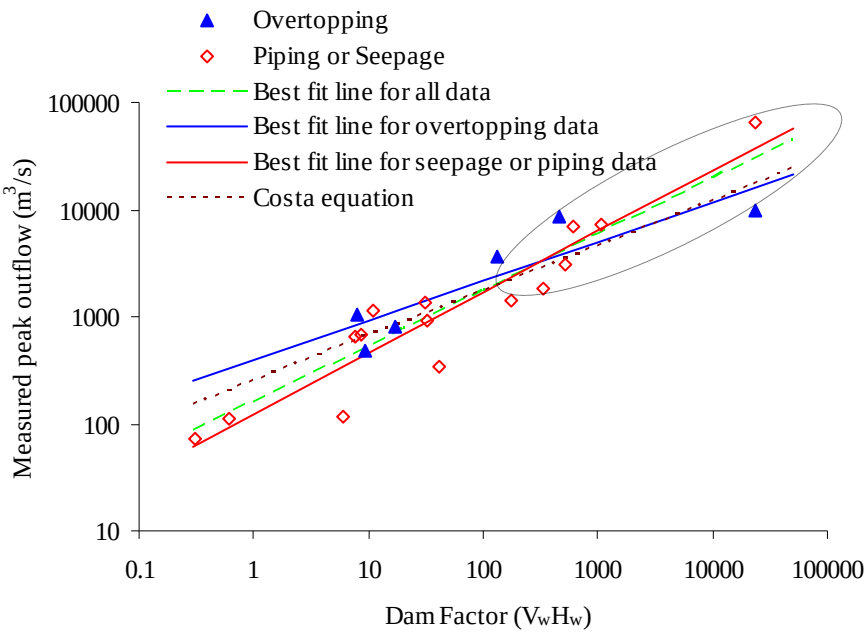

Figure 2.19 Comparison of peak discharge for different mode of failure for embankment dam (Data Compiled by: David C. Froehlich,1995)

failure, as shown in Figure 2.18, partial collapse of the dam body proceeds upward until it ends as a large failure at the moment the partial collapse reaches the location of the blocked water behind the dam. At that moment the collapsed mass moves very fast and height of collapsed mass around crest of the dam is also higher compared with instantaneous slip failure. These are

the main reasons behind higher peak discharge in the case of progressive failure compared with other failure modes. However, the peak discharge in progressive failure will be influenced by the water level in the upstream reservoir.

The data set of peak discharge for different failure modes of actual landslide dam failure are not available so the data set of embankment dam failure used by Froehlich (1995) was used to check the peak discharge for different failure modes. Figure 2.19 shows the comparison of peak discharge produced by embankment dam failure for different failure modes. Froehlich (1995) classified failure modes as overtopping, piping or seepage or foundation defects. However, Figure 2.19 just shows two failure modes i.e. overtopping and piping or seepage. From Figure 2.19 it is clear that peak discharge produced by seepage or piping is high compared with overtopping for higher dam factor. This study used small data set and peak outflow discharge for all dam failures were estimated by either slope area measurement or reservoir volume change. So the peak discharge estimated by two methods may not be consistent.

2.5.7 Results and discussions

Expression for critical slope of channel for sediment Mix 1-6 and Mix 1-7 based on number of experiments can be used to quick guess of failure mode. However numbers of assumptions are made to derive these expressions like slope of dam body, constant channel width, homogeneous and non-cohesive dam body, and uniform moisture content throughout the whole dam body close to residual moisture content. It is difficult to derive such all parameters for actual landslide dam. If we can predict failure mode in the beginning we can use individual model to predict outflow hydrograph based on predicted failure mode.

If we have huge data set for different sediment mix, it is possible to use data mining techniques like Artificial Neural Network (ANN) to determine failure mode based on number of input parameters. Alternatively, it is possible to develop physically based model by integrating different individual models like seepage flow model, slope stability model, surface overtopping erosion and channel breach so that the model itself define the failure mode based on input parameters, initial and boundary conditions.

Peak discharge is also governed by failure modes. From experimental data it is clear that peak discharge produced by progressive failure is higher compared with peak discharge produced by

instantaneous slip failure and overtopping. Data set of embankment dam failure also shows that peak discharge produced by piping or seepage is higher compared with overtopping for higher dam factor.

Summary

Brief introduction of different measuring apparatus with their basic principle and procedure of measurement are discussed. Although the shape of the actual landslide dam depends on many factors for simplicity the shape of the dam body used in this study is triangular and prepared from homogeneous sediment mix. Critical channel slope for sediments Mix 1-6 and Mix 1-7 are derived from flume experiments. However these relationships are applicable only to those sediments. Numbers of assumptions are made to derive these expressions so it is difficult to apply in the case of actual landslide dam. If we can predict failure mode in advance individual model can be used to determine outflow hydrograph based on predicted failure mode. The concept of physically based integrated model is another alternative which can detect failure mode based on initial and boundary conditions and predict outflow hydrograph based on predicted failure mode.

Set of flume experimental data was used to compare the peak discharge for different failure modes. Progressive failure produced maximum peak discharge compared with other failure modes. Based on data set of embankment dam compiled by Froehlich (1995), peak discharge produced by seepage or piping failure is higher compared with overtopping failure for higher dam factor.

Chapter 3

Seepage Flow Modeling

3.1 Introduction

Failure of landslide dam is one of the potential causes of flash flood and the study on their formation and failure mechanism has relevant importance in the perspective of flood risk assessment and management. Failure of landslide dam may occur with a variety of failure processes which includes overtopping, seepage or piping, and mass movements etc. Many of these failure processes are related to variations in pore water pressures during filling of landslide dammed reservoirs by river discharge and rainfall. The seepage flow modeling is one of the important components of an integrated model to predict outflow hydrograph. Firstly, it helps to predict the time to overflow the landslide dammed reservoir and secondly, it will help to predict stability of the dam body. Proper quantification of various processes such as infiltration, evaporation, river flow etc has to be modeled as accurately as possible. Such process can be modeled through a conceptual frame work and mathematical tools, which can be used to represent the processes and solve the problems.

The main objective of the development of seepage flow model is to develop and validate a computationally simple two-dimensional and three-dimensional variably saturated flow model to investigate movement of moisture inside landslide dam so that it can easily be integrated with slope stability model for transient slope stability analysis of landslide dam. The literature of variably saturated flow modeling is very vast however the following section covers two-dimensional model with various boundary conditions and solution technique to solve the governing equation and brief introduction of extended three-dimensional seepage flow model.

3.2 Two-dimensional seepage flow modeling

3.2.1 Governing equations

The seepage flow in the dam body is caused by the blocked water stage behind the dam. The transient flow in the dam body after formation of landslide dam can be analyzed by Richards'

equation (1931). To evaluate the change in pore water pressure in variably saturated soil, pressure based Richards' equation is used (Sharma et al., 2005; Awal et al, 2007).

$$C\frac{\partial h}{\partial t}=\frac{\partial}{\partial x}\left(K_x(h)\frac{\partial h}{\partial x}\right)+\frac{\partial}{\partial z}\left(K_z(h)\left(\frac{\partial h}{\partial z}+1\right)\right) \tag{3.1}$$

where h is the water pressure head, $K_x(h)$ and $K_z(h)$ are the hydraulic conductivity in x and z direction, C is the specific moisture capacity $(\partial\theta/\partial h)$, θ is the soil volumetric water content, t is the time, x is the horizontal spatial coordinate and z is the vertical spatial coordinate taken as positive upwards.

Equation 3.1 represents flow in both the unsaturated domain as well as in the saturated domain. The unsaturated flow involves a two-phase flow of air and water, however only the flow of the water has been considered, where the air phase is continuous and is at atmospheric pressure, and it does not affect the dynamics of the water phase. Richards' equation is a non-linear parabolic partial differential equation in the unsaturated zone and elliptic in the saturated zone. Line-successive over-relaxation (LSOR) is often a very effective method of treating cross-sectional problem grids. LSOR scheme is used in this study for the numerical solution of Richards' equation.

3.2.2 Soil Constitutive Relationships (*K-h-θ*)

Richards' equation is nonlinear in nature, since the flow and storage properties are functions of the dependent variable. In order to solve Richards' equation, the constitutive equations, which relate the pressure head to the moisture content and the relative hydraulic conductivity, are required. Many empirical relationships have been developed in the past based on field experiments for soil moisture constitutive relationships and are reported in the literature. The most popular being Brookes and Corey (1964), Campbell (1974), Haverkamp (1977), van Genuchten (1980), Kosugi (1994) and Assouline et al. (1998) relationships. In this study, following constitutive relationships proposed by van Genuchten (1980) are used for establishing relationship of $\theta-h$ and $K-\theta$, with $m=1-(1/\eta)$.

$\theta - h$ Relationship

The water retention characteristic ($\theta - h$ relationship) of the soil describes the soil ability to store and release water. This relationship is called soil moisture characteristic curve. The shape of the curve depends upon the pore size distribution of the soil.

$$S_e = \frac{\theta - \theta_r}{\theta_s - \theta_r} \tag{3.2}$$

$$S_e = \begin{cases} \dfrac{1}{\left(1 + |\alpha h|^{\eta}\right)^m} & \text{for } h < 0 \\ 1 & \text{for } h \geq 0 \end{cases} \tag{3.3}$$

where, α and η are parameters related with matric potential of soil and are measure of capillary fringe thickness and pore size distribution of soil respectively, S_e is the effective saturation, θ_s and θ_r are saturated and residual moisture content respectively.

$K - \theta$ Relationship

The unsaturated hydraulic conductivity, K is a nonlinear function of the moisture content, θ and it can be expressed as a power function of the effective saturation.

$$K = \begin{cases} K_s S_e^{0.5}\left[1 - (1 - S_e^{1/m})^m\right]^2 & \text{for } h < 0 \\ K_s & \text{for } h \geq 0 \end{cases} \tag{3.4}$$

where, K_s is the saturated hydraulic conductivity.

3.2.3 Initial and boundary conditions

Governing Equation 3.1 needs initial and boundary conditions to get a solution. The values of pressure head or moisture content throughout the domain are specified as initial conditions. To get a unique solution for a given initial condition, two dimensional model (in a vertical cross section) needs boundary values on four sides (Figure 3.1). As a boundary condition two different types of conditions can be defined, (i) Drichlet condition, value of the dependent variable is specified, (ii) Neuman condition, flux at the bottom boundary is specified. The process such as infiltration due to rainfall or river flow, evaporation which occur at the dam

body constitute the upper, left and right boundary conditions for unsaturated flow. However, rainfall and evaporation effect are not included in the present model. Bottom boundary condition is used as no-flow boundary. Upper, left and right boundary may be no flow boundaries or head boundary based on water level in the upstream reservoir. A seepage face is an external boundary of the saturated zone, where water leaves the soil and pressure head is uniformly zero (atmospheric pressure). The height of the seepage face is not known a priori and is determined iteratively.

3.2.4 Solution methods

There are many available methods of numerical solution, however in this study; line-successive over-relaxation (LSOR) scheme used by Freeze (1971, 1976) is used. Equation 3.1 is solved by the implicit iterative finite difference scheme, using the over-relaxation technique.

The numerical grid is block centered nodal grid in the *x-z* plan as shown in Figure 3.1 with a block size (Δx, Δz). In the x-direction the nodes are labeled i = 1, 2,…N and in the z-direction they are labeled j = 1, 2,…M. The value of pressure head at (x_i, y_i) and t is denoted by h_{ij}^t. The finite difference form of Equation 3.1 used in the mode1 is

$$\frac{1}{\Delta x}\left[K(h_I)\left(\frac{h_{i+1,j}^t + h_{i+1,j}^{t-1} - h_{i,j}^t - h_{i,j}^{t-1}}{2\Delta x}\right) - K(h_{II})\left(\frac{h_{i,j}^t + h_{i,j}^{t-1} - h_{i-1,j}^t - h_{i-1,j}^{t-1}}{2\Delta x}\right)\right] +$$
$$\frac{1}{\Delta z}\left[K(h_{III})\left(\frac{h_{i,j+1}^t + h_{i,j+1}^{t-1} - h_{i,j}^t - h_{i,j}^{t-1}}{2\Delta z} + 1\right) - K(h_{IV})\left(\frac{h_{i,j}^t + h_{i,j}^{t-1} - h_{i,j-1}^t - h_{i,j-1}^{t-1}}{2\Delta z} + 1\right)\right]$$
$$= C(h_V)\left(\frac{h_{i,j}^t - h_{i,j}^{t-1}}{\Delta t}\right) \qquad (3.5)$$

For vertical LSOR, the term can be grouped as

$$-A_j h_{i,j+1}^t + B_j h_{i,j}^t - C_j h_{i,j-1}^t = D_j \qquad (3.6)$$

where, A_j, B_j, C_j and D_j are developed from the groupings of the coefficients of Equation 3.5 as bellows:

$$A_j = \frac{K(h_{III})}{2\Delta z^2} \qquad (3.7)$$

$$B_j = \frac{C(h_V)}{\Delta t} + \frac{K(h_I)}{2\Delta x^2} + \frac{K(h_{II})}{2\Delta x^2} + \frac{K(h_{III})}{2\Delta z^2} + \frac{K(h_{IV})}{2\Delta z^2} \tag{3.8}$$

$$C_j = \frac{K(h_{IV})}{2\Delta z^2} \tag{3.9}$$

$$D_j = \frac{C(h_V)}{\Delta t} h_{i,j}^{t-1} + K(h_I)\left(\frac{h_{i+1,j}^{t} + h_{i+1,j}^{t-1} - h_{i,j}^{t-1}}{2\Delta x^2}\right) - K(h_{II})\left(\frac{h_{i,j}^{t-1} - h_{i-1,j}^{t} - h_{i-1,j}^{t-1}}{2\Delta x^2}\right)$$
$$+ K(h_{III})\left(\frac{h_{i,j+1}^{t-1} - h_{i,j}^{t-1}}{2\Delta z^2} + \frac{1}{\Delta z}\right) - K(h_{IV})\left(\frac{h_{i,j}^{t-1} - h_{i,j-1}^{t-1}}{2\Delta z^2} + \frac{1}{\Delta z}\right) \tag{3.10}$$

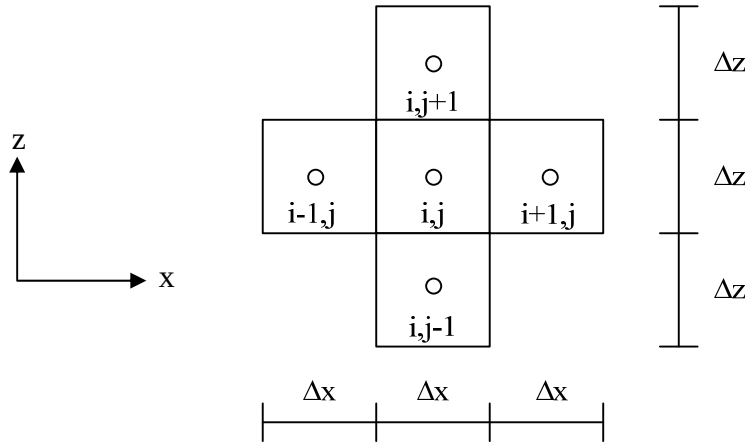

Figure 3.1 Grid scheme

The set of Equations 3.6 for a line scan, form a tri-diagonal matrix equation that can be solved by the well-known triangularization scheme embodied in the following recurrence relation.

$$\left.\begin{aligned} h_{ij}^{t} &= E_j h_{i,j+1}^{t} + F_j \quad \text{for } j < M \\ h_{ij}^{t} &= F_j \quad \text{for } j = M \end{aligned}\right\} \tag{3.11}$$

where,

$$E_j = \frac{A_j}{B_j - C_j E_{j-1}} \quad \text{for } j > 1; \qquad E_1 = \frac{A_1}{B_1} \tag{3.12}$$

$$F_j = \frac{D_j + C_j F_{j-1}}{B_j - C_j E_{j-1}} \quad \text{for } j > 1; \qquad F_1 = \frac{D_1}{B_1} \tag{3.13}$$

The E and F coefficients are calculated from j = 1 to j = M using Equations 3.12 and 3.13 and

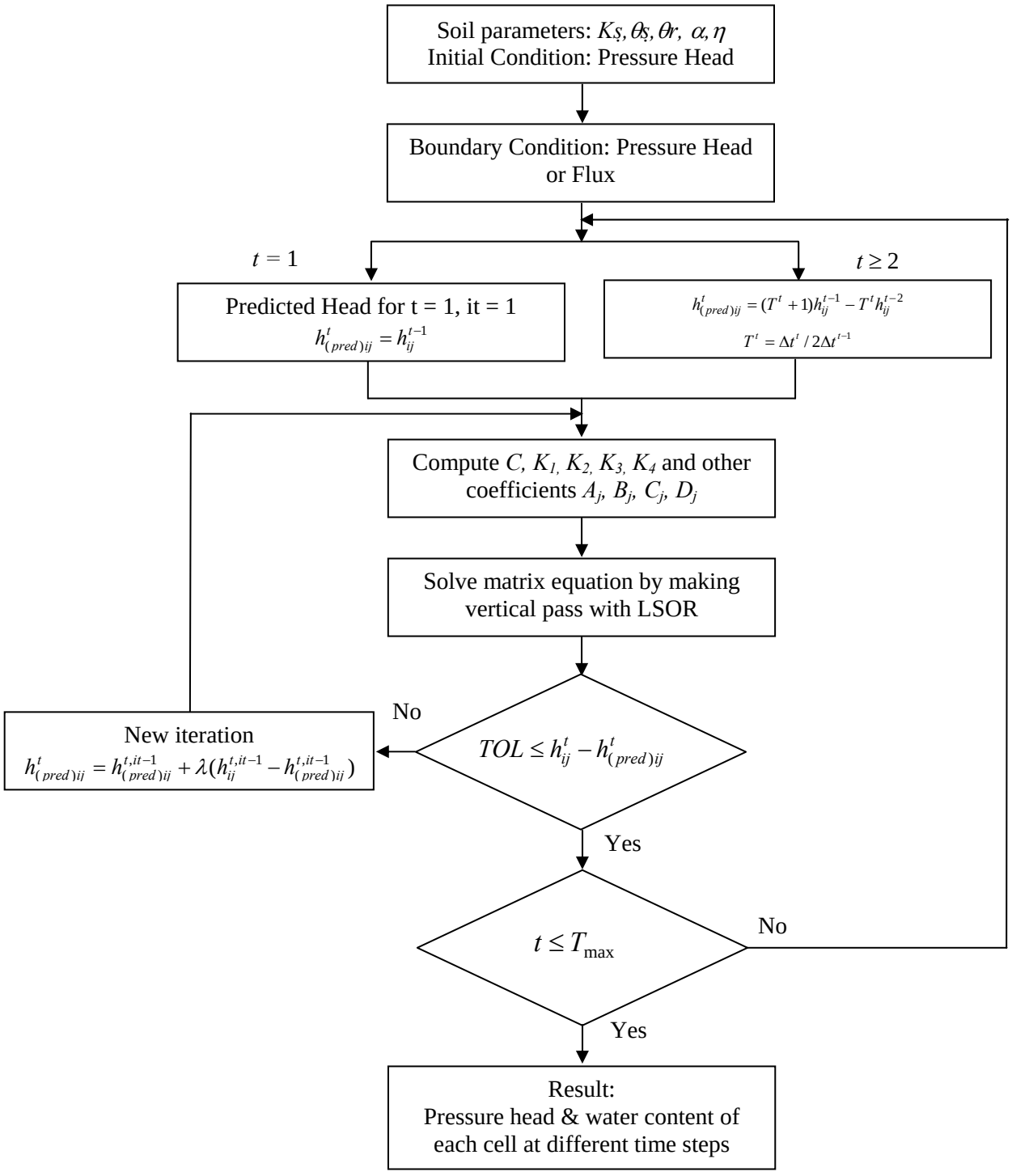

Figure 3.2 Flow chart of seepage flow model

the h_{ij}^{t} s are back calculated from j = M to j = 1 using Equation 3.11. The flowchart of seepage flow model is shown in Figure 3.2. At each iteration, it is necessary to predict a pressure head value $h_{(pred)ij}$ at each node from which the current estimates of K and C can be calculated. For the first iteration of the first time step:

$$h_{(pred)ij}^{t} = h_{ij}^{t-1} \tag{3.14}$$

For the first iteration of later time step:

$$h_{(pred)ij}^{t} = (T^{t} + 1)h_{ij}^{t-1} - T^{t} h_{ij}^{t-2} \tag{3.15}$$

where,

$$T^{t} = \Delta t^{t} / 2\Delta t^{t-1} \quad , \quad T^{t} = \frac{1}{2} \text{ for } \Delta t^{t} = \Delta t^{t-1} \tag{3.16}$$

For later iterations of all time steps:

$$h_{(pred)ij}^{t} = h_{(pred)ij}^{t,it-1} + \lambda(h_{ij}^{t,it-1} - h_{(pred)ij}^{t,it-1}), \qquad 0 \le \lambda \le 1 \tag{3.17}$$

The value of h_I in Equation 3.5 is the predicted value of h at the boundary between two nodal blocks and h_I is determined by

$$h_I = \frac{1}{2}\left(h_{(pred)ij} + h_{(pred)i+1,j}\right) \tag{3.18}$$

The value of h_{II}, h_{III} and h_{IV} are determined analogously and h_V is equal to $h_{(pred)ij}$.

The iterations are repeated until the given tolerance is achieved. Although the implicit scheme is unconditionally stable, some difficulties due to the strong nonlinearity of the Richards' equation may occur. Which can be overcome by the adaptable time step, however in this model very small time step is used. At the boundary node, Equation 3.5 is modified to reflect time-dependent boundary conditions. Water level in the upstream reservoir in each time step is determined by water-volume balance equation considering inflow discharge, rate of infiltration inside the dam body and flume geometry (width and slope).

3.2.5 Verification of model with experiments

Laboratory experiments

The rectangular flume shown in Figure 2.1 was used. The slope of the flume was set at 17^o. The shape and size of dam body is shown in Figure 3.3. Mixed Silica sand (Mix 1-7) was used to prepare dam body. The grain size distribution of sediment mixture is shown in Figure 2.9. van Genuchten parameters (including θ_r) were estimated by non-linear regression analysis of soil moisture retention data obtained by pF meter experiment. The hysteresis effect is not considered in these parameters. Some other parameters of mixed sand are listed in Table 2.1. Measured saturated hydraulic conductivity was 0.0004m/sec.

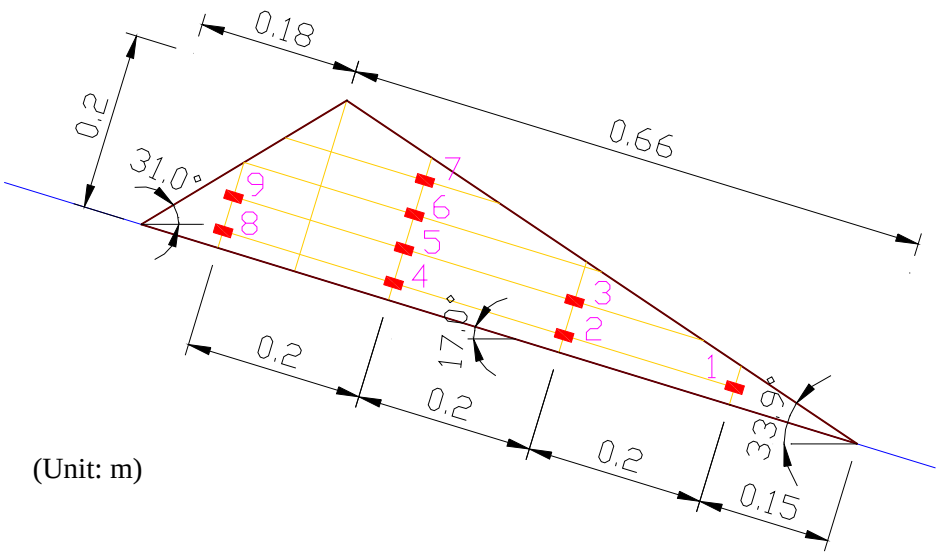

Figure 3.3 Shape and size of the dam body

Two cases of experiments are considered. Water level of reservoir was kept constant in Case I; where as steady discharge was supplied in Case II. For both cases, water content reflectometers (WCRs) were used to measure the temporal variation of moisture content during seepage process. Nine WCRs were inserted inside the dam body from a sidewall of the flume. The arrangements of WCRs are shown in Figure 3.4. The data acquisition interval for WCRs was 1 sec. The probe rods disturb the sliding of the dam body so water content was measured in separate experiment under same experimental conditions that used in experiment of slope stability.

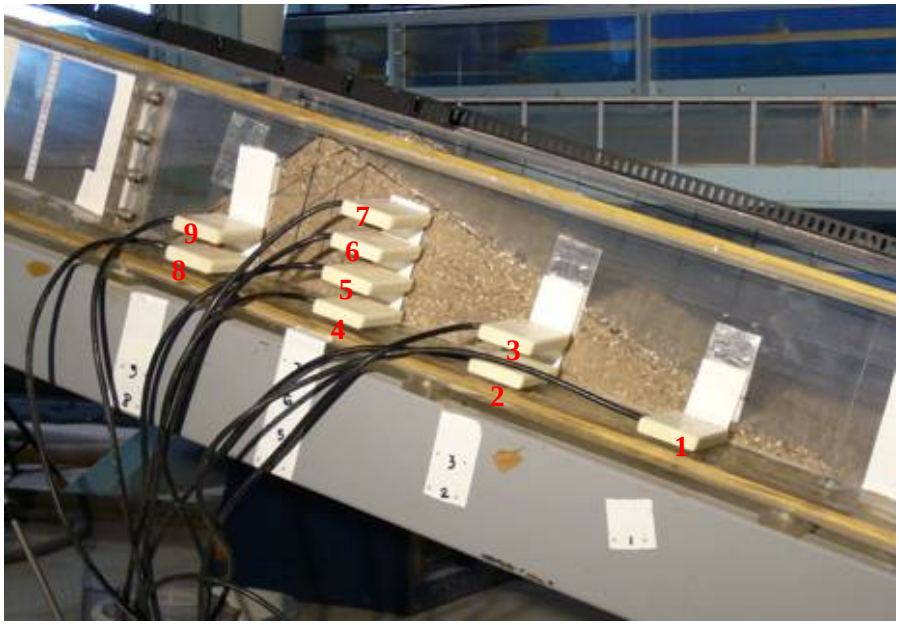

Figure 3.4 Arrangement of WCRs (1-9)

All the WCRs were calibrated prior to the experiment. The relationship between volumetric water content and output period of WCR was represented by different linear equation for different WCR.

Results and discussions

In seepage flow analysis, the boundaries of the dam body are not parallel to space coordinates as shown in Figure 3.5. The rectangular finite-difference grid is used to approximate the geometry of the dam body in a step-wise manner, resulting in some part of cells outside of the dam body.

In order to simulate boundary conditions, cells are grouped as inactive (or no flow) cells, variable-head cells and known-head or no flow cell based on the water level in the upstream reservoir. Inactive cells do not allow flow into or out of the cell. The finite difference Equation 3.1 is formulated for each variable-head cell in the mesh. The system of finite difference equations is solved by LSOR scheme for each time step in the simulation. The cell size shown in Figure 3 is 10mm x 10mm however finer cell size of 2mm x 2mm is used in the simulations.

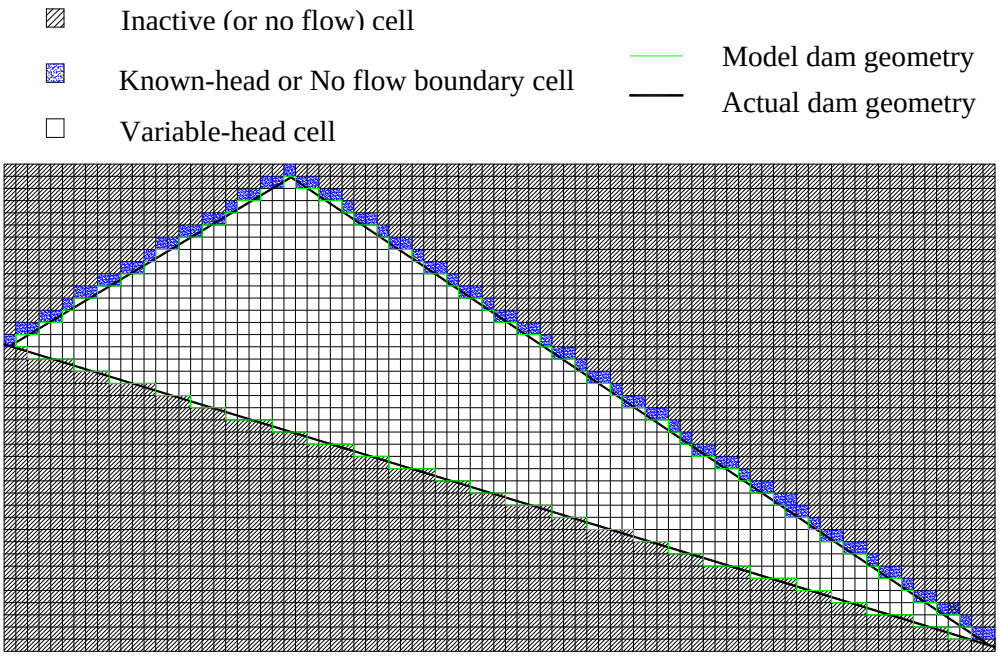

Figure 3.5 Discretized dam body and cell designations (For cell size of 10mm x 10mm)

Following two cases are considered for the validation of seepage flow model:

Case I: Constant water level in the upstream reservoir

The reservoir in the upstream of the dam was filled by water up to16mm below crest level of the dam in 25 seconds. Simulated and experimental results of variation of moisture content at WCR-4 through WCR-9 are shown in Figure 3.6. The results of numerical simulation of moisture profile in the dam body are in good agreement with the experimental results. However the result might have been influenced due to assumption of immobile air phase in unsaturated flow and variation of saturated hydraulic conductivity since it was difficult to make sand mixture perfectly homogeneous and uniform compaction.

Case II: Steady discharge in the upstream reservoir

Steady discharge of 39.8cm^3/sec was supplied from the upstream end of the flume. Moisture content in the dam body was measured using WCRs. Figure 3.7 shows the simulated and experimental results of moisture profile at WCR-4 through WCR-9 which are quite close.

The numerical simulation and experimental results of moisture profile are in good agreement for both cases.

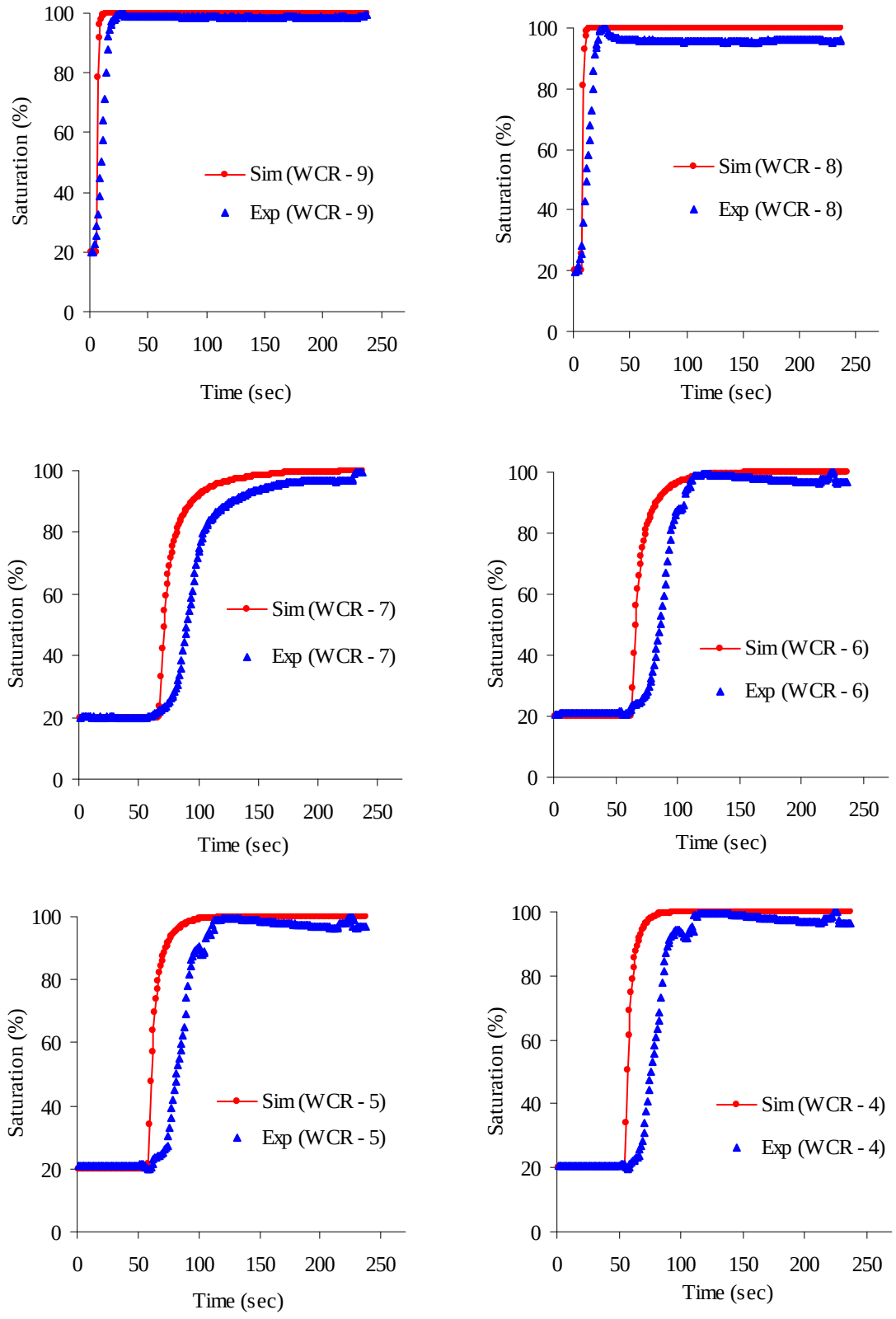

Figure 3.6 Simulated and experimental results of water content profile for constant water level in the upstream reservoir (WCR – 9,8,7,6,5 and 4)

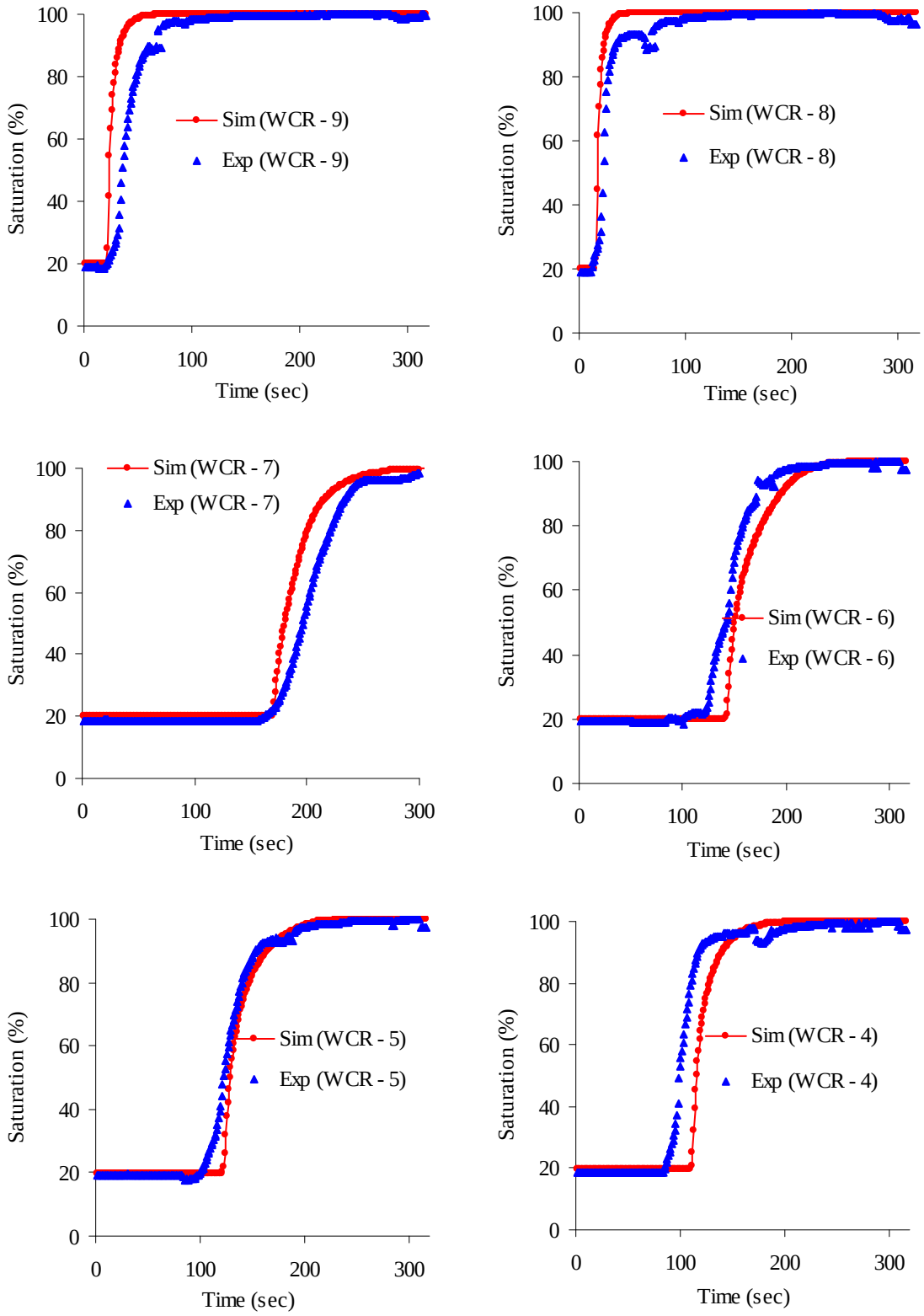

Figure 3.7 Simulated and experimental results of water content profile for steady discharge in the upstream reservoir (WCR – 9,8,7,6,5 and 4)

3.3 Three-dimensional seepage flow modeling

Seepage flows through landslide dam formed in narrow valleys are likely to have three-dimensional effects, so the two-dimensional simplifications may not be consistent with field conditions. To consider three-dimensional water infiltration into originally unsaturated landslide dam, 3D seepage flow model is developed by incorporating 3D Richards' equation.

3.3.1 Governing equation and solution method

The three-dimensional movement of blocked water of constant density through porous landslide dam can be described by the partial-differential equation (Freeze, 1971):

$$\frac{\partial}{\partial x}\left(K_x(h)\frac{\partial h}{\partial x}\right)+\frac{\partial}{\partial y}\left(K_y(h)\frac{\partial h}{\partial y}\right)+\frac{\partial}{\partial z}\left(K_z(h)\left(\frac{\partial h}{\partial z}+1\right)\right)=C\frac{\partial h}{\partial t} \tag{3.19}$$

where h is the water pressure head, $K_x(h)$, $K_y(h)$ and $K_z(h)$ are the hydraulic conductivity in x, y and z directions, C is the specific moisture capacity $(\partial\theta/\partial h)$, θ is the soil volumetric water content, t is the time, x and y are the horizontal spatial coordinates and z is the vertical spatial coordinate taken as positive upwards.

The Equation 3.19 is the extended form of two-dimensional Equation 3.1 with additional terms in y direction. The solution of $h=h(x,y,z,t)$ describes the sequential and spatial variations in the pressure head field. The location of the $h=0$ isobar delineates the water table position. In the regions with $h<0$, conditions are unsaturated.

Figure 3.8 shows the block size of $(\Delta x,\Delta y,\Delta z)$ and indicies for the six adjacent cells surrounding cell *i,j,k*. Equation 3.20 is the finite difference form of Equation 3.19 with additional terms in y direction. The coefficients of Equation 3.21, A_j, B_j, C_j and D_j with additional terms are given by Equations 3.22 , 3.23, 3.24 and 3.25 respectively. The set of Equations 3.21 for a line scan, forms a tri-diagonal matrix equation that can be solved by triangularization scheme whose solution is similar to Equation 3.6 and has already been discussed in two-dimensional seepage flow model.

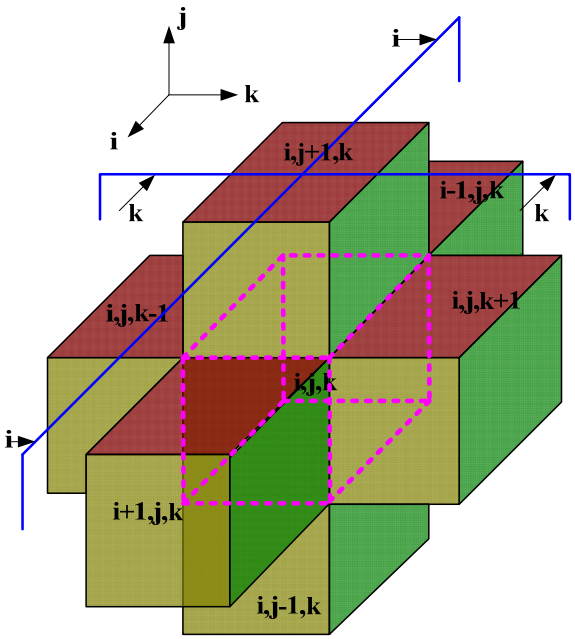

Figure 3.8 Indices for the six adjacent cells surrounding cell i,j,k (contd.)

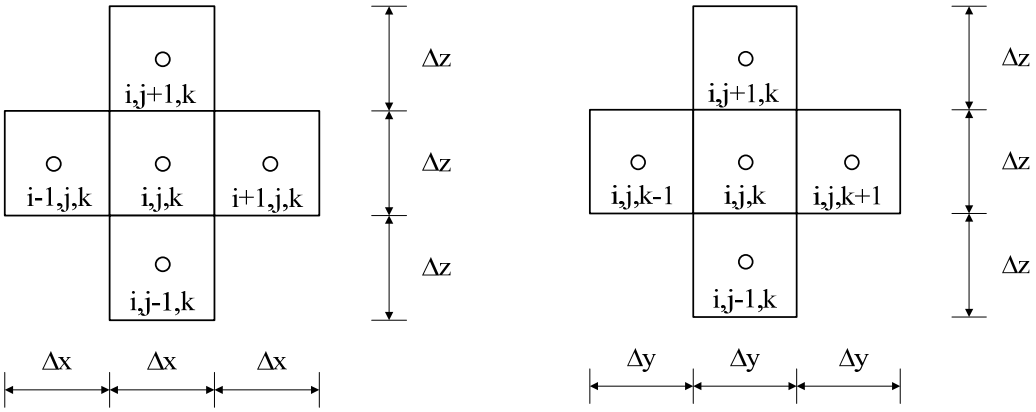

Figure 3.8 Indices for the six adjacent cells surrounding cell i,j,k

$$\frac{1}{\Delta x}\left[K(h_I)\left(\frac{h^t_{i+1,j,k}+h^{t-1}_{i+1,j,k}-h^t_{i,j,k}-h^{t-1}_{i,j,k}}{2\Delta x}\right)-K(h_{II})\left(\frac{h^t_{i,j,k}+h^{t-1}_{i,j,k}-h^t_{i-1,j,k}-h^{t-1}_{i-1,j,k}}{2\Delta x}\right)\right]+$$

$$\frac{1}{\Delta y}\left[K(h_V)\left(\frac{h^t_{i,j,k+1}+h^{t-1}_{i,j,k+1}-h^t_{i,j,k}-h^{t-1}_{i,j,k}}{2\Delta y}\right)-K(h_{VI})\left(\frac{h^t_{i,j,k}+h^{t-1}_{i,j,k}-h^t_{i,j,k-1}-h^{t-1}_{i,j,k-1}}{2\Delta y}\right)\right]+$$

$$\frac{1}{\Delta z}\left[K(h_{III})\left(\frac{h^t_{i,j+1,k}+h^{t-1}_{i,j+1,k}-h^t_{i,j,k}-h^{t-1}_{i,j,k}}{2\Delta z}+1\right)-K(h_{IV})\left(\frac{h^t_{i,j,k}+h^{t-1}_{i,j,k}-h^t_{i,j-1,k}-h^{t-1}_{i,j-1,k}}{2\Delta z}+1\right)\right]$$

$$=C(h_{VII})\left(\frac{h^t_{i,j,k}-h^{t-1}_{i,j,k}}{\Delta t}\right) \qquad (3.20)$$

For vertical LSOR, the term can be grouped as

$$-A_j h^t_{i,j+1,k} + B_j h^t_{i,j,k} - C_j h^t_{i,j-1,k} = D_j \tag{3.21}$$

where,

$$A_j = \frac{K(h_{III})}{2\Delta z^2} \tag{3.22}$$

$$B_j = \frac{C(h_{VII})}{\Delta t} + \frac{K(h_I)}{2\Delta x^2} + \frac{K(h_{II})}{2\Delta x^2} + \frac{K(h_{III})}{2\Delta z^2} + \frac{K(h_{IV})}{2\Delta z^2} + \frac{K(h_V)}{2\Delta y^2} + \frac{K(h_{VI})}{2\Delta y^2} \tag{3.23}$$

$$C_j = \frac{K(h_{IV})}{2\Delta z^2} \tag{3.24}$$

$$D_j = \frac{C(h_{VII})}{\Delta t} h^{t-1}_{i,j,k} + K(h_I)\left(\frac{h^t_{i+1,j,k} + h^{t-1}_{i+1,j,k} - h^{t-1}_{i,j,k}}{2\Delta x^2}\right) - K(h_{II})\left(\frac{h^{t-1}_{i,j,k} - h^t_{i-1,j,k} - h^{t-1}_{i-1,j,k}}{2\Delta x^2}\right)$$

$$+ K(h_{III})\left(\frac{h^{t-1}_{i,j+1,k} - h^{t-1}_{i,j,k}}{2\Delta z^2} + \frac{1}{\Delta z}\right) - K(h_{IV})\left(\frac{h^{t-1}_{i,j,k} - h^{t-1}_{i,j-1,k}}{2\Delta z^2} + \frac{1}{\Delta z}\right)$$

$$+ K(h_V)\left(\frac{h^t_{i,j,k+1} + h^{t-1}_{i,j,k+1} - h^{t-1}_{i,j,k}}{2\Delta y^2}\right) - K(h_{VI})\left(\frac{h^{t-1}_{i,j,k} - h^t_{i-1,j,k-1} - h^{t-1}_{i-1,j,k-1}}{2\Delta y^2}\right) \tag{3.25}$$

3.3.2 Verification of model with experiments

Laboratory experiments

The flume of 500cm long, 30cm wide and 50cm high (Figure 3.9) was used. The rectangular shape of the flume was modified to make cross slope of 20^o. The slope of the flume was set at 20^o. The shape and size of the dam body is shown in Figure 3.10 and 3.11. The height of the dam is 30cm in side A and decrease uniformly towards side B to 19.08cm. Mixed Silica sand (Mix 1-7) was used to prepare dam body. The grain size distribution of sediment mix is shown in Figure 2.9 and some parameters are listed in Table 2.1. Measured saturated hydraulic conductivity was 0.0003m/sec.

Water content reflectometers (WCRs) were used to measure the temporal variation of moisture content during seepage process. The arrangements of WCRs are shown in Figure 3.11. The holes were prepared in the side B of the flume and twelve WCRs were inserted inside the dam body from that side. Two set of experiments were carried out to measure moisture profile at different location of the dam body. The discharge used in 'Experiment A' was 29.8cm^3/sec and 'Experiment B' was 30.5cm^3/sec.

Figure 3.9 Photo of the flume

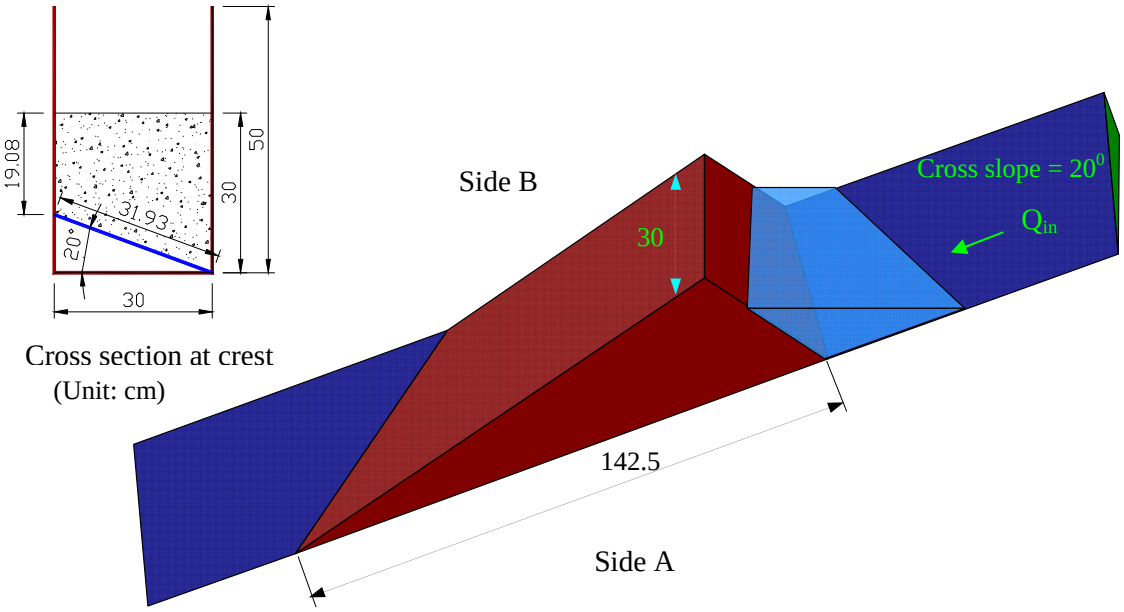

Figure 3.10 Shape of the dam body and cross section at the crest

Results and discussions

Steady discharge was supplied from the upstream of the flume. Moisture content in the dam body was measured by using WCRs. The measured moisture content is the average of 18cm length from the side of the flume (Figure 3.11). The moisture along WCR may not be constant due to three dimensional effect of water movement inside the dam body. The comparison of measured moisture profile for ‘Experiment A’ and ‘Experiment B’ are shown in Figure 3.12.

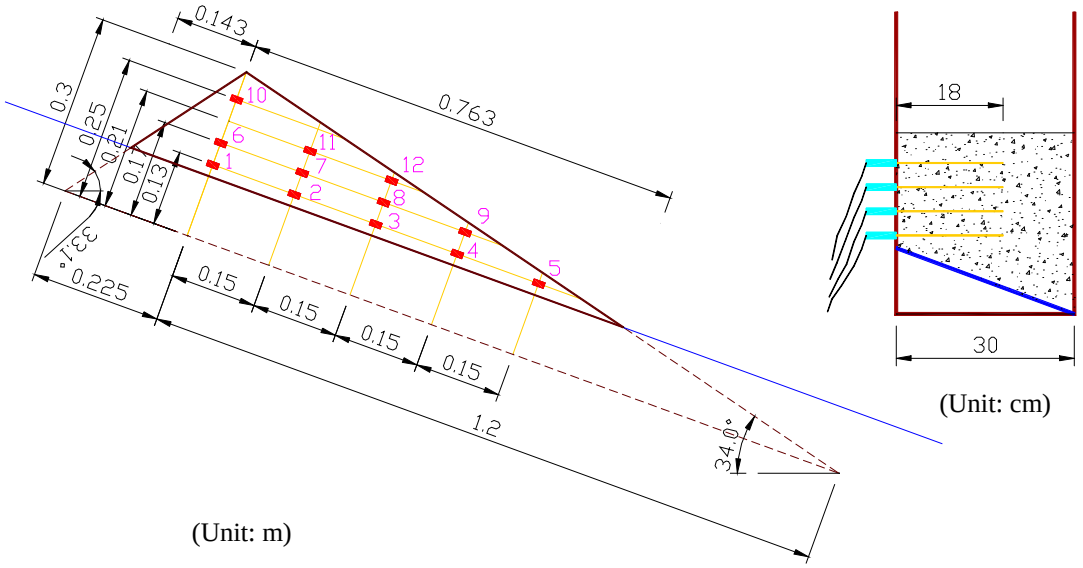

Figure 3.11 Arrangement of WCRs (1-12), view from Side B

Although discharges used in both experiments are nearly equal, the variation of moisture profile for different WCRs is slightly different. This may be due to variation of hydraulic conductivity in two experiments.

Figures 3.13 and 3.14 show the comparison of simulated and measured moisture profile at different WCRs. The results are in good agreement for all WCRs.

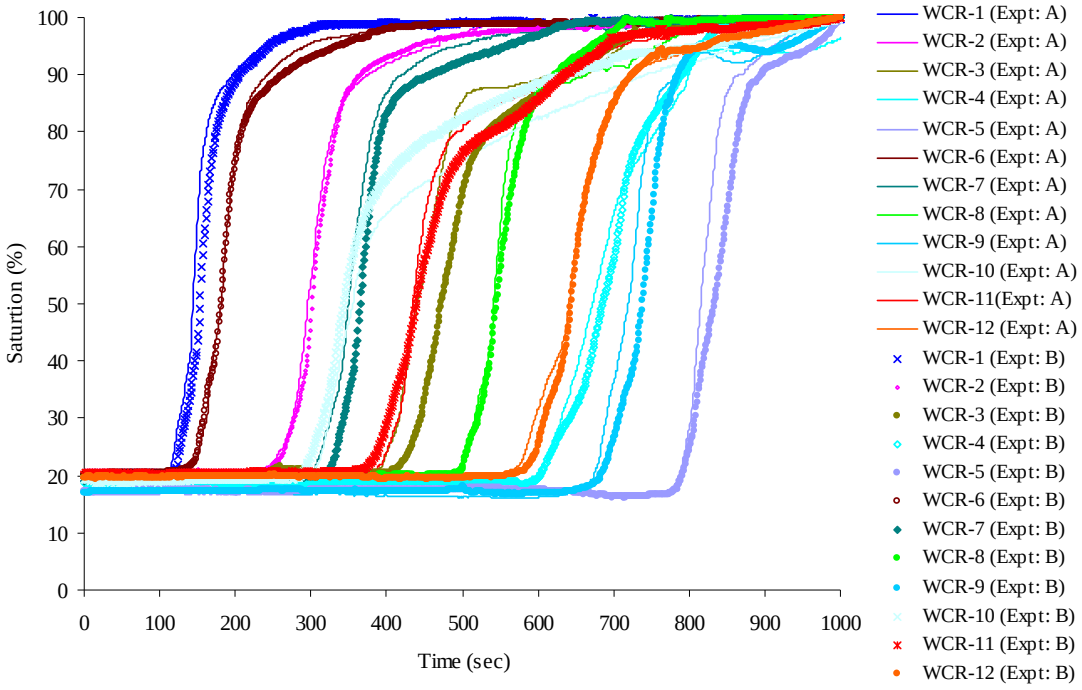

Figure 3.12 Comparison of moisture profile (Experiment A and Experiment B)

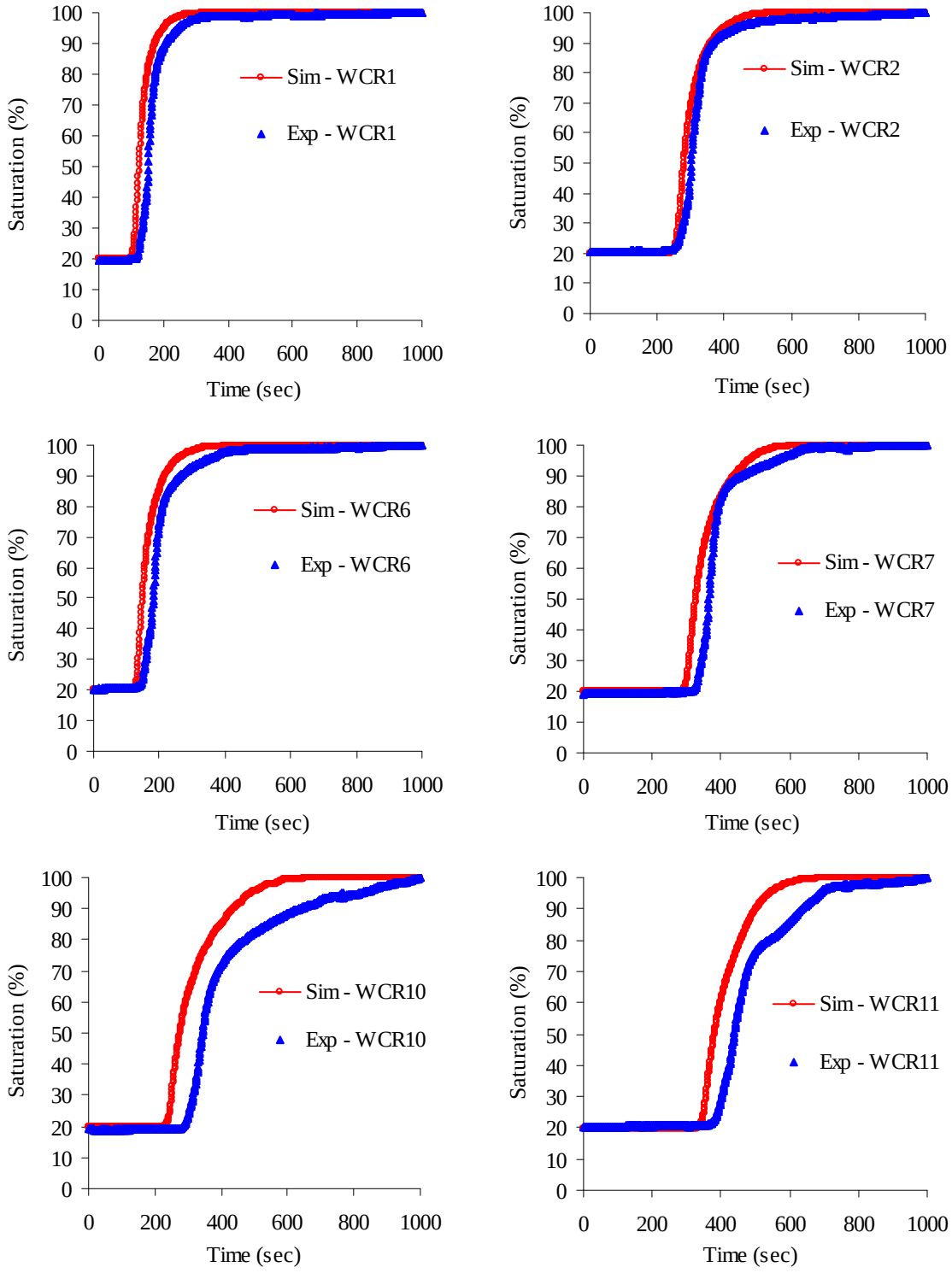

Figure 3.13 Simulated and experimental results of water content profile for steady discharge in the upstream reservoir (WCR – 1,2,6,7,10 and 11)

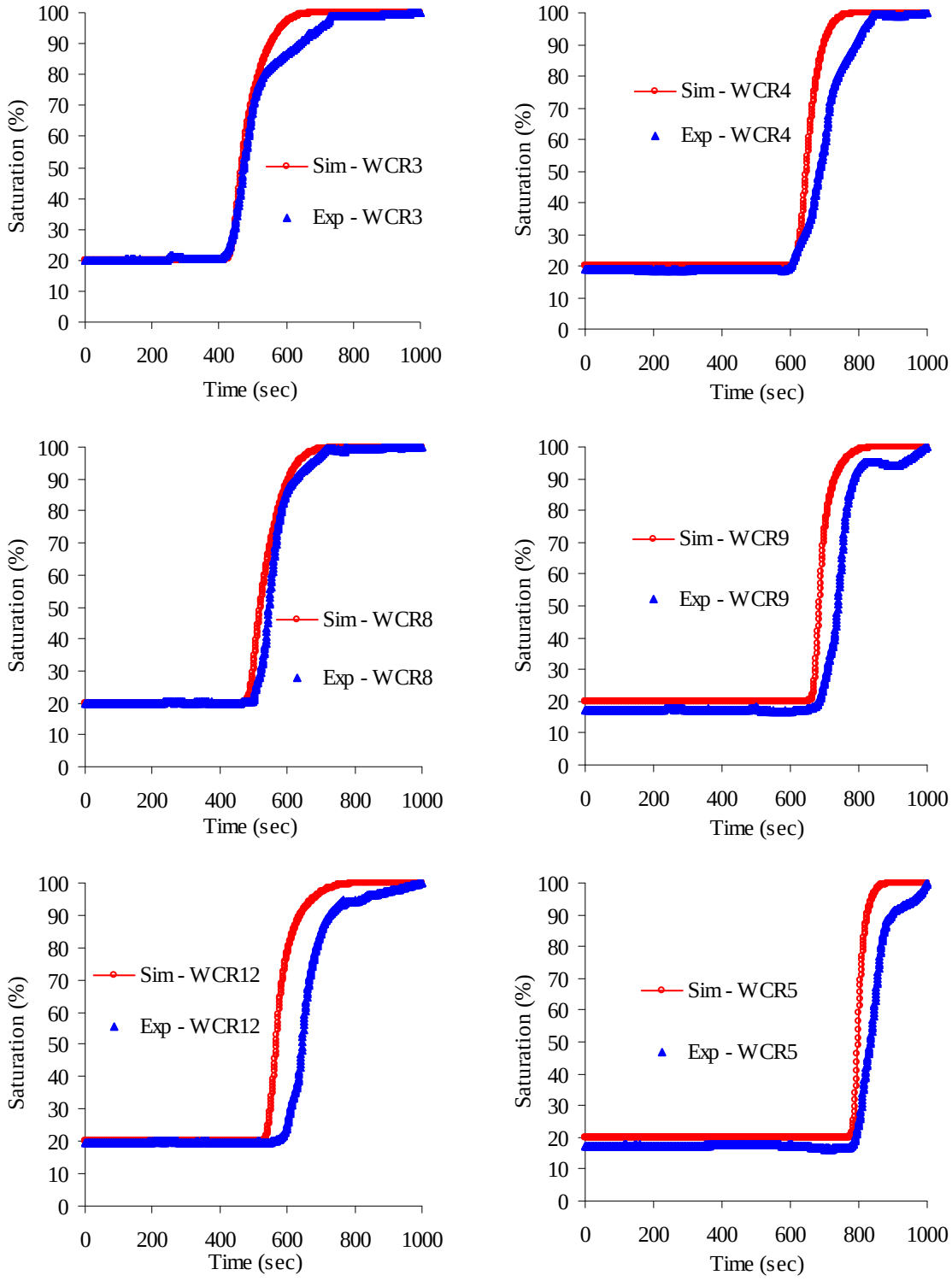

Figure 3.14 Simulated and experimental results of water content profile for steady discharge in the upstream reservoir (WCR – 3,4,8,9,12 and 5)

Summary

Infiltration into variably saturated porous media is governed by the Richards' equation. The pressure based Richards' equation discretized by finite differences technique was used in numerical simulations. Numerical simulations and experimental studies were carried out for two cases to verify 2D seepage flow model. In first case water level in the upstream reservoir was kept constant where as in the second case steady discharge was supplied in the upstream reservoir. In the case of 3D seepage flow model steady discharge was used. A high constant water level or gradual rise of water level in the reservoir causes water to penetrate into the dam body and it reduce shear strength of dam body. The numerical simulation and experimental results of movements of moisture in the dam body are in good agreement for both cases. The seepage flow model can be combined with slope stability model. The combined model can be used for transient slope stability analysis of landslide dam.

Chapter 4

Slope Stability Analysis

4.1 Introduction

A high water level or rise of water level in the landslide dammed reservoir causes water to infiltrate into the dam body increasing both ground water pressures and weight of the dam body. Sliding of the dam body occurs when the mobilized shear stress, which is increased by the weight increase of the dam body, becomes larger than resisting shear stress, which is decreased by the increase of the pore water pressures. Water infiltrates through the landslide dam in a transient manner, so the slope stability analysis coupled with transient seepage analysis is useful to study stability of landslide dam.

Different analytical procedures have been developed over the years for slope stability analyses. They include limit equilibrium methods, boundary element methods and finite element methods. Limit equilibrium methods of slices are the most commonly used methods among others since simplicity and ease of use are their main advantages. The analysis of slope stability consists of computing a factor of safety using one of several limit equilibrium procedures of analysis for a given sliding surface and searching for the critical slip surface. Critical slip surface with the minimum factor of safety can be determined by using different numerical optimization techniques. The majority of these are based on mathematical programming, particularly nonlinear programming. Several comprehensive reviews of slope stability analysis have appeared recently (e.g. Duncan, 1992, 1996(a), (b); Morgenstern, 1992).

Transient slope stability analysis of many studies are focused on stability analysis of natural slopes, embankments and collapsible dams which may fail by seepage and mass movement due to rainfall and change in river stage. Awal et al. (2007, 2008) used a combined model of seepage flow analysis and slope stability analysis by combining dynamic programming for the transient slope stability analysis of landslide dam.

This chapter presents an optimization algorithm for finding non-circular critical slip surface by using Janbu's simplified method of slope stability analysis combined with dynamic

programming for both two-dimensional (2D) and three-dimensional (3D) methods. The result of seepage flow analysis, i.e. change in pore water pressure and moisture content inside the dam body are incorporated in the transient slope stability analysis.

4.2 Two-dimensional slope stability analysis

4.2.1 Introduction

Two-dimensional slope stability methods are the most commonly used methods due to their simplicity. However, these methods are based on simplifying assumptions to reduce the three-dimensional problem to a two-dimensional. In addition, simplified assumptions in 2D slope stability methods have led to factors of safety that differ from the more rigorous 3D slope stability analysis methods. In practice, 3D analysis of slope stability is not performed unless the geometry of the slope is very complicated or the failure mechanism is complex.

Once appropriate shear strength properties, pore water pressures, slope geometry and other soil and slope properties are established, slope stability analysis can be performed by several limit equilibrium procedures of analysis. The method of slices is one of the widely used limit equilibrium methods for the analysis of the stability of slopes. The sliding mass is divided into a number of vertical slices. The static equilibrium of the slices and the mass as a whole are used to solve the problem. All methods of slices are statically indeterminate and involve assumptions in order to make the problem statically determinate. Analysis techniques differ from each other in respect of the equilibrium equations employed and the particular assumptions made with regards to the inter-slice forces. The next subsections briefly discuss Janbu's simplified method and present the relevant equations to calculate the factor of safety and dynamic programming used for locating critical surface.

4.2.2 Janbu's simplified method

Janbu's simplified method (1956) is based on the assumption that the interslice forces are horizontal. This method is over specified and may violate moment equilibrium for the soil mass as a whole. Janbu's simplified method includes the effect of pore water by taking the water pressure to be hydrostatic below the phreatic surface.

The failure surface is defined by nodal points connected by straight lines. The points are equidistant from each other with the first and last points at the ground surface. These two points may move along the ground surface and consequently all the nodal points have the possibility of moving horizontally together with the freedom of vertical movement. This results in a general formulation of the failure surface position.

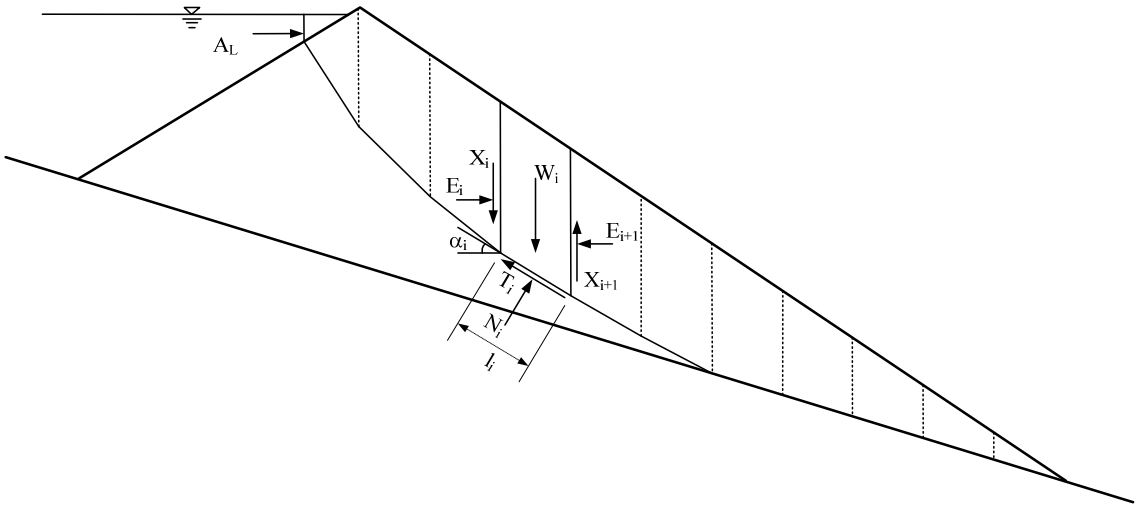

Figure 4.1 Forces acting on a slice through a sliding mass

Janbu's simplified method can be used to calculate the factor of safety for slip surfaces of any shape. The sliding mass is divided into vertical slices and the static equilibrium conditions of each slice are considered as sum of the vertical forces equal to zero and sum of the forces parallel to failure surface equal to zero. For the soil mass as a whole, sum of the vertical forces $\sum F_y = 0$ and sum of the horizontal forces $\sum F_x = 0$ are considered as equilibrium condition.

Figure 4.1 shows all the forces acting on a slip surface. For slice shown in the figure,

Shear strength (available)

$$s_i = c + (\sigma_i - u_i)\tan\phi \tag{4.1}$$

where, s_i is the shear strength, c is the effective cohesion, ϕ is the effective angle of internal friction, σ_i is the total normal stress and u_i is the pore water pressure.

Shear strength (mobilized)

$$\tau_i = \frac{s_i}{F_s} \tag{4.2}$$

The total normal force, N_i, and mobilized shear force T_i in each slice can be expressed as

$$N_i = \sigma_i l_i, \qquad T_i = \tau_i l_i = \frac{1}{F_s}\left(cl_i + \left(N_i - u_i l_i\right)\tan\phi\right) \tag{4.3}$$

Resolve vertically,

$$N_i \cos\alpha_i + T_i \sin\alpha_i = W_i - \left(X_{i+1} - X_i\right) \tag{4.4}$$

Assume $X_i = X_{i+1} = 0$ (i.e. interslice forces horizontal)

Rearranging and substituting for T_i gives

$$N_i = \frac{W_i - \frac{1}{F_s}\left(cl_i - u_i l_i \tan\phi \sin\alpha_i\right)}{\cos\alpha_i\left(1 + \frac{\tan\alpha_i \tan\phi}{F_s}\right)} \tag{4.5}$$

Resolve parallel to base of slice

$$T_i + \left(E_{i+1} - E_i\right)\cos\alpha_i = \left(W_i - \left(X_{i+1} - X_i\right)\right)\sin\alpha_i \tag{4.6}$$

Assume $X_i = X_{i+1} = 0$, rearrange and substitute for T_i

$$\left(E_{i+1} - E_i\right) = W_i \tan\alpha_i - \frac{1}{F_s}\left(cl_i + \left(N_i - u_i l_i\right)\tan\phi\right)\sec\alpha_i \tag{4.7}$$

Overall force equilibrium

Summing above expression from one end to other end of sliding mass

$$\sum_{i=1}^{n}\left(E_{i+1} - E_i\right) = 0 - A_L \tag{4.8}$$

where, A_L is the resultant external water force in the left side of slope. If the water level in the upstream reservoir is below slip surface then $A_L = 0$.

So, $\sum_{i=1}^{n}\left(E_{i+1} - E_i\right) + A_L = \sum_{i=1}^{n} W_i \tan\alpha_i - \frac{1}{F_s}\sum_{i=1}^{n}\left(cl_i + \left(N_i - u_i l_i\right)\tan\phi\right)\sec\alpha + A_L = 0$ (4.9)

$$F_s = \frac{\sum_{i=1}^{n}\left(cl_i + \left(N_i - u_i l_i\right)\tan\phi\right)\sec\alpha}{\sum_{i=1}^{n} W_i \tan\alpha_i + A_L} \tag{4.10}$$

By eliminating N_i in the Equation 4.10 the factor of safety, F_s for Janbu's simplified method can be expressed as:

$$F_s = \frac{1}{\left(\sum_{i=1}^{n} W_i \tan\alpha_i + A_L\right)} \times \sum_{i=1}^{n} \left\{ \frac{cl_i \cos\alpha_i + (W_i - u_i l_i \cos\alpha_i)\tan\phi}{\cos^2\alpha_i \left(1 + \frac{1}{F_s}\tan\alpha_i \tan\phi\right)} \right\} \tag{4.11}$$

where W_i is the weight of each slice including surface water, A_L is the resultant external water force in the left side of slope, l_i is the length of the base of each slice, u_i is the average pore water pressure on the base of the slice, α_i is the inclination of the base to the horizontal, *n* is the total number of slices, and c and ϕ are the Mohr-Coulomb strength parameters.

A modified form of the Mohr-Coulomb equation (Fredlund et al., 1978) can be used to account the shear strength of an unsaturated soil (i.e., a soil with negative pore-water pressures) to derive Equation 4.11. However in this model increase in shear strength due to the negative pore water pressures is ignored.

The partial submergence by impounded water in the upstream is modeled as a material with no strength; the model uses a vertical slip surface through the water and applies a hydrostatic horizontal force on the vertical portion of the slip surface, as shown in Figure 4.1.

4.2.3 Application of Dynamic Programming to slope stability analysis

Dynamic programming has been developed as a numerical algorithm for the rapid optimization of sequential multistage decision problems (Bellman, 1957). Such problems are characterized by two features: firstly, that at any stage the system may exist in any one of a finite number of states and, secondly, that it is required to find the minimum system "cost". The minimum cost depends on the trajectory between stages and is defined as the sum of the costs incurred on passing between adjacent stages. The problem of locating the critical slip surface and hence the minimum factor of safety of a slope may readily be formulated in this manner.

The dynamic programming method to determine critical slip surface has been the subject of interest of a number of researchers, since the 80's. Baker (1980) combined the Spencer method with dynamic programming, Yamagami and Ueta (1986) coupled the Janbu's simplified method

with dynamic programming involving Baker's ideas, Yamagami and Ueta (1988) extended the dynamic programming method and replaced the Spencer limit equilibrium method with stresses computed in a finite element (FE) stress analysis. More recent studies have been presented by Zou et al. (1995) and Pham et al. (2002).

Use of the dynamic programming method requires the definition of a grid of state points that overlaps the potential slip region. The state points are arranged in a series of stages. The numerical procedure behind the identification of critical noncircular slip surface with the minimum factor of safety based on dynamic programming and the Janbu's simplified method is mainly based on research by Yamagami and Ueta. The algorithm combines the Janbu's simplified method with dynamic programming on the basis of Baker's successful procedure.

Equation 4.11 can be generalized as

$$F_s = \frac{\sum R_i}{\sum T_i + A_L} \quad (i = 1 \sim n) \tag{4.12}$$

where,

$$R_i = \frac{cl_i \cos\alpha_i + (W_i - u_i l_i \cos\alpha_i)\tan\phi}{\cos^2\alpha_i \left(1 + \frac{1}{F_s}\tan\alpha_i \tan\phi\right)} \tag{4.13}$$

$$T_i = W_i \tan\alpha_i \tag{4.14}$$

The factor of safety, defined in Equation 4.12, can be minimized by the introduction of the 'auxiliary function', G, and minimization of F_s is equivalent to minimizing the function G.

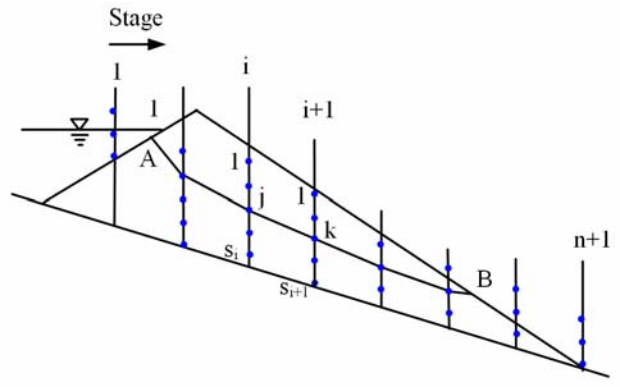

Figure 4.2 Schematic representation of stages, states and slip surface

$$G = \sum_{i=1}^{n} (R_i - F_s T_i) - F_s A_L \tag{4.15}$$

When applying dynamic programming, minimization of G is carried out over all admissible slip surfaces:

$$G_m = \min G = \min\left[\sum_{i=1}^{n} (R_i - F_s T_i) - F_s A_L \right] \tag{4.16}$$

where, G_m is the minimum of the function G, which yields the critical slip surface. F_s in Equation 4.16 is not known in advance, so that starting with an initial assumed value of F_s, we must iterate the computation process. As shown in Figure 4.2, an arbitrary line *jk* which connects points (i, j) and $(i+1, k)$ is considered as a part of assumed slip surface. R_i and T_i on the surface *jk* are obtained from Equation 4.13 and Equation 4.14 and the return function is calculated using Equation 4.17.

$$DG_i(j,k) = R_i - F_s T_i \tag{4.17}$$

If $H_i(j)$, optimal value function in dynamic programming, is the minimum value of G from the point A (Figure 4.2) to the point (i, j), then the minimum G value from A to $(i+1, k)$ is given by Equation 4.18. According to Bellman's principle of optimality, Equation 4.18 is the recurrence relation in dynamic programming for the present situation.

$$H_{i+1}(k) = \min\left[H_i(j) + DG_i(j,k)\right], \qquad i = 1 \sim n,\ j = 1 \sim S_i,\ k = 1 \sim S_{i+1} \tag{4.18}$$

The boundary conditions are

$$H_1(j) = 0,\ j = 1 \sim S_1 \tag{4.19}$$

$$G_m = \min G = \min\left[H_{n+1}(j)\right] \left(j = 1 \sim S_{n+1}\right) \tag{4.20}$$

Difference between the value of F_s calculated by Equation 4.12 after this procedure and initially assumed value of F_s should be within tolerance, therefore, iteration is required to obtain exact value of F_s along the slip surface.

The Janbu's simplified method uses a correction factor f_o to account for the effect of the

interslice shear forces. However, in this study correction factor is not considered since the range of correction factor for non-cohesive soil is small.

4.2.4 Coupling slope stability model with seepage flow model

The model of the dam failure due to sliding consists of two models. As already described in Chapter 3, the seepage flow model calculates both positive and negative pore water pressure and moisture content in each grid inside the dam body. However, for slope stability analyses the pore water pressures are assumed to be zero in the region where negative pressures have been calculated. The average pore water pressures at the center of the base of individual slices along a slip surface are determined by averaging the pore water pressure of block grid just above the slip surface. The model of slope stability calculates the factor of safety and the geometry of critical slip surface according to pore water pressure and moisture movement in the dam body. Water level in the upstream reservoir (h) in each time step is determined by water-volume balance equation considering inflow discharge (Q_i), rate of infiltration inside the dam body (Q_{sh}) and flume geometry (width and slope). The general flow chart of combined model for transient slope stability analysis is shown in Figure 4.3.

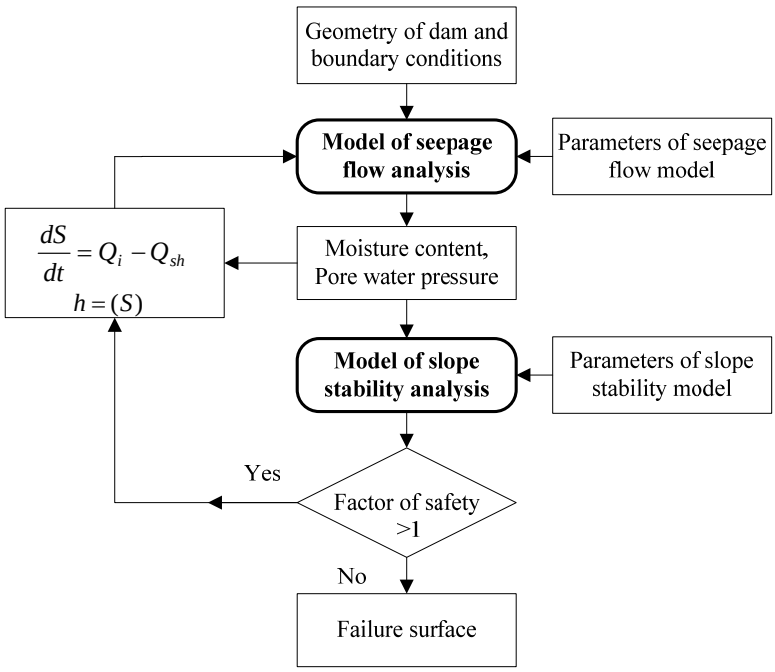

Figure 4.3 General flow chart of coupled model for transient slope stability analysis

4.2.5 Verification of model with experiments

Laboratory experiments

The rectangular flume of length 5m, width 20cm and depth 21cm was used. The slope of the flume was set at 17 degree. Sediment Mix 1-7 was used to prepare dam body. Different parameter of sediment mix is shown in Table 2.1.

Triangular dam was prepared on the rigid bed of flume by placing mixed sand on the flume. The upstream and downstream faces of landslide dam are slightly smaller than the angle of repose of the sand mixture. The height of the dam was 20cm and the longitudinal base length was 84cm. The schematic diagram of the flume is shown in Figure 2.1. To measure the movement of dam slope during sliding, red colored sediment strip was placed in the dam body at the face of flume wall. A digital video camera was placed in the side of the flume to capture the shape of slip surface due to sudden sliding. Water level of reservoir was kept constant in Case I; where as steady discharge was supplied in Case II. Temporal weight of debris flow was also measured in the downstream end of the flume with the help of load cell. The shape of slip surface during sliding of the dam body was measured by analyses of video taken from the flume side.

Results and discussions

Many experiments were performed to observe the failure of the dam by sudden sliding. Two cases are considered:

Case I: Constant water level in the upstream reservoir

The reservoir in the upstream of the dam was filled by water up to16mm below crest level of the dam in 25 seconds. Then water level was maintained constant. Sudden sliding of the dam was observed at 255sec. Figure 4.4 shows the observed sliding surface in the experiment. The slip surface was determined by the measurement of tilting of the red color strips with the help of snaps captured by the video camera positioned on the side of flume. Figure 4.5 shows simulated and experimental slip surface. The simulated failure time was 237sec after start of filling of reservoir. The simulated time was slightly earlier than the experimentally observed time that may be due to the assumption of immobile air phase in unsaturated flow and variation of saturated hydraulic conductivity since it was difficult to make sand mixture perfectly homogeneous. Moreover, the effects of vertical interslice forces are ignored in Janbu's

simplified method. Increase in shear strength due to the negative pore-water pressures are not considered in the formulation of factor of safety.

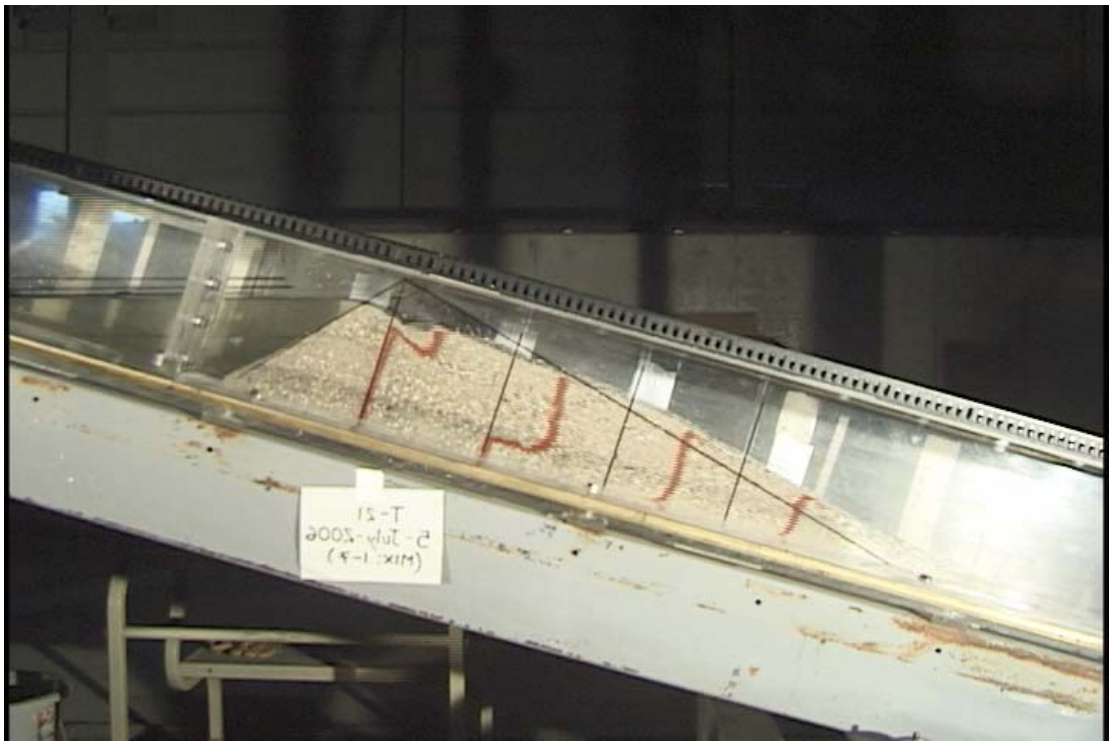

Figure 4.4 Slope sliding of the dam (constant water level in the upstream reservoir)

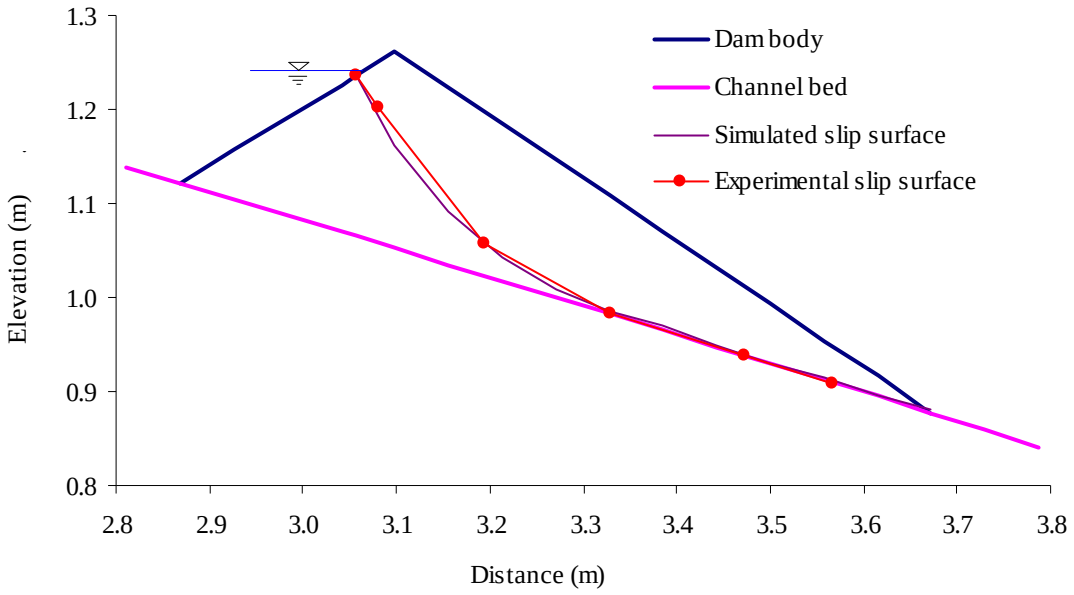

Figure 4.5 Comparison of simulated and experimental slip surface

Case II: Steady discharge in the upstream reservoir

Steady discharge of 39.8cm^3/sec was supplied from the upstream end of the flume. The sliding surface observed in the experiment is shown in Figure 4.6. The sliding of the dam body was

Figure 4.6 Slope sliding of the dam (steady discharge in the upstream reservoir)

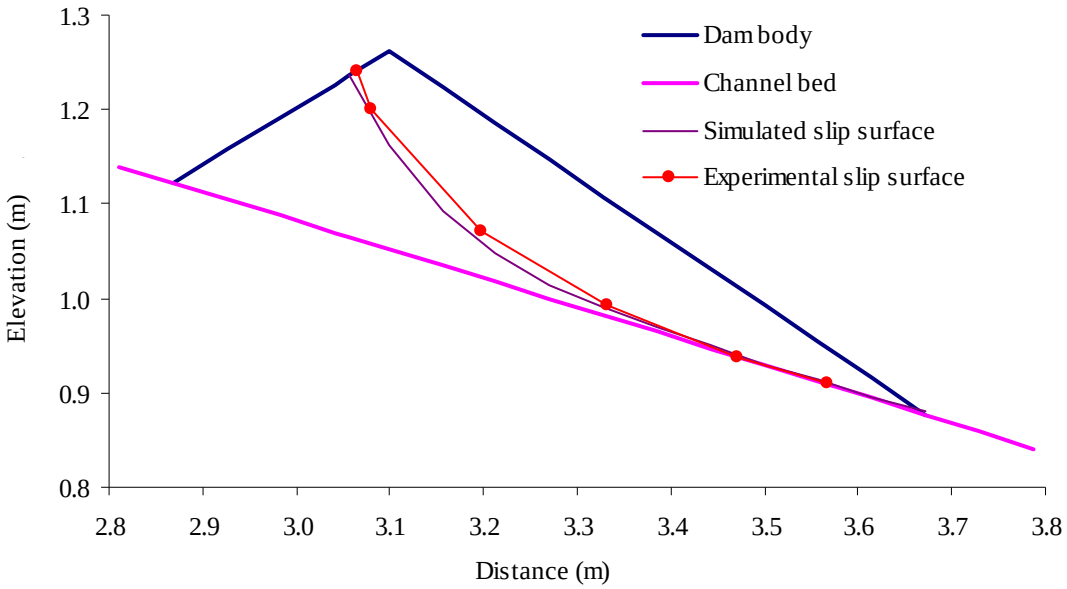

Figure 4.7 Comparison of simulated and experimental slip surface

observed at 350sec in the experiment whereas in the simulation it was observed at 317sec. Figure 4.7 shows the comparison of simulated and experimental slip surface. The numerical simulation and experimental results of the geometry of predicted critical slip surface was similar. So the model developed by coupling the seepage flow model with the stability model in this study is promising.

4.3 Three-dimensional slope stability analysis

4.3.1 Introduction

The limit equilibrium method is employed to evaluate the transient slope stability. It involves calculating the factor of safety and searching for the critical slip surface that has the lowest factor of safety according to infiltration of water inside the dam body. A 2D analysis is only valid for slopes which are long in the third dimension. However, failure of natural slopes and landslide dams confined in a narrow U- or V-shaped valley occurs in three dimensions. Therefore 3D approach is more appropriate to analyze such stability problems. The 3D slope stability analysis based on dynamic programming and random number generation incorporated with 3D simplified Janbu method is used to determine minimum factor of safety and the corresponding critical slip surface for landslide dam in the V-shaped valley.

4.3.2 The 3D Simplified Janbu method

Most of the three-dimensional slope stability analysis procedures are based on a method of columns. The method of columns are the 3D equivalent of the 2D procedures of slices. The soil mass is subdivided into a number of vertical columns. A considerable number of assumptions must be made to achieve a statically determinate solution with the method of columns. Several procedures employ simplifying approaches comparable to the Ordinary Method of Slices, rather than fully satisfying the six equations of static equilibrium, i.e. three equations for force equilibrium and three equations for equilibrium of moments about three axes (Duncan and Wright, 2005).

Several methods have been proposed to determine factor of safety for three dimensions based on limit equilibrium analysis of columns which are valid for an arbitrary slip surface. Ugai (1988) and Ugai and Hosobori (1988) extended the simplified Janbu method and Spencer method in 2-

D problem to three-dimensions. 3D simplified Janbu method proposed by Ugai et al. is simple and comparatively rigorous one. This method possesses a definite advantage in that when the slope under consideration is gentle (less than 45^{o}), a factor of safety can be determined by only one formula rather than by simultaneous equations in general cases and therefore iterative

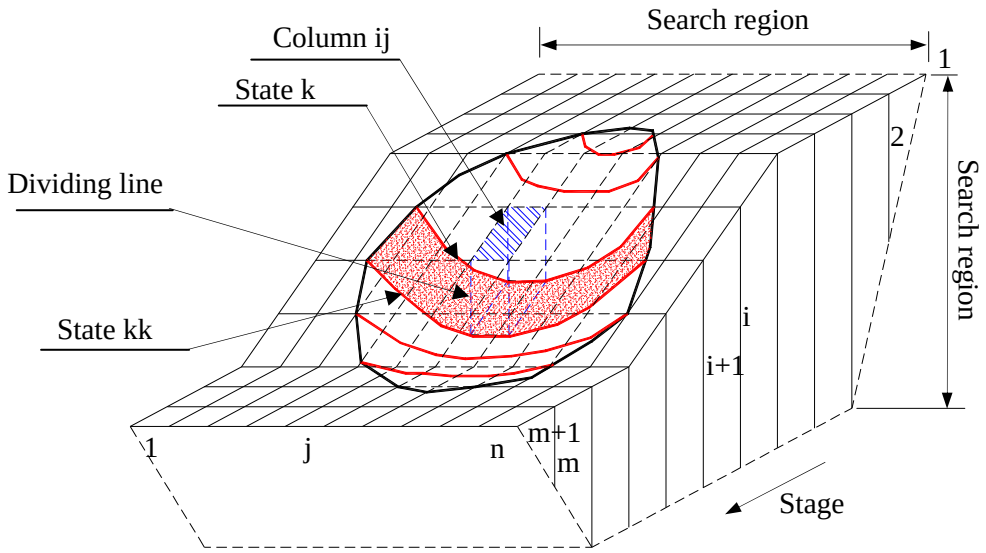

Figure 4.8 A stage-state system and dividing scheme for a 3D slope (Modified from Yamagami and Jiang, 1997)

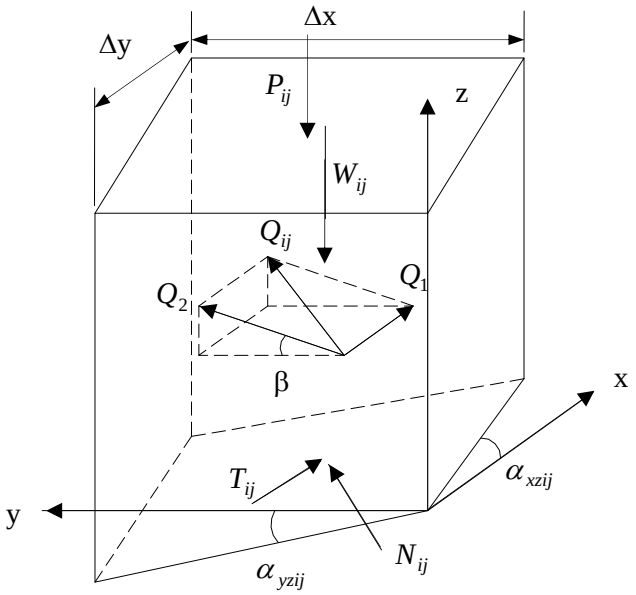

Figure 4.9 Forces acting on a typical column

procedures will be significantly simplified (Yamagami and Jiang, 1997). The proposed model incorporates 3D simplified Janbu method proposed by Ugai et al. couple with the minimization approach based on dynamic programming and the method of Random Number Generation. The model is further coupled with seepage flow model for transient slope stability analysis.

A 3D sliding mass and vertically divided columns within a slope is shown in Figure 4.8. Figure 4.9 shows the forces acting on a typical column taken from Figure 4.8. These forces are: W_{ij} is the weight of column, P_{ij} is the vertical external force acting on the top of the column, T_{ij} and N_{ij} are the shear force and total normal force acting on the column base, Q_{ij} is the resultant of all intercolumn forces acting on the column sides. In addition other symbols in Figure 4.9 include: Δx and Δy are discretized widths of the columns in the $x-$ and $y-$ direction, α_{xzij} and α_{yzij} are the inclination angles of the column base to the horizontal direction in the xz and yz planes, respectively. The direction of forces W_{ij}, P_{ij}, T_{ij} and N_{ij} are given by the following unit vectors:

W_{ij} : $(0,0,-1)$

P_{ij} : $(0,0,-1)$

T_{ij} : $\left(1/J',0,\tan\alpha_{xzij}/J'\right)$

N_{ij} : $\left(-\tan\alpha_{xzij}/J,-\tan\alpha_{yzij}/J,1/J\right)$

where, $J'=\left(1+\tan^2\alpha_{xzij}\right)^{1/2}$ and $J=\left(1+\tan^2\alpha_{xzij}+\tan^2\alpha_{yzij}\right)^{1/2}$

According to Ugai's (1988), Q_{ij} is decomposed to a component Q_1 parallel to $x-$axis and a component Q_2 inclined at an angle $\beta=\tan^{-1}\left(\eta\tan\alpha_{xzij}\right)$ to the $y-$axis, where η is unknown constant. Based on these assumptions and the failure condition T_{ij} and N_{ij} can be derived from the equilibrium of the forces in the direction perpendicular to the plane composed of Q_1, Q_2 and Q_{ij}. The failure condition, in combination with the definition of the safety factor, F_s can be written as

$$T_{ij}=\left[cJ\Delta x\Delta y+\left(N_{ij}-u_{ij}J\Delta x\Delta y\right)\tan\phi\right]/F_s \tag{4.21}$$

where, c and ϕ are the effective strength parameters of soil, u_{ij} is the pore water pressure at the column base.

Applying equilibrium conditions in horizontal and vertical directions for the entire sliding mass, Ugai (1988) defined two safety factors F_{sh} and F_{sv}. Equations 4.22 and 4.23 are the expression for F_{sh} and F_{sv} considering P_{ij} and u_{ij} in Ugai's analysis.

$$F_{sh} = \frac{\sum_{i=1}^{m}\sum_{j=1}^{n}\left[\left(c - u_{ij}\tan\phi\right)\left(1+\eta\cos^2\alpha_{xzij}\tan^2\alpha_{yzij}\right)\Delta x\Delta y + \left(W_{ij}+P_{ij}\right)\left(\tan\phi + \frac{\eta F_{sh}\sin\alpha_{xzij}\tan^2\alpha_{yzij}}{J}\right)\right]/\cos\alpha_{xzij}\, m_\alpha}{\sum_{i=1}^{m}\sum_{i=1}^{n}\tan\alpha_{xzij}\left(W_{ij}+P_{ij}\right)} \tag{4.22}$$

$$F_{sv} = \frac{\sum_{i=1}^{m}\sum_{i=1}^{n}\left[\left(c - u_{ij}\tan\phi\right)\eta\sin\alpha_{xzij}\tan^2\alpha_{yzij}\Delta x\Delta y + \left(W_{ij}+P_{ij}\right)\left(\sin\alpha_{xzij}\tan\phi + \frac{F_{sv}}{J}\right)\right]/m_\alpha}{\sum_{i=1}^{m}\sum_{i=1}^{n}\left(W_{ij}+P_{ij}\right)} \tag{4.23}$$

where, $m_\alpha = \left(1+\eta\tan^2\alpha_{yzij}\right)/J + \sin\alpha_{xzij}\tan\phi/F_s$.

Both of these factors depend on η and they become equal to each other at a certain η value. It has been shown that the equation $F_s = F_{sh} = F_{sv}$ is usually satisfied at small η values (Ugai, 1987; Jiang and Yamagami, 1999). For such small values of η, calculated F_{sh} values show little change with variation of η. In other words, sufficiently accurate values of the 3D factor of safety can be calculated based on F_{sh} evaluated at $\eta = 0$ (Ugai, 1987; Jiang and Yamagami, 1999) and based on this approximation, factor of safety F_s can be expressed by following expression:

$$F_s = \frac{\sum_{i=1}^{m}\sum_{j=1}^{n}\left[\left(c - u_{ij}\tan\phi\right)\Delta x\Delta y + \left(W_{ij}+P_{ij}\right)\tan\phi\right]/\left[\left(1/J + \sin\alpha_{xzij}\tan\phi/F_s\right)\cos\alpha_{xzij}\right]}{\sum_{i=1}^{m}\sum_{j=1}^{n}\tan\alpha_{xzij}\left(W_{ij}+P_{ij}\right)} \tag{4.24}$$

This simplified formula can provide sufficiently accurate results when the slope is less than 45^o (Ugai and Hosobori, 1988).

Coupling 3D slope stability model with 3D seepage flow model

In Equation 4.24, W_{ij}, P_{ij} and u_{ij} ($c = 0$ for cohesionless soil) are time dependent and can be determined at each time step by coupling with 3D seepage flow model. The output (pore water pressure and moisture content of each cell) and boundary condition (depth of surface water) of seepage flow model can be used to determine these quantities.

Weight of a column, $W_{ij} = \sum \theta(x, y, z, t)\gamma_w dxdydz + \sum c_* \gamma_s dxdydz$

Vertical external force (surface water), $P_{ij} = \sum \gamma_w H_s(x, y, t)dxdy$

Pore water pressure, $u_{ij} = Average \sum \gamma_w h(x, y, z, t)$ for $h(x, y, z, t) > 0$

where, dx, dy and dz are the size of cell used in 3D seepage flow model, γ_w and γ_s are the unit weight of water and solids respectively, c_* is the volume concentration of the solids fraction in the dam body, $\theta(x, y, z, t)$ and $h(x, y, z, t)$ are the moisture content and pressure head in each cell and $H_s(x, y, t)$ is the depth of surface water in submerged cell of dam body in the upstream reservoir.

4.3.3 Extension of Dynamic Programming to 3D slope stability analysis

A search procedure for determination of critical 3D surfaces developed by Yamagami and Jiang (1997) is used in this study. This study extends their work to transient slope stability analysis by incorporating seepage flow model.

Equation 4.24 can be rewritten as

$$F_s = \frac{\sum_{i=1}^{m} R_i}{\sum_{i=1}^{m} T_i} \tag{4.25}$$

where,

$$R_i = \sum_{j=1}^{n} \frac{\left(c - u_{ij} \tan\phi\right)\Delta x \Delta y + \left(W_{ij} + P_{ij}\right)\tan\phi}{\cos\alpha_{xzij}\left(1/J + \sin\alpha_{xzij} \tan\phi / F_s\right)} \tag{4.26}$$

$$T_i = \sum_{j=1}^{n} \tan \alpha_{xzij} \left(W_{ij} + P_{ij} \right) \tag{4.27}$$

To use dynamic programming, it is necessary to introduce an auxiliary function *G* that transforms the factor of safety equation from ratio of two summations into an additive function (Baker, 1980).

$$G = \sum_{i=1}^{m} \left[R_i - F_s T_i \right] = \sum_{i=1}^{m} DG_i \tag{4.28}$$

Application of dynamic programming to a particular problem requires a stage-state system (Baker, 1980). Figure 4.8 illustrates such a stage-state system for a 3D slope (Yamagami and Jiang, 1997). In the present case, 'stages' are vertical planes perpendicular to the sliding direction and a state in a stage is represented by a curve in the stage plane. One state curve for each stage is shown in Figure 4.10. However a large number of state curves in each stage plane are necessary to search for a smooth 3D critical slip surface. The state curves in each stage plane are produced by use of Random Number Generation techniques. The details of state curves generation is discussed at the end of this section.

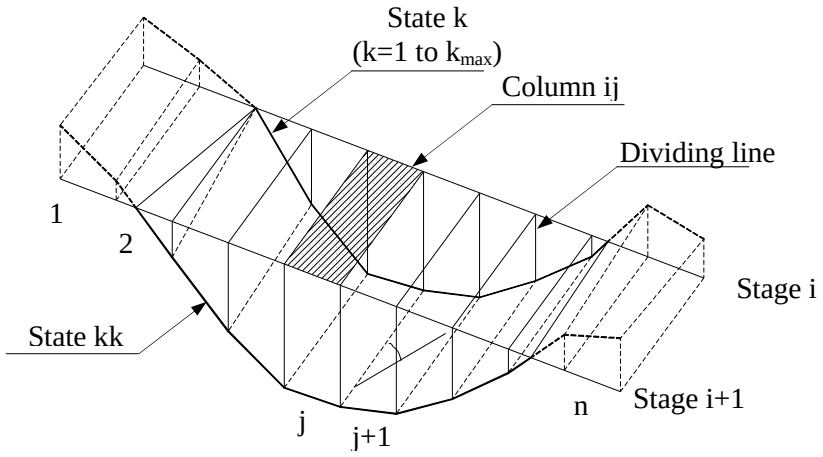

Figure 4.10 Columns between two adjacent stages *i* and *i*+1

To obtain a sufficiently accurate solution for a general slope, a few hundred state curves usually need to be produced in each stage plane prior to the dynamic programming search. If a state curve k in a stage i and a state curve kk in the stage $i+1$ are selected, as shown in Figure 4.8,

the shaded concave segment sandwiched between these two state curves constitutes a part of a potential 3D slip surface. Referring to Figure 4.8, Figure 4.10 can be drawn in which the earth mass between the two adjacent stage planes i and $i+1$ has been discretized into (n) vertical columns by two groups of $(n+1)$ vertical dividing lines located respectively in stage i and stage $i+1$. Since the state curves k and kk were chosen from those produced by the random number generation technique, the location of the (n) columns are determined. Consequently, R_i and T_i in Equation 4.28 can be calculated, and thus Equation 4.28 may be written as

$$G = \sum_{i=1}^{m} [R_i - F_s T_i] = \sum_{i=1}^{m} DG_i = \sum_{i=1}^{m} DG_i(k, kk) \tag{4.29}$$

in which $DG_i(k, kk) = R_i - F_s T_i$ is referred to as the return function in dynamic programming. The function $DG_i(k, kk)$ represents a change in G between two state curves k and kk located in two adjacent stage planes i and $i+1$. Since the return function has been defined, the same recurrence relation and boundary conditions for 3D analysis as those in 2D problem can be constructed through introducing optimal value function. By solving the recurrence relation, the minimum factor of safety and the corresponding critical slip surface in three-dimensions can be obtained at the same time.

Generation of states based on random number generation

States in three-dimensions are indicated by curves in each stage plane. Numbers of state curves are generated by Random Number Generation method. Number of points in each dividing line are determined based on search region and Δz (Figure 4.11). Random integers are generated at each dividing lines. Connecting in sequence those points indicated by the random integers generates a state curve. A large number of curves so generated are recorded and used for states in the stage plane. This procedure is repeated over all the stage planes. To make the generated state curves smooth, concave and to exclude states that oscillate violently different constraints are used.

Constraint to generate concave curve:

$$\frac{(z_{i+1} + z_{i-1})}{2} - z_i \geq 0 \tag{4.30}$$

where, z_i coordinate of the j^{th} dividing line on the state as shown in Figure 4.11.

Maximum lateral slope of slip surface (α_{max}) is considered as equal as or less than 45^o. This angle varies based on material properties of the dam body.

Constraint of minimum thickness (t_m) of sliding mass (at any dividing line of specified region) can be also used to prevent generation of very shallow slips as shown in Figure 4.11.

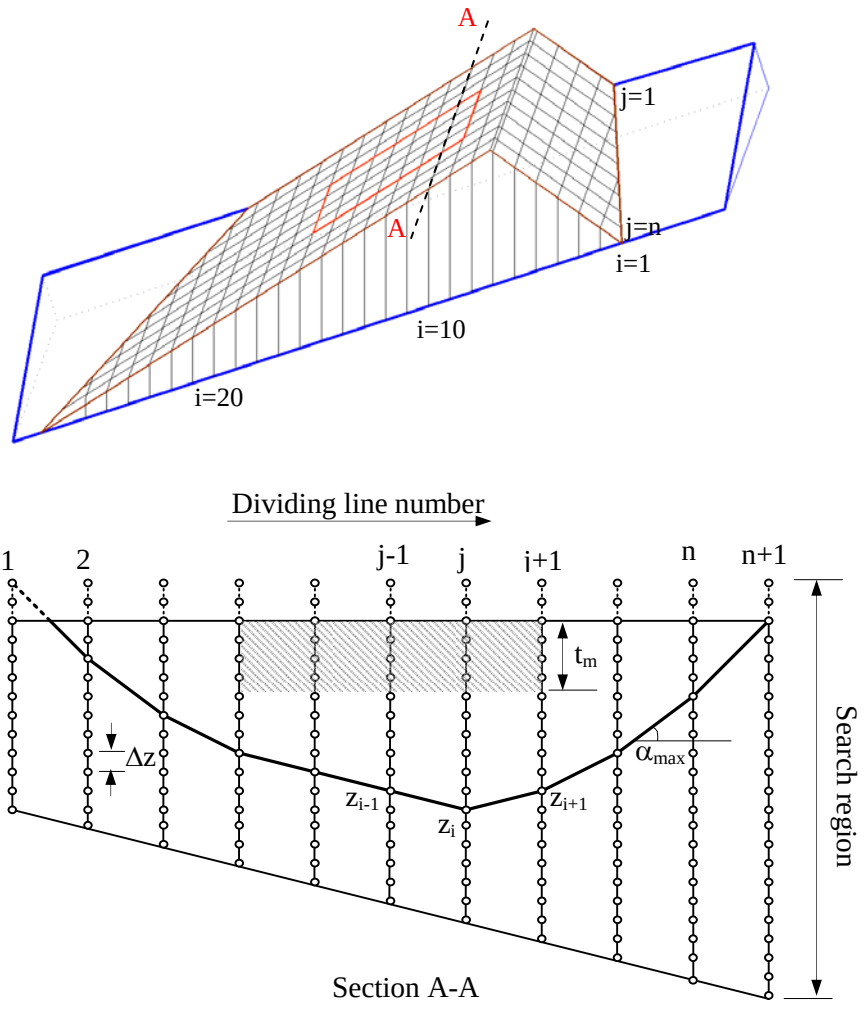

Figure 4.11 The discretization scheme for the generation of state

Constraints used in combining two states:

Range of exit point to combine two state curves in two stage planes is considered as $-\Delta y$ to $+\Delta y$

to prevent irregular shaped column in the boundary and to make smooth shape in plan view. As shown in Figure 4.12 state curves having exit point beyond range of $-\Delta y$ to $+\Delta y$ (e.g., state k = 4) are excluded.

Steepest longitudinal slope of sliding surface is also considered as less than 45^o from the horizontal to prevent generation of steep slip surface.

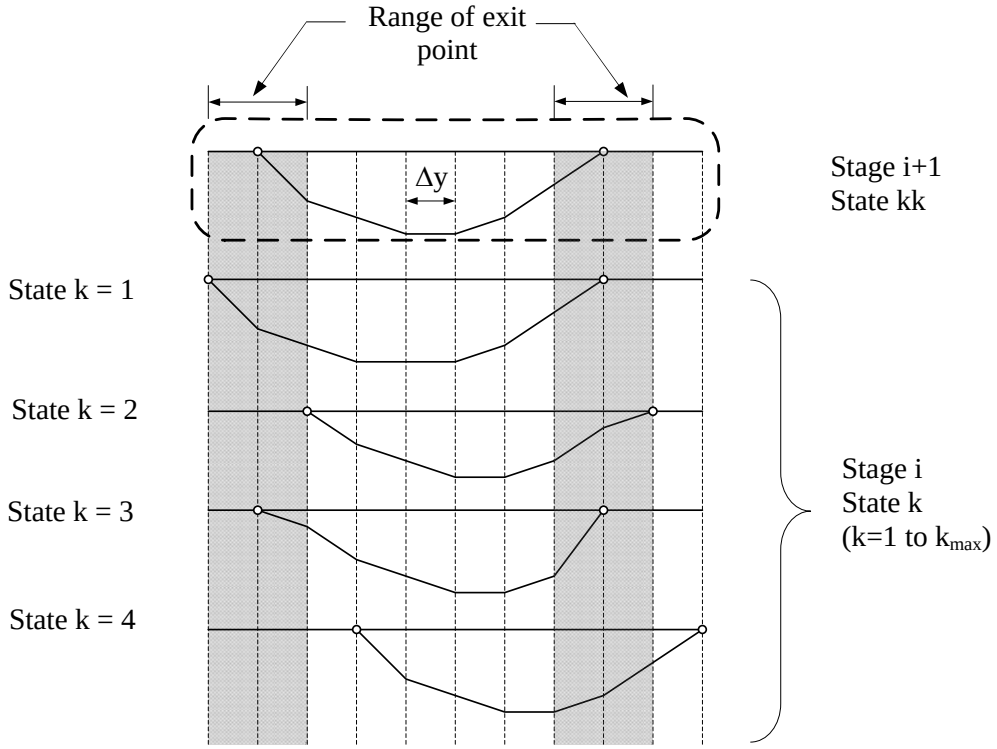

Figure 4.12 Range of exit point to combine two state curves in two stage planes

4.3.4 Verification of model with experiments

Laboratory experiments

The rectangular flume of length 500cm, width 30cm and depth 50 cm was used. The bed of flume was modified to make cross slope of 20^o as already explained in Chapter 3. The shape, size, material properties of the dam body was same as that used for seepage flow experiment, three-dimensional case. To measure the movement of the dam slope during sliding, red colored sediment strip was placed in the dam body at the both faces of the flume wall. Three digital video cameras were used, two in side A and side B and one in the front to capture the shape of

slip surface due to sudden sliding. The shape of slip surface during sliding of the dam body was measured by analyses of videos taken from the flume sides.

Results and discussions

Two experiments were carried out for nearly equal discharge. Steady discharge of 29.8cm^3/sec was used in 'Experiment C' and 30.1 cm^3/sec was used in 'Experiment D'. Figure 4.13 shows the movement of slide at different time steps in case of 'Experiment C'. Although the movement appears at about 930sec the distinct movement can be seen just at about 978sec. In case of 'Experiment D', failure was observed at 1030sec and slide mass is also deeper than 'Experiment C' as shown in Figure 4.14. This may be due to difference in non uniformity in sediment mixing, compaction, hydraulic conductivity between two experiments. However efforts were made to make uniformity in both experiments.

Based on preliminary analysis of 3D slope stability, state curves were generated with following constraints: falter cross slope $\left(\alpha_{\max} = 20^0\right)$, minimum thickness of slipped mass $\left(t_m\right)$ at any dividing line = 10cm (Figure 4.11, i = 9 to 16 and j = 4 to 8), $\Delta z = 5mm$. Thousand numbers of states were generated at each stage plane. Different parameters of sediment, Mix 1-7 are shown in the table 2.1. The other hydraulic conditions/parameters and grid systems used in the simulation are Q_{in} = 29.8cm^3/sec, K_s =0.0003m/sec, $\Delta t = 0.01$sec, block size of 10mm was used in seepage flow model. Column size of $\Delta x = 5cm$ and $\Delta y = 3cm$ was used in slope stability model. Convergence criterion (difference between the factors of safety from the final two interactions) of less than 0.002 was used.

Although it is possible to determine factor of safety at each time step (longer simulation time), factor of safety was calculated just at 10sec interval close to failure time. The simulated critical slip surfaces in the beginning and at 770 sec are shown in Figure 4.15 and 4.16 respectively. The simulated factor of safety was less than 1 at 770sec however the observed failure time in the experiment was about 930sec. The simulations were also carried out for reduced discharge of 29cm^3/sec to account evaporation as well as reduced saturated hydraulic conductivity of 0.00028m/sec to account uncertainty of hydraulic conductivity. In both cases dam was failed at 790sec. The simulated failure time was 830sec for saturated hydraulic conductivity, K_s = 0.00025m/sec. So, the failure time is also depends on saturated hydraulic conductivity. 3D Simplified Janbu method satisfies the horizontal and vertical force equilibrium while it does not satisfy the moment equilibrium. In addition, the method assumes that the resultant interslice

Figure 4.13 Movement of slide at different time steps - Experiment C (contd.)

Figure 4.13 Movement of slide at different time steps - Experiment C

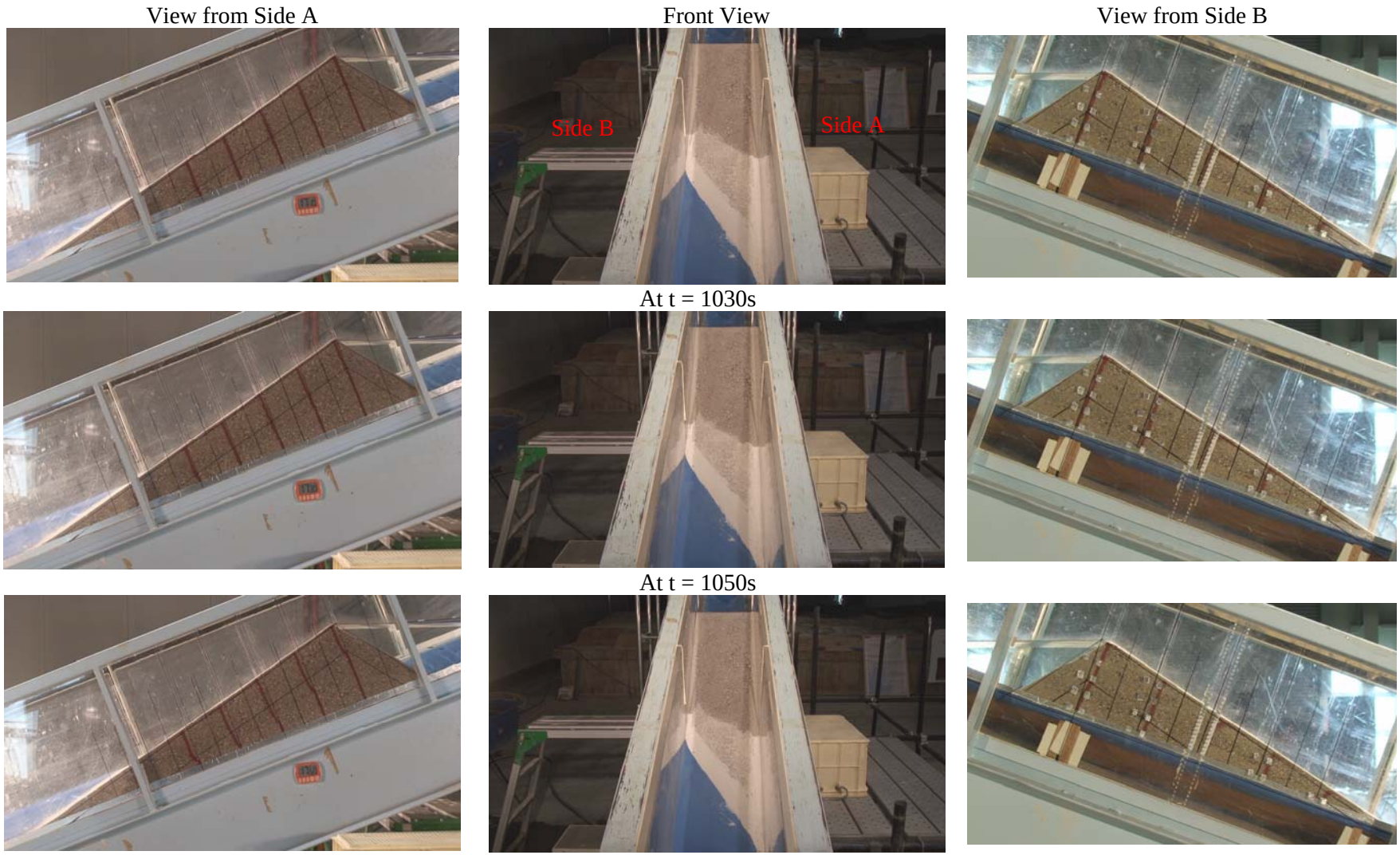

Figure 4.14 Movement of slide at different time steps - Experiment D

Note: Dimensions are in cm.

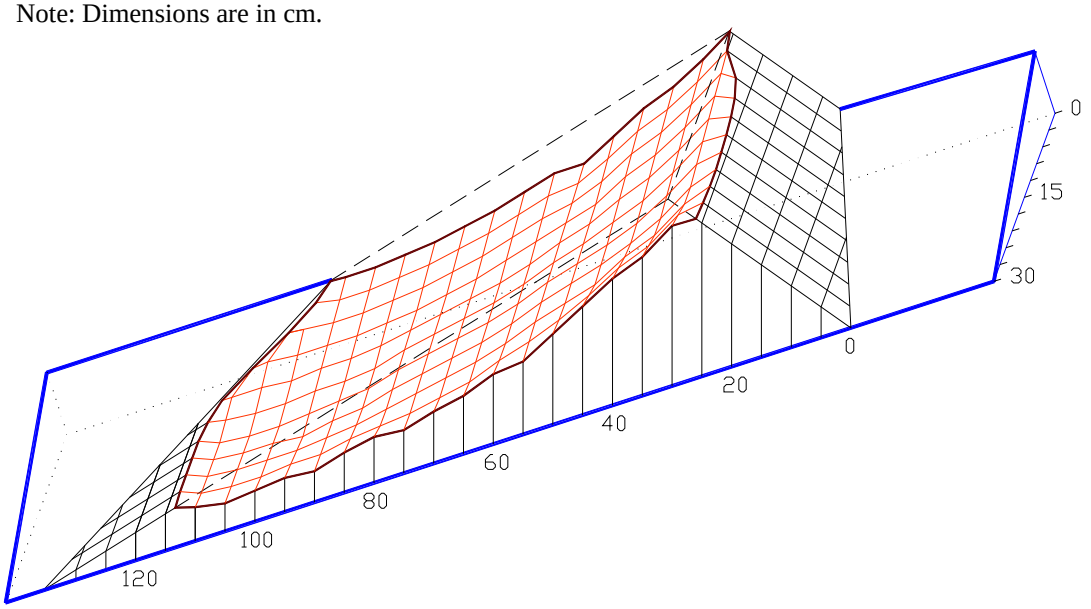

Figure 4.15 Simulated critical slip surface at t = 0sec.

Note: Dimensions are in cm.

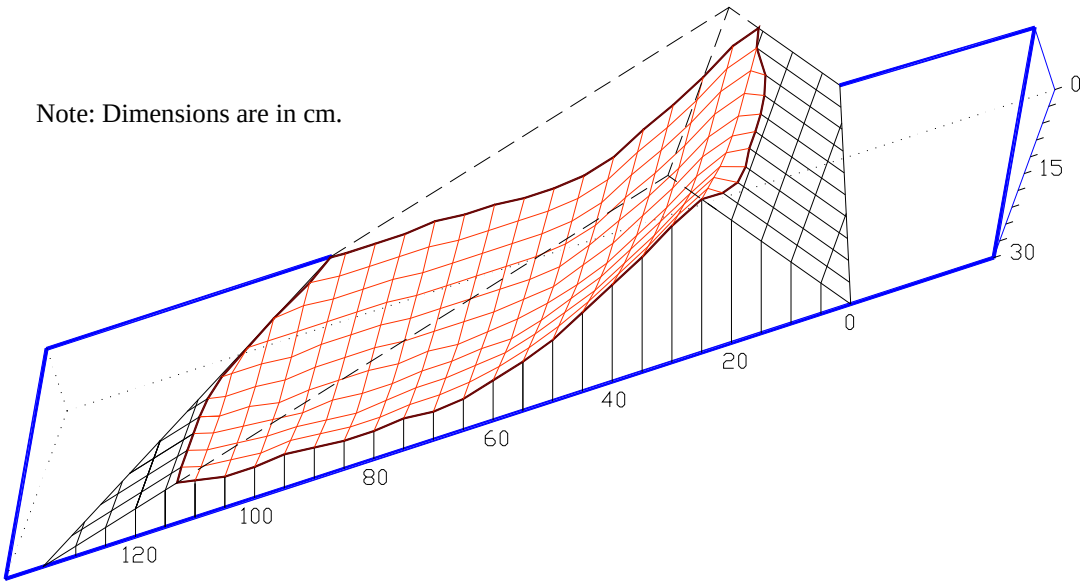

Figure 4.16 Simulated critical slip surface at t = 770sec.

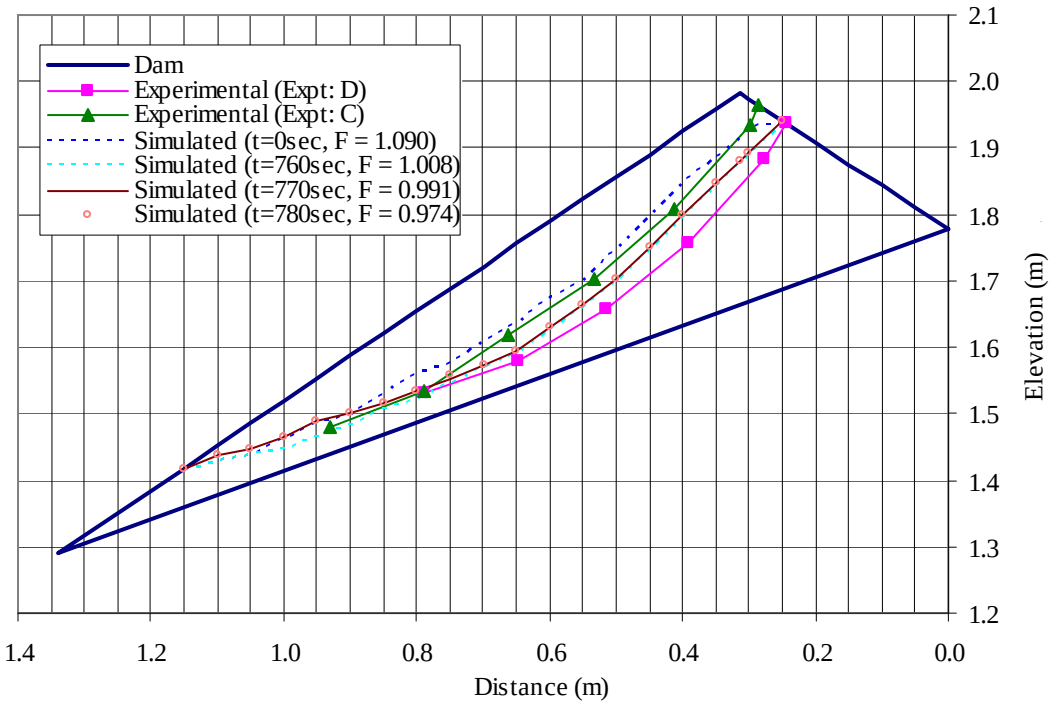

Figure 4.17 Critical slip surface in Side A

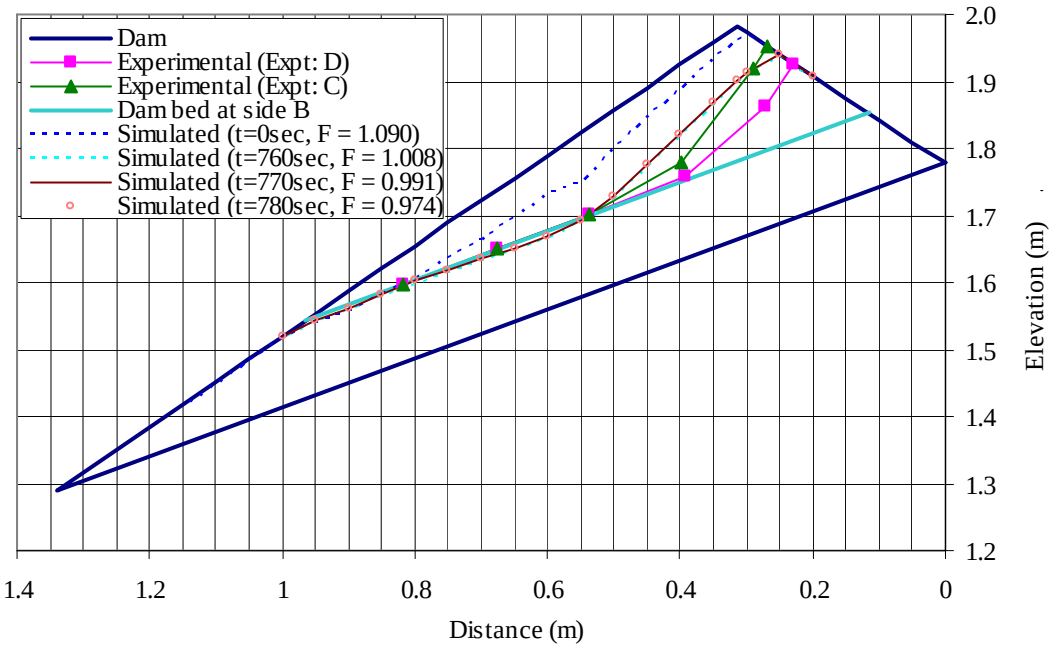

Figure 4.18 Critical slip surface in Side B

forces are horizontal while a correction factor is applied to account for the vertical interslice forces in 2D analysis. However, the correction factor is only available for 2D slope stability analysis and no correction is available for the intercolumn forces in the extended 3D slope stability method. For the same critical slip surface factor of safety calculated by other methods which also satisfies moment equilibrium will be higher. Moreover, the friction in the side wall of flume was also ignored in the computation. The comparison of failure surface in two faces of flume (Figures 4.17 and 4.18) shows the good agreement with experiment. The shape of the slip surface depends on many factors. Data of actual slip surfaces in natural landslide are still lacking to generalize the constraints to generate the state curves based on soil properties. Further improvement of model by incorporating more rigorous method of slope stability analysis is essential for the practical application of 3D transient slope stability analysis.

Summary

Sudden failure of landslide dam was studied in experimental flume for constant head and steady discharge in the upstream reservoir. A high and constant water level or a gradual rise of water level in the reservoir causes water to penetrate into the dam body, increasing mobilized shear stress and causing dam to fail by sudden collapse after it becomes larger than resisting shear stress. Transient slope stability model coupling with seepage flow model was developed. The limit equilibrium method was employed to evaluate the transient slope stability. The numerical procedure used for the identification of critical noncircular slip surface with the minimum factor of safety was based on dynamic programming and the Janbu's simplified method.

A 2D analysis is only valid for slopes which are long in the third dimension. However, failure of natural slopes and landslide dams confined in a narrow U- or V-shaped valley occurs in three dimensions. Therefore 3D approach is more appropriate to analyze such stability problems. The 3D slope stability analysis based on dynamic programming and random number generation incorporated with 3D Simplified Janbu's method was used to determine minimum factor of safety and the corresponding critical slip surface for landslide dam in the V-shaped valley. The 3D seepage flow model was coupled with 3D slope stability model so the combined model was capable for transient slope stability analysis.

Numerical simulations and flume experiments were performed to investigate the mechanism of landslide dam failure due to sliding for both 2D and 3D cases. The lateral slope of the flume bed was horizontal for 2D case and was inclined for 3D case. The shape of the slip surface during

sliding of the dam body was measured by analyses of videos taken from the flume sides. Comparisons show that results of numerical simulation and experimental measurement are quite close in terms of movement of moisture in the dam body, predicted critical slip surface and time to failure of the dam body.

Chapter 5

Dam Surface Erosion and Flow Modeling

5.1 Introduction

Landslide dam which may form suddenly and fail rapidly pose unpredictable threats to human life and infrastructure. Considerable work has been done in the past (and continues today) to predict breach formation for embankment dam. However, mathematical models available so far for landslide dam failure are few. Different methods available to predict peak discharge and outflow hydrograph due to overtopping can be classified (according to Manville, 2001) as empirical methods, parametric methods, dimensionless analysis and physically based models. Empirical methods and dimensionless techniques are simple and rapid method to determine approximate peak discharge and outflow hydrograph. Brief introduction of these methods and details of physically based two dimensional flow overtopping and erosion model are described in this section.

Empirical Relationships

Many empirical relationships are derived to determine peak discharge from dataset of historic dam failures for landslide, glacier, moraine and earth and rock-fill dam. Regression equations that relate peak discharge of landslide dam failure to some measure of impounded water volume such as depth, volume, or some combination thereof are shown in Table 5.1.

Tabata et al. (2002) developed an empirical equation to predict peak discharge from landslide dam failure based on experimental peak discharge observed in the flume experiments.

$$q_p = 0.542 \times q_{in} \times \left\{ \frac{\left(g \times D^3\right)^{0.5}}{\tan\alpha \times q_{in}} \right\}^{0.565} \tag{5.1}$$

where, q_p is the peak outflow discharge per unit width, q_{in} is the inflow discharge per unit width, α is the torrent bed gradient, g is the gravitational acceleration and D is the height of the landslide dam.

Table 5.1 Empirical relationships for estimation of peak discharge in landslide dams

Regression Equation	Dataset	R^2	S.E. (%)	Reference
$Q_p = 0.0158(PE)^{0.41}$	12	0.81	185	Costa & Schuster 1988
$Q_p = 672(V_o/10^6)^{0.56}$	10	0.73	142	Costa 1985
$Q_p = 6.3 d_l^{1.59}$	10	0.74	147	Costa 1985
$Q_p = 181(d_l V_o/10^6)^{0.43}$	10	0.76	129	Costa 1985
$Q_p = 1.6 V_o^{0.46}$	19	0.73		Walder & O'Connor 1997
$Q_p = 6.7 d_l^{1.73}$	19	0.53		Walder & O'Connor 1997
$Q_p = 0.99(d_l V_o)^{0.40}$	19	0.76		Walder & O'Connor 1997

Note: Q_p = Peak discharge (m^3/s), V_o = volume released (m^3), d_l = drop in water level (m), PE = Potential energy (joules) = dam height (m) * volume (m^3) * specific weight of water (9800 N/m^3), R^2 = Coefficient of determination, S.E. = standard error

Dimensionless analysis

Walder and O'Connor (1997) revised statistical relations (derived from data for past constructed and natural dam failures) between peak discharge (Q_p) and water volume released (V_o) or drop in lake level (d_l) considering breach growth rate, breach geometry (width to depth ratio and sidewall slope) and lake hypsometry on the peak discharge. Analysis of a simple, physically based model of dam-breach formation show that the hydrograph at the breach depends primarily on a dimensionless parameter:

$$\eta_d = \frac{kV_o}{g^{0.5} d_l^{3.5}} \tag{5.2}$$

where, k is the mean erosion rate of the breach and g is acceleration due to gravity.

The functional relationship between Q_p and η_d takes asymptotically distinct forms depending on whether $\eta_d << 1$ (relatively slow breach formation or small lake volume) or $\eta_d >> 1$ (relatively fast breach formation or large lake volume).

They proposed different curves for dimensionless peak discharge $\left(Q_p^*\right)$ versus dimensionless parameter (η_d) with different variables such as breach shape factor (r), breach side slope (θ_b), lake shape factor (m), drop in lake level as fraction of initial lake level (ξ) based on theoretical model for the case in which the dam fails by overtopping when water level equals the height of the dam and breach then cut to the base of dam. Similar curve for dam failure by piping was also proposed for variable initial water level as fraction of dam height (ζ).

Using three parameters an approximate outflow hydrograph from a dam breach can be predicted. The parameters are drop in water level, d_l (typically 50-100% of the dam height), water volume released (V_o) and erosion rate, k (typically 10-100m/hr). η_d can be determined using Equation 5.2 and following equations can be used to determine peak discharge and time to peak flow:

For $\eta_d < 0.6$

$$Q_p = 1.51\left(g^{0.5} {d_l}^{2.5}\right)^{0.06}\left(\frac{kV_o}{d_l}\right)^{0.94} \tag{5.3}$$

For $\eta_d > 5$

$$Q_p = 1.94 g^{0.5} {d_l}^{2.5}\left(\frac{D_c}{d_l}\right)^{3/4} \tag{5.4}$$

For $0.6 < \eta_d < 5$

Q_p^* may be read off the appropriate curve purposed by Walder and O'connor (1997) or approximately calculated as (for r = 2.5, θ_b = 35°, m = 2):

$$Q_p^* = 2.307 + \frac{1.191}{\eta_d^{0.5}} \tag{5.5}$$

Then Q_p may be determined from following equation

$$Q_p = g^{0.5} {d_l}^{2.5} Q_p^* \tag{5.6}$$

The time to peak flow t_p can be calculated using the following asymptotic relations:

For $\eta_d << 1$

$$t_p = 1.24\left(\frac{V_o}{k^2 (g d_l)^{0.5}}\right)^{1/3} \tag{5.7}$$

For $\eta_d >> 1$

$$t_p = \frac{d_l}{k} \tag{5.8}$$

An approximate breach hydrograph, assumed to be triangular, may then be constructed with a peak value Q_p at time t_p and a termination at an elapsed time of $2V_o / Q_p$.

Although dimensionless technique has advantage of rapid prediction of peak discharge, this method does not consider the role of breach width.

5.2 Two-dimensional dam surface erosion and flow modeling

5.2.1 Introduction

Almost all existing model assumes a breach location at center within a dam (Mohamed et al., 2002). However, overtopping failure may occur near bank of river valley. Hence, the breach growth and outflow from a centrally located breach is likely to be different from a side breach in terms of time to peak discharge, peak value, and hydrograph shape. In such cases, two dimensional models (2D) are essential.

There are only a few two 2D numerical models for dam-break erosion by overtopping flow. Takahashi and Nakagawa (1994) used 2D model to predict flood/debris flow hydrograph due to natural dam failure caused by overtopping. Broich (1998) used 2d model using different numerical schemes for shallow water equations, Exners equation and sediment transport formulae. Unrealistic modeling of the vertical and lateral erosion, no stability mechanism, and parabolic breach shape are the some limitations of this model (Morris and Hassan, 2002).

The mathematical model developed by Takahashi and Nakagawa (1994) was used for the modeling of surface erosion and flow. The model was capable to analyse the whole phenomena from the beginning of overtopping to the complete failure of the dam as well as to predict flood/debris flow hydrograph in the downstream. The infiltration in the dam body was not considered in their model; therefore, time to overflow after formation of landslide dam could not be predicted from the previous model. In this study, infiltration in the dam body is also incorporated.

The proposed model is two-dimensional and it can also collapse to treat one-dimensional for overtopping from full channel width. In case of sudden sliding failure, simplified assumption is made for initial transformation of the dam body after the slip failure. Based on many experiments the slipped mass is assumed to stop at the sliding surface where slope is less than angle of repose and the shape of the slipped mass is assumed as trapezium. There is some time lag between slip failure and movement of the slipped soil mass but the time necessary for such a deformation is assumed as nil in the model. The erosion process by the overspilled water is analysed for the modified dam shape.

The erosive action of the overtopping flow removes material from the top part of the dam. The overtopped flow grows to debris flow by adding the eroded dam material in it, if the slope and length of dam body satisfy the critical condition for the occurrence of a debris flow.

5.2.2 Governing equations

The main governing equations are briefly discussed here. The depth-wise averaged two-dimensional momentum conservation equation for the x-wise (down valley) direction is

$$\frac{\partial M}{\partial t} + \beta' \frac{\partial (uM)}{\partial x} + \beta' \frac{\partial (vM)}{\partial y} = gh \sin\theta_{bxo} - gh \cos\theta_{bxo} \frac{\partial (h + z_b)}{\partial x} - \frac{\tau_{bx}}{\rho_T} \tag{5.9}$$

and for the y-wise (lateral) direction,

$$\frac{\partial N}{\partial t} + \beta' \frac{\partial (uN)}{\partial x} + \beta' \frac{\partial (vN)}{\partial y} = gh \sin\theta_{byo} - gh \cos\theta_{byo} \frac{\partial (h + z_b)}{\partial y} - \frac{\tau_{by}}{\rho_T} \tag{5.10}$$

The continuity of the total volume is

$$\frac{\partial h}{\partial t} + \frac{\partial M}{\partial x} + \frac{\partial N}{\partial y} = i\{c_* + (1 - c_*)s_b\} - q \tag{5.11}$$

The continuity equation of the particle fraction is

$$\frac{\partial (ch)}{\partial t} + \frac{\partial (cM)}{\partial x} + \frac{\partial (cN)}{\partial y} = ic_* \tag{5.12}$$

The equation for the change of bed surface elevation is

$$\frac{\partial z_b}{\partial t} + i = i_{sml} + i_{smr} \tag{5.13}$$

where $M = uh$ and $N = vh$ are the x and y components of flow flux, u and v are the x and y components of mean velocity, h is the flow depth, z_b is the elevation, ρ_T is the apparent density of the flow, $\rho_T = c(\sigma - \rho) + \rho$, c is the volume concentration of the solids fraction in the flow, σ is the density of the solids, ρ is the density of water, β' is the momentum correction coefficient, τ_{bx} and τ_{by} are the x and y components of resistance to flow, i is the erosion (> 0) or deposition velocity (< 0), c_* is the solids fraction in the bed, s_b is the degree of saturation in the bed (applicable only in cases of erosion, when deposition takes place substitute $s_b = 1$), i_{sml} and i_{smr} are the mean recessing velocity of the left and right hand side banks of the incised channel, respectively, t is the time, g is the acceleration due to gravity and q is the infiltration rate.

According to Takahashi (1991), the flow can be divided into three categories based on sediment concentration in the flow: (a) stony debris flow, (b) immature debris flow and (c) turbulent flow. Different flow resistance equations are proposed for different types of flow. The flow is called stony debris flow when the volume concentration of the solids fraction in the flow (c) is more

than 40% of the volume concentration in the bed (c_*) i.e. $c > 0.4c_*$. In stony type debris flow, the laminarly moving particles are dispersed in the entire flow depth when the channel slope is steeper than about 9°. The flow is called immature debris flow if the volume concentration of the solids is larger than 1% and smaller than 40% of c_*. In immature debris flow (channel slope flatter than 9°), the sediment mixture layer can occupy only the lower part of the entire depth of the flow. If the volume concentration of the solid is less than 1%, the flow is called turbulent flow and the sediment flow regime is bed load or suspended load. If the downstream slope of the dam is steeper than 9° and the dam composing material is course the early stage of the overtopping flow may form the stony-inertial debris flow, with the progress of erosion dam slope flattens to generate the immature debris flow and then the ordinary flood flow.

Shear stress, erosion or deposition velocity and channel enlargement for overtopping from partial channel width were evaluated using the model presented in Takahashi and Nakagawa (1994).

Shear stress equations

The resistance at the bottom τ_{bx} and τ_{by} are described for different types of flow as follows:

For stony-type debris flow

$$\tau_{bx} = \frac{1}{8}\left(\frac{d_p}{h}\right)^2 \sigma\lambda^2 u\sqrt{u^2+v^2} = \frac{\rho_T}{8}\left(\frac{d_p}{h}\right)^2 \frac{u\sqrt{u^2+v^2}}{\{c+(1-c)\rho/\sigma\}\{(c_*/c)^{1/3}-1\}^2} \tag{5.14}$$

$$\tau_{by} = \frac{1}{8}\left(\frac{d_p}{h}\right)^2 \sigma\lambda^2 u\sqrt{u^2+v^2} = \frac{\rho_T}{8}\left(\frac{d_p}{h}\right)^2 \frac{v\sqrt{u^2+v^2}}{\{c+(1-c)\rho/\sigma\}\{(c_*/c)^{1/3}-1\}^2} \tag{5.15}$$

For immature debris flow

$$\tau_{bx} = \frac{\rho_T}{0.49}\left(\frac{d_p}{h}\right)^2 u\sqrt{u^2+\upsilon^2} \tag{5.16}$$

$$\tau_{by} = \frac{\rho_T}{0.49}\left(\frac{d_p}{h}\right)^2 v\sqrt{u^2+\upsilon^2} \tag{5.17}$$

For ordinary flow (bed load transportation)

$$\tau_{bx} = \frac{\rho g n^2 u\sqrt{u^2+\upsilon^2}}{h^{1/3}} \tag{5.18}$$

$$\tau_{by} = \frac{\rho g n^2 v\sqrt{u^2+\upsilon^2}}{h^{1/3}} \tag{5.19}$$

where n is the Manning's roughness coefficient and d_p is the mean diameter of particles.

Erosion equations

The bed erosion in the incised channel proceeds under unsaturated bed condition and it continues as long as the entrained-solids concentration in the flow is less than the equilibrium value. Therefore, the equation of bed erosion velocity for unsaturated bed may be written as

$$\frac{i}{\sqrt{gh}} = K_e \sin^{3/2}\theta\left\{1-\frac{\sigma-\rho}{\rho}c\left(\frac{\tan\phi}{\tan\theta}-1\right)\right\}^{1/2}\cdot\left(\frac{\tan\phi}{\tan\theta}-1\right)\left(c_{eq}-c\right)\frac{h}{d_p} \tag{5.20}$$

where ϕ is the internal friction angle of the bed, K_e is the parameter of erosion velocity and c_{eq} is the equilibrium solids concentration defined by the following equations.

$$c_{eq} \equiv c_\infty = \frac{\rho\tan\theta}{(\sigma-\rho)(\tan\phi-\tan\theta)} \tag{5.21}$$

If the slope is steeper than about 9 degrees and $c_{s\infty}$ by Equation 5.22 calculates the value less than c_∞

$$c_{eq} \equiv c_{s\infty} = 6.7c_\infty^2 \tag{5.22}$$

and for the slope on which $c_{s\infty}$ by Equation 5.22 count less than 0.01, c_{eq} should be obtained by using appropriate bed load equation. The value of $\tan\theta$ in the above equations is the energy gradient and

$$\tan\theta = \sqrt{\tau_{bx}^2+\tau_{by}^2}\,/\left(\rho_T gh\right) \tag{5.23}$$

The Takahashi's bed load formula (Takahashi, 1987) applicable to a steep slope channel can be used to determine c_{eq} in turbulent flow:

$$\frac{q_b}{\left\{\left(\sigma/\rho-1\right)gd_p^3\right\}^{1/2}} = \frac{1+5\tan\theta}{\cos\theta}\sqrt{\frac{8}{f}}\tau_*^{3/2}\left(1-\alpha_c^2\frac{\tau_{*c}}{\tau_*}\right)\left(1-\alpha_c\sqrt{\frac{\tau_{*c}}{\tau_*}}\right) \tag{5.24}$$

where q_b is the bed load discharge per unit width, τ_* is the non-dimensional shear stress and τ_{*c} is the non-dimensional critical shear stress, α_c is a coefficient and f is the resistance coefficient. The critical shear stress is given by Equation 5.25

$$\tau_{*c} = 0.04\times10^{1.72\tan\theta} \tag{5.25}$$

The α_c and f can be calculated by using Equations 5.26 and 5.27 respectively.

$$\alpha_c^2 = \frac{2\{0.425 - \sigma \tan\theta/(\sigma - \rho)\}}{1 - \sigma \tan\theta/(\sigma - \rho)} \tag{5.26}$$

$$\sqrt{\frac{8}{f}} = \begin{cases} A + 5.75\log\left[\dfrac{(\sigma/\rho - 1)\tau_*}{\tan\theta(1 + 2\tau_*)}\right] & ; \quad \tau_* \geq 2 \\ A + 5.75\log\left[\dfrac{0.2(\sigma/\rho - 1)}{1.4\tan\theta}\right] & ; \quad \tau_* < 2 \end{cases} \tag{5.27}$$

where

$A = 0.04\tan^{-2}\theta$; $\tan\theta \geq 0.08$

$A = 6$; $\tan\theta < 0.08$

The relationship between f and Manning's roughness coefficient (n) is:

$$n = \left(\frac{f}{8g}\right)^{1/2} h^{1/6} \tag{5.28}$$

From Equations 5.24 through 5.28, the equilibrium solids concentration in the case of bed load transport is given by:

$$c_{b\infty} = q_b / q_T \tag{5.29}$$

The value of θ in Equations 5.24 to 5.27 is considered as the gradient of flow surface to the direction of velocity vector and is given by:

$$\tan\theta = \frac{u\sin\theta_{bx}^{'} + v\sin\theta_{by}^{'}}{\sqrt{u^2\cos^2\theta_{bx}^{'} + v^2\cos^2\theta_{by}^{'}}} \tag{5.30}$$

where,

$\tan\theta_{bx}^{'} = \tan(\theta_{bx0} + \theta_{bzhx})$; $\tan\theta_{by}^{'} = \tan(\theta_{by0} + \theta_{bzhy})$

$\tan\theta_{bzhx} = \dfrac{-\partial(z_b + h)}{\partial x}$; $\tan\theta_{bzhy} = \dfrac{-\partial(z_b + h)}{\partial y}$

Deposition equations

If the flow on the dam body develops to a stony type debris flow and it comes down to the flat area, it begins to decelerate and then it starts to deposit when the velocity becomes pu_e $(p < 1)$, in which u_e is the equilibrium velocity defined by

$$U_e = \frac{2}{5d_p}\left(\frac{g\sin\theta_e}{0.02}\left\{c+(1-c)\frac{\rho}{\sigma}\right\}\right)^{1/2}\left\{\left(\frac{c_*}{c}\right)^{1/3}-1\right\}h^{3/2} \tag{5.31}$$

where θ_e is the slope on which concentration c is in equilibrium; therefore, $\tan\theta_e$ is given by substituting c into c_∞ in Equation 5.21

$$\tan\theta_e = \frac{c(\sigma-\rho)\tan\phi}{c(\sigma-\rho)+\rho} \tag{5.32}$$

The deposition velocity equation which takes account such inertial motion is given by

$$i = \delta_d\left(1-\frac{\sqrt{u^2+v^2}}{pu_e}\right)\frac{c_\infty - c}{c_*}\sqrt{u^2+v^2} \tag{5.33}$$

If the flow is immature debris flow or ordinary water flow, the inertial motion may be neglected and

$$i = \delta_d\,\frac{c_{eq}-c}{c_*}\sqrt{u^2+v^2} \tag{5.34}$$

where δ_d is a constant and if in Equation 5.33 $\sqrt{u^2+v^2} > pu_e$, $i = 0$.

Lateral erosion equations

Lateral erosion velocity is assumed as a function of the shear stress on the side wall assigned by the interstitial fluid of the overlying sediment-laden flow, τ_{sf}. The value of τ_{sf} is then assumed as the half of the bed shear stress τ_f. One may write the recession velocity of the wetted sidewall under the surface of the flow i_s as

$$\frac{i_s}{\sqrt{gh}} = \left(\frac{1}{2}\right)^{3/2} K_{es}\sin^{3/2}\theta\left\{1-\frac{\sigma-\rho}{\rho}c\left(\frac{\tan\phi}{\tan\theta}-1\right)\right\}^{1/2}\cdot\left(\frac{\tan\phi}{\tan\theta}-1\right)(c_{eq}-c)\frac{h}{d_p} \tag{5.35}$$

where K_{es} is a constant.

By recession of the wetted sidewall, the part of the wall upward of the surface of the flow may lose its stability and fall into the flow. If one assumes the recession of the whole sidewall is parallel as shown in Figure 5.1, the mean recession velocity of the side walls would be

$$i_{sml} = \frac{h_l}{l_l+h_l}i_{sl} \quad , \quad i_{smr} = \frac{h_r}{l_r+h_r}i_{sr} \tag{5.36}$$

The finite difference calculation of the system of equations referred to above on the two dimensional rigid grid system set on the horizontal plane requires a little contrivance, because on such grid the channel can enlarge its width only discretely in spite of the actual continuous

widening. To overcome this problem, one may assume that the sediment produced by the recession of banks, e.g. $i_{smr}(z_{bs} - z_b)\Delta t$, is supplied only to the cell adjacent to the bank, e.g. cell **A** in Figure 5.1, and it instantaneously raises the elevation of that cell to be eroded by the flow in the channel in the next time step. The channel width is considered not to be changed until the total volume of the sediment supplied, for example, to the cell **A** becomes equal to the volume of the sediment in the side bank cell at the beginning of the side bank erosion, t_0. At the moment when the two respective volumes of sediment become equal, the channel is considered to be widened by one cell width and the bottom elevation of the new cell adjacent to the new bank is set to be equal to that of the former adjacent cell at time t_0. The formulation of the procedure is as follows:

$$\int_{t_0}^{t} i_{sr} h_r \Delta x dt = \left(z_{bs} + z_{s0} - z_b - z_0\right)\Big|_{t=t_0} \Delta x \Delta y \quad \Rightarrow \quad z_b = z_b\Big|_{t=t_0} \tag{5.37}$$

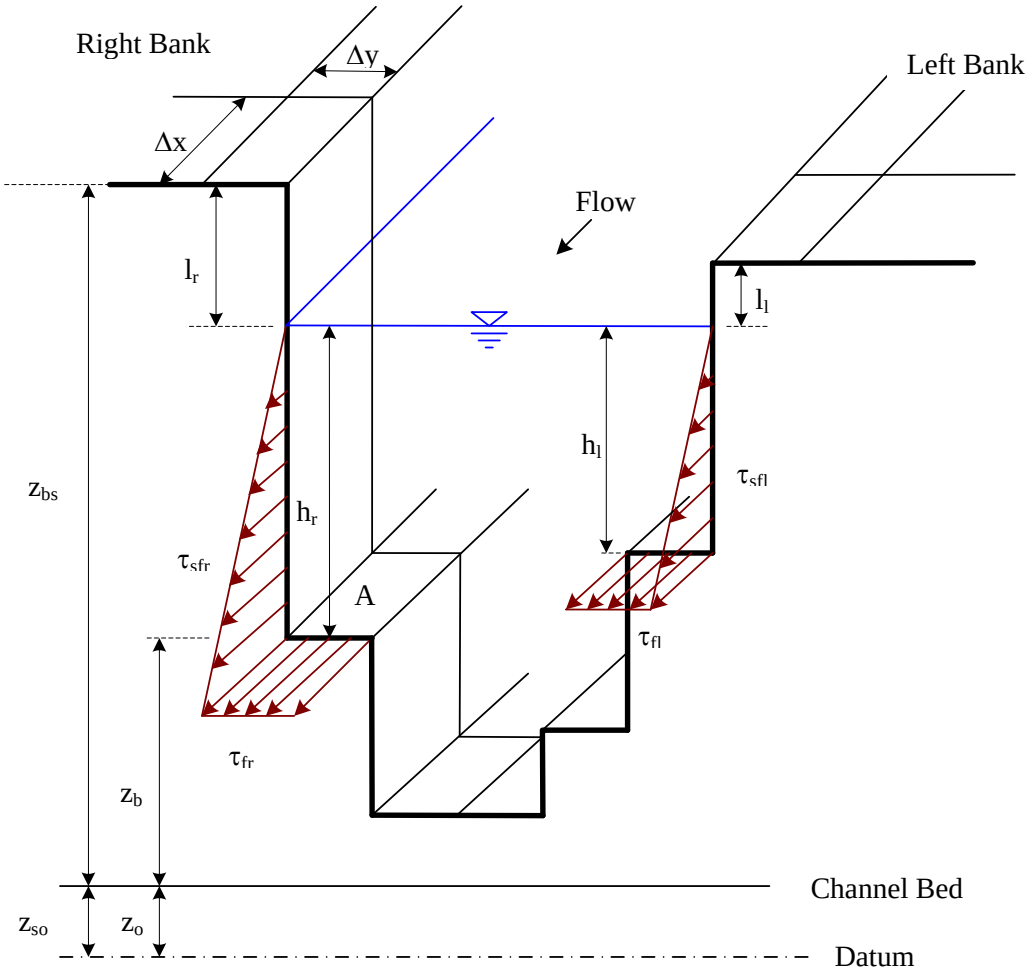

Figure 5.1 A cross-section of the incised channel on a dam

5.2.3 Coupling with seepage flow model

The coordinate system used for dam surface erosion and flow model is different from seepage flow model. In dam surface erosion flow model, x-axis is parallel to the channel bed and the depth and cross section measured perpendicular to the bed whereas in seepage flow model x-axis is horizontal and the depth is measured vertically. Thus, inclined flow depth calculated by dam surface erosion and flow model is changed to vertical flow depth to use boundary condition in seepage flow model.

Coupling of dam surface erosion and flow model and seepage flow model can be made by imposing boundary condition in seepage flow model. The flow depth calculated by dam surface erosion and flow model is used as boundary condition in the grid cell of seepage flow model expose to water surface as a known head boundary. Grid system of seepage flow model and dam surface erosion and flow model is shown in Figure 5.2. Infiltration rate, q in Equation 5.11 is calculated by averaging infiltration rate of number of cells exposed to water between $x = i$ to $x = i + 1$.

Infiltration rate in each cell is calculated using following equation:

$$q_k = K\left(\frac{\partial h}{\partial z_{sh}} + 1\right)_{top} + K\left(\frac{\partial h}{\partial x_{sh}}\right)_{left} + K\left(\frac{\partial h}{\partial x_{sh}}\right)_{right} \tag{5.38}$$

where, q_k is infiltration rate of cell j, K is the hydraulic conductivity, h is pressure head, dz_{sh} and dx_{sh} are the unit grid dimension of seepage flow model in vertical and horizontal direction.

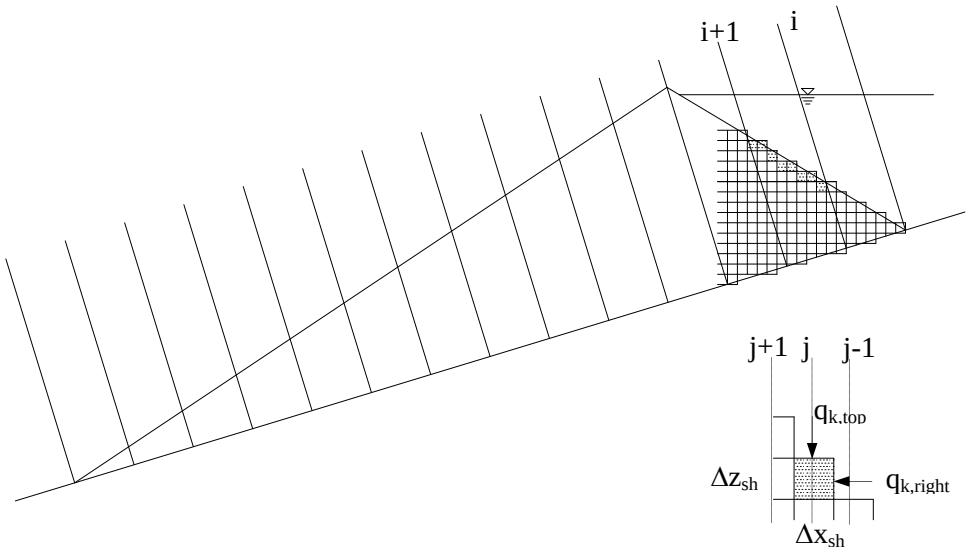

Figure 5.2 Grid system of seepage flow model and dam surface erosion and flow model

5.2.4 Verification of model with experiments

Laboratory Experiments

The schematic diagram of the flume is shown in Figure 2.1. The slope of the flume was set at 17, 10 and 5 degrees. Sediment, Mix 1-7 was used to prepare triangular dam in the flume. The height of the dam was 20cm and the longitudinal base length was 84cm for channel slope 17 and 10 degree whereas 90cm for 5 degree. van Genuchten parameters and other parameters of mixed sand, Mix 1-7, listed in Table 2.1 were used. Measured saturated hydraulic conductivity, K_s in different experiment varies but average of 0.00018m/sec was used. The K_s value is smaller compared to other cases because initial moisture content used to make dam body is higher and degree of compaction is different from other cases.

The shape of the dam body at different time step due to surface erosion after overtopping were measured by analyses of video taken from the flume side. The outflow hydrograph at the outlet of channel was measured. The flow discharge was calculated by measuring water level by using servo type water level gauge in the tank at the outlet of flume. Sediment discharge was determined by measuring submerged weight of sediment collected in the container with the help of load cell.

Table 5.2 Summary of experiments

Expt. No.	Case	Flume Slope	Moisture content	Discharge (cm^3/s)	Dam size in cm			Remarks
					Ht.	U/S L	D/S L	
(I) Overtopping from full channel width								
1	OFCW17	17	50 %	550	20	18	66	
2	OFCW10	10	47 %	550	20	18	66	
3	OFCW05	5	42 %	530	20	24	66	
(II) Overtopping from partial channel width								
4	OPCW17	17	50 %	49	20	18	66	
5	OPCW10-1	10	43 %	98	20	18	66	No data of load cell
6	OPCW10-2	10	45 %	99	20	18	66	Simulated case
7	OPCW10-3	10	15.7%	99	20	18	66	
8	OPCW05-1	5	45 %	201	20	24	66	Simulated case
9	OPCW05-2	5	15.7%	203	20	24	66	

Results and discussions

Numerical simulations and flume experiments were performed to investigate the mechanism of landslide dam failure and resulting hydrograph due to overtopping and channel breach. Table 5.2 summarizes the geometry of the dams and hydraulic conditions used in different experimental cases. The parameters and the grid systems used in the calculation are K_e = 0.11, $K_{es} = 1$, δ_d = 0.05, c_* = 0.655, σ = 2.65g/cm^3, d_p = 1mm, Δx = 60mm, Δy = 6.25mm and $\Delta t = 0.002$ sec.

The model simulation and experimental results are divided into two cases. The results were analysed to study the model performance.

Case I: Overtopping (from full channel width)

Steady discharge as shown in Table 5.2 for different cases was supplied from the upstream part of the flume. The model started simulation after the start of inflow. Overtopping occurred after the filling of the reservoir. Overtopped water proceeds downstream eroding the crest as well as the downstream slope of the dam body.

The simulated and experimental outflow hydrograph at 66cm downstream of the dam are represented in Figures 5.3, 5.5 and 5.7 for channel slope 17, 10 and 5 degrees respectively. Transformation of the dam body with time is shown in Figures 5.4, 5.6 and 5.8 for channel slope 17, 10 and 5 degrees respectively. The shape of the simulated surface of the dam body at each time steps are similar to observed. The shape of the simulated hydrograph is similar to measured outflow hydrograph however they are not matching perfectly. Time of overtopping for simulations and experiments are slightly different in all cases. Simulated hydrographs are the plot of averaged (for some time period) instantaneous discharge whereas measured hydrographs are the average discharge of 2 sec time period. The outflow hydrographs are determined by measuring water level in the tank at the outlet of the flume. When the flow suddenly drops in the tank the water level slightly fluctuates even if precautionary measures are employed such as baffle, number of filter layers etc. These factors also affect the simulated and measured outflow hydrographs.

Channel Slope: 17 degree

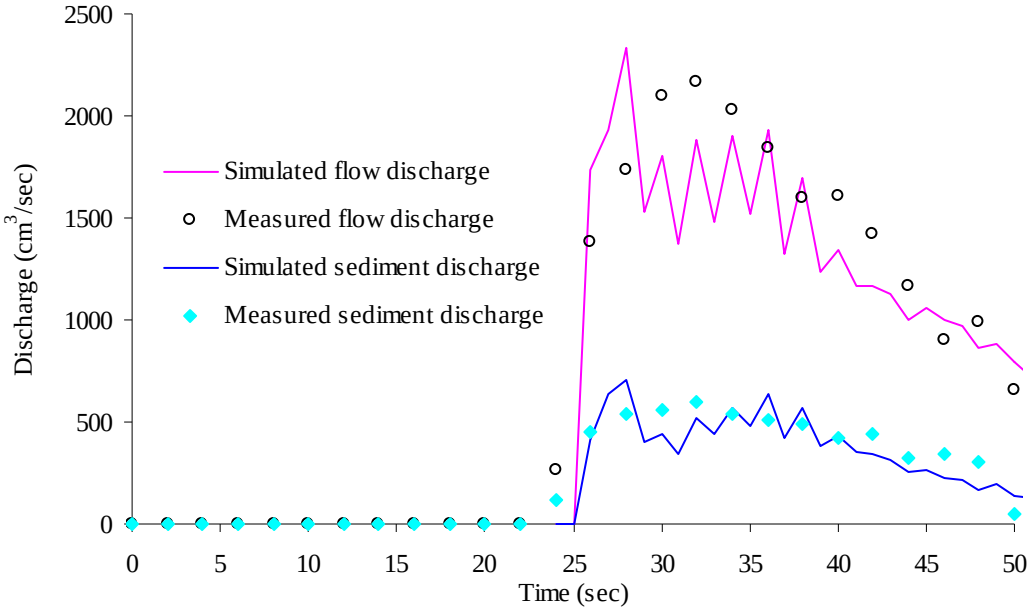

Figure 5.3 Outflow hydrograph (channel slope = 17^{o})

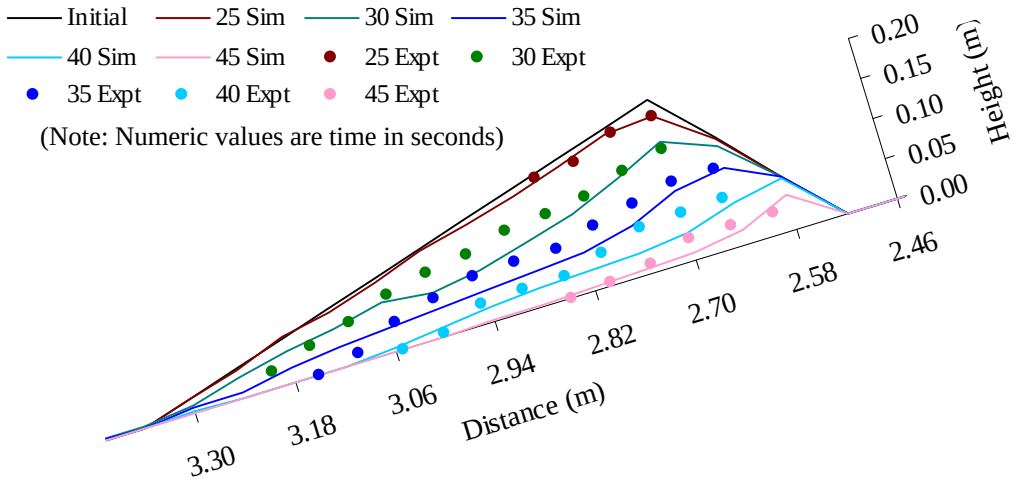

Figure 5.4 Comparison of dam surface erosion (channel slope = 17^{o})

Channel Slope: 10 degree

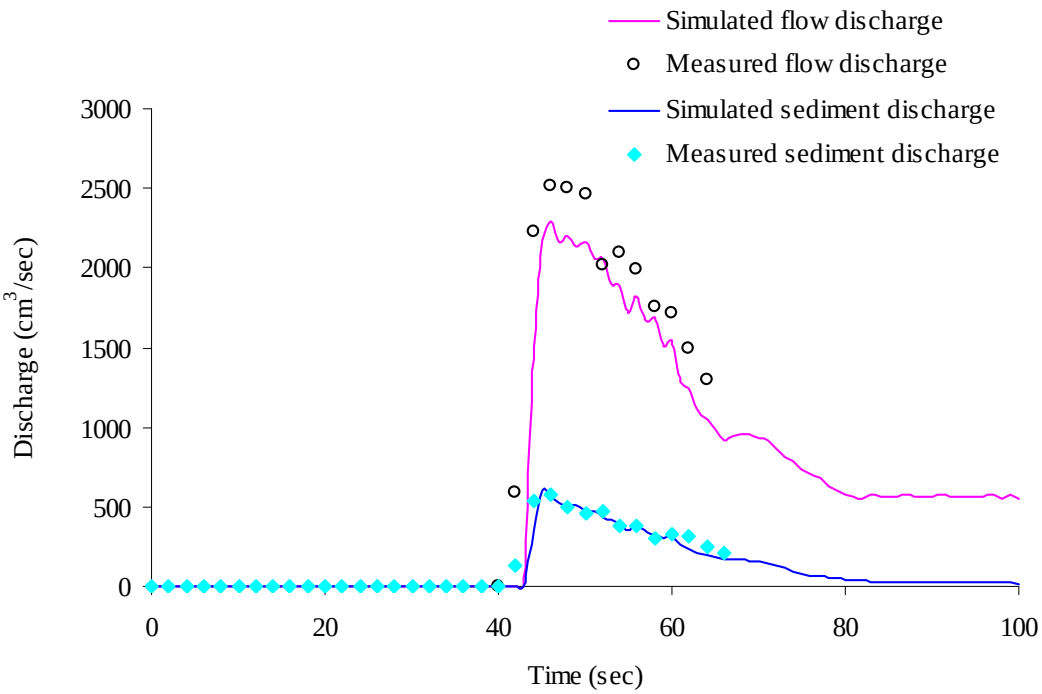

Figure 5.5 Outflow hydrograph (channel slope = 10^{o})

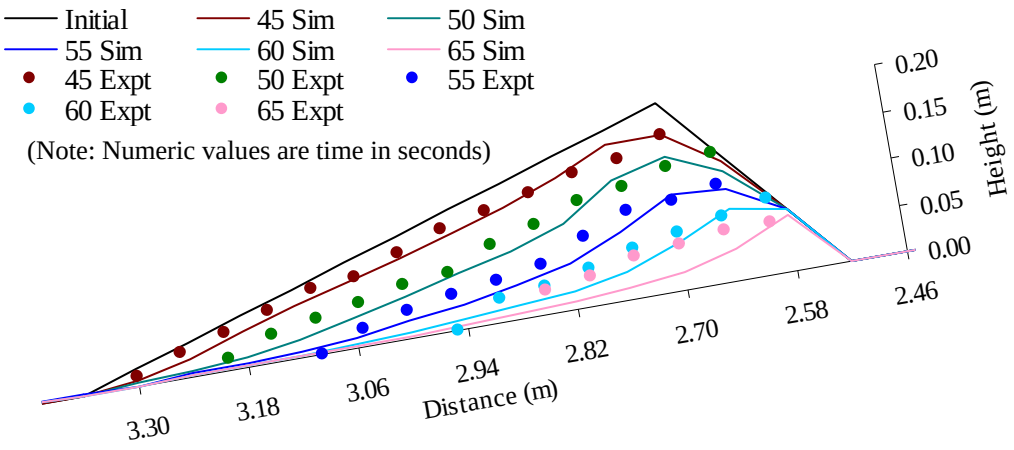

Figure 5.6 Comparison of dam surface erosion (channel slope = 10^{o})

Channel Slope: 5 degree

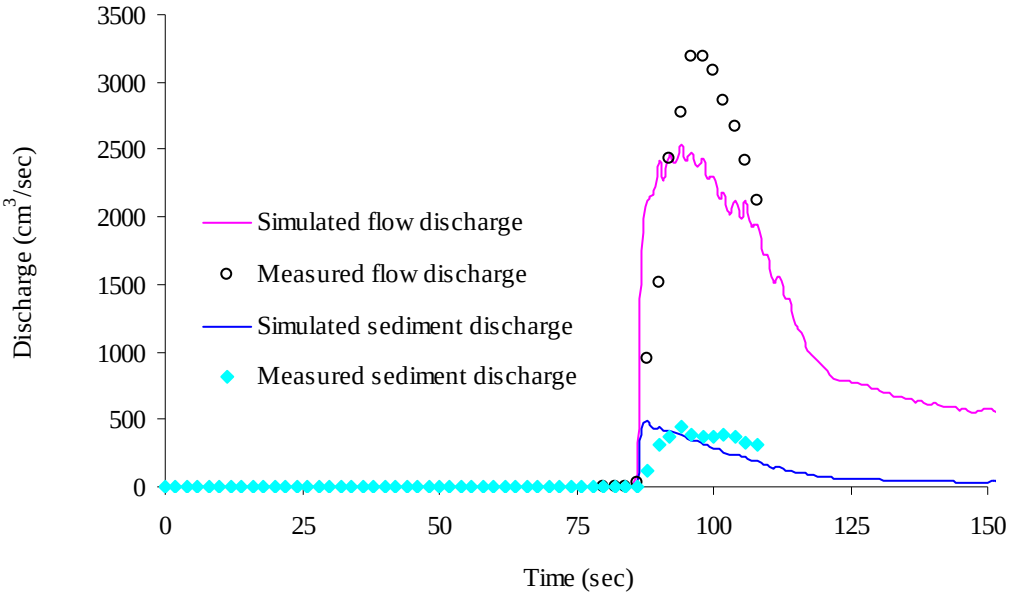

Figure 5.7 Outflow hydrograph (channel slope = 5°)

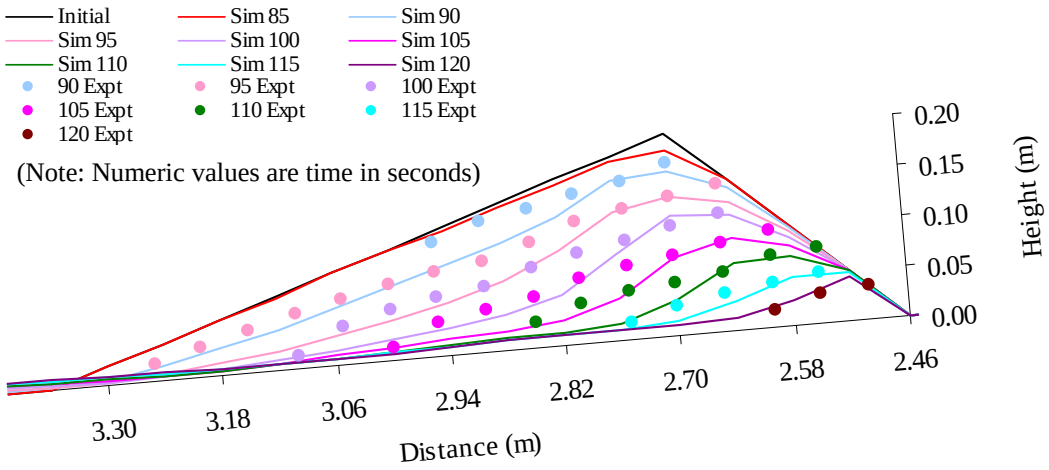

Figure 5.8 Comparison of dam surface erosion (channel slope = 5°)

Case II: Overtopping and channel breach (from partial channel width)

Notch of the width 5cm and depth 0.5cm was incised at the crest and downstream face of the dam in the left side of the dam body so that the erosion of the surface of the dam body can be observed from left side of the flume. Steady discharge as shown in Table 5.2 for different cases was supplied from the upstream part of the flume, after the filling of the reservoir; it overflowed from the notch at the crest of the dam. The overtopping flow incised a channel on the slope of the dam and that channel increased its cross-sectional area with time caused by the erosion of released water. The simulated and experimental outflow hydrographs are represented in Figures 5.9, 5.11 and 5.13 for channel slope 17, 10 and 5 degree respectively. Figures 5.10, 5.12 and 5.14 show the comparison of the simulated and experimental shapes of dam surface at different time steps for channel slope 17, 10 and 5 degree respectively. The simulated outflow hydrographs are similar to experimental.

In the both experiment and simulation the channel incised almost vertically in channel slope 17 degree that may be due to rapid drawdown of reservoir and small inflow rate. The overflowing water depth was very small so the shear stress due to flowing water in the side wall of incised channel was also small. Figure 5.15 shows the simulated cross sectional shape of incised channel at two points, one at the crest of the dam and another at 30cm downstream from the crest. The simulated breach channel widths are larger in flatter channel slopes due to side erosion however slumping of side slope of breached channel occurs at irregular time steps and is depending on condition of flow and material of dam body. During breach formation, breach enlargement proceeded rapidly below the water surface in the breach channel. Above the water level there was some apparent cohesion added by water content and adhesion so the side wall was very steep and undermines the slope. The erosion process continues until slope stability was encountered. Armouring effect was also negligible due to small particle size of the dam body. The peak discharge and width of breached channel depends on inflow discharge and reservoir volume (flume slope). The slope failure of channel bank around crest of the dam is one of the main causes of higher peak discharge (both flow and sediment discharge) in the experiment compared to simulation. Measured outflow hydrograph in different experiments for similar hydraulic condition (Figure 5.11) is different due to uncertainty in material properties (degree of compaction, mixing of sediment etc.) of dam the body.

Channel Slope: 17 degree

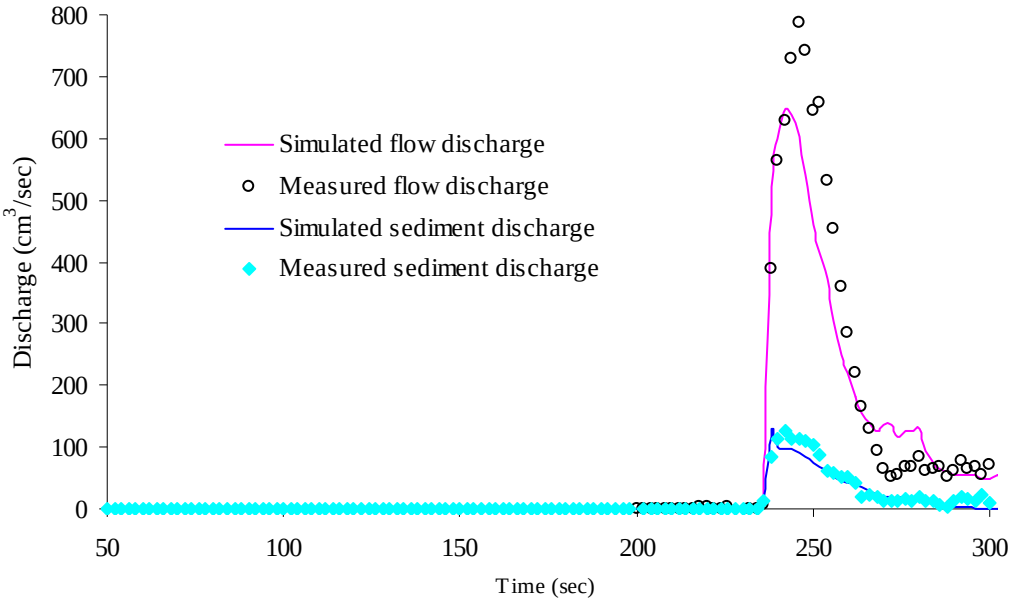

Figure 5.9 Outflow hydrograph (channel slope = 17^{o})

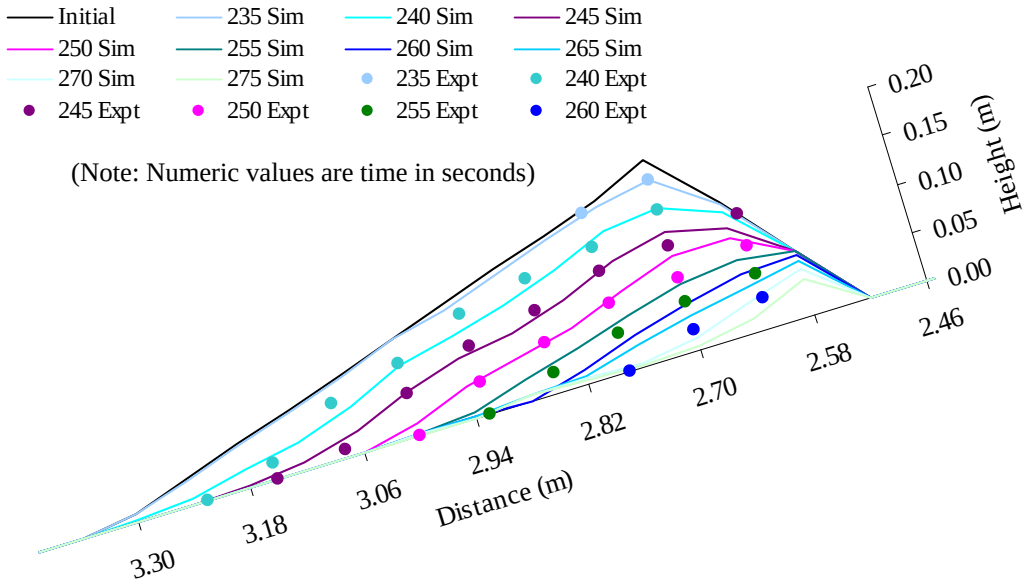

Figure 5.10 Comparison of dam surface erosion at incised channel (channel slope = 17^{o})

Channel Slope: 10 degree

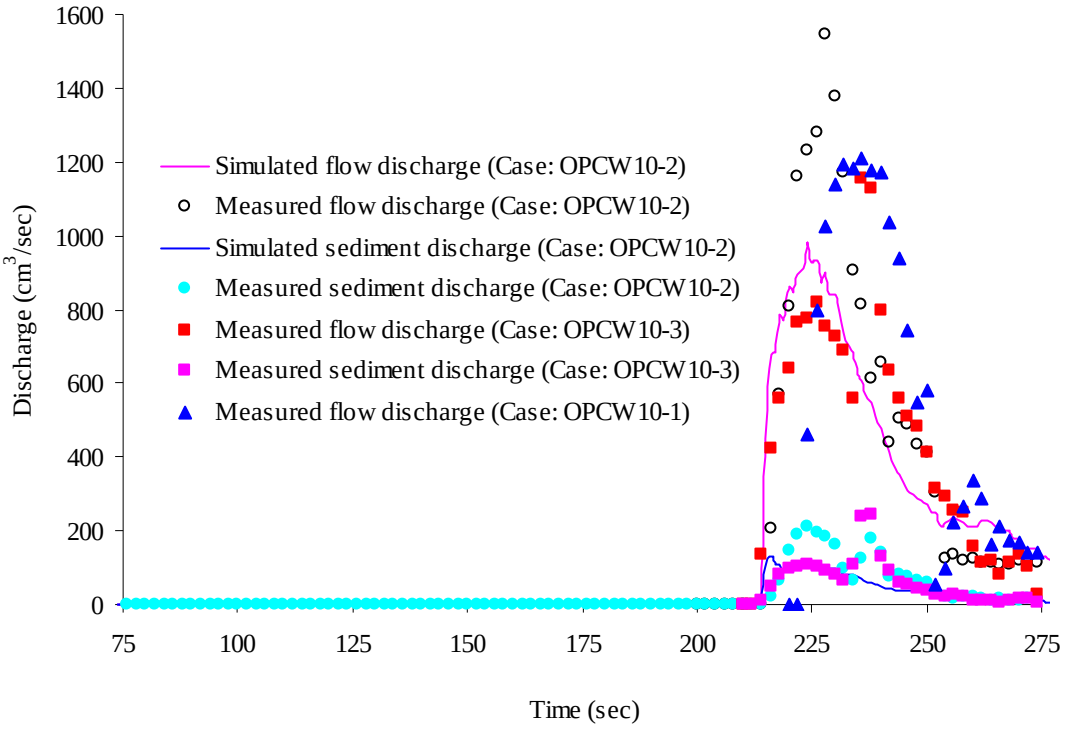

Figure 5.11 Outflow hydrograph (channel slope = 10^{o})

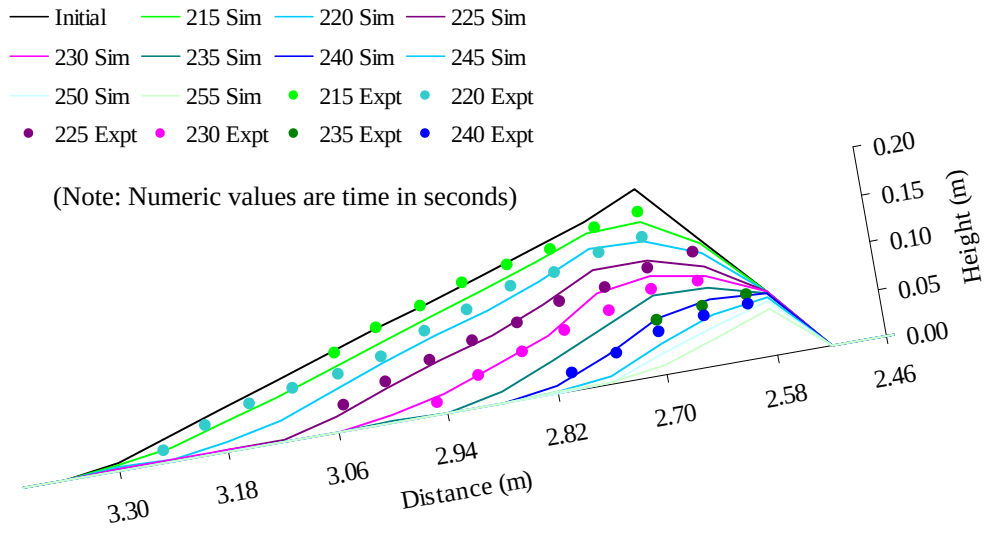

Figure 5.12 Comparison of dam surface erosion at incised channel, (channel slope = 10^{o})

Channel Slope: 5 degree

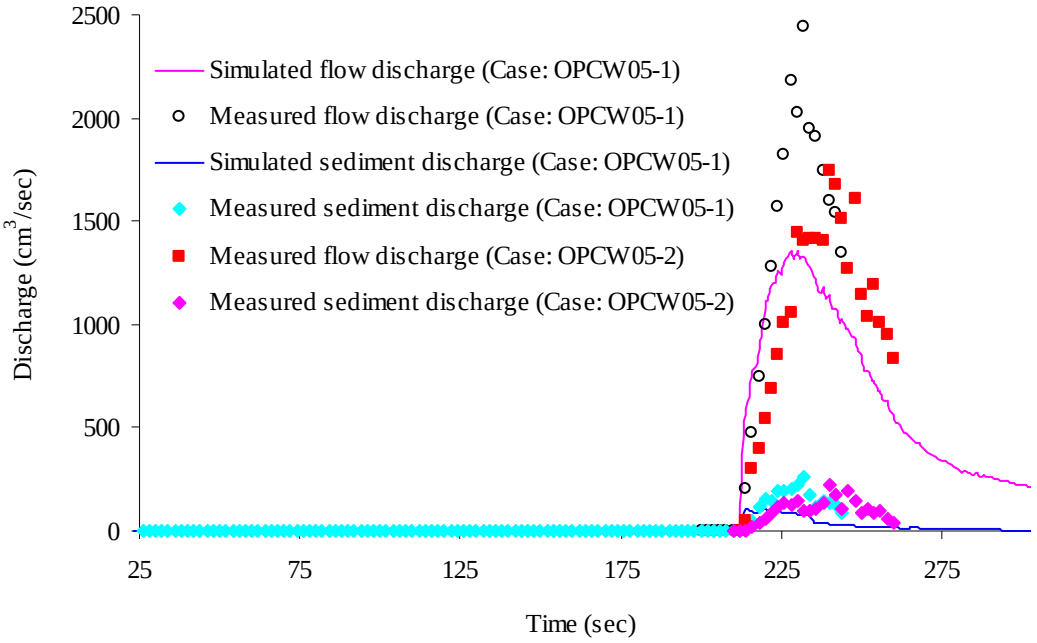

Figure 5.13 Outflow hydrograph (channel slope = 5^{o})

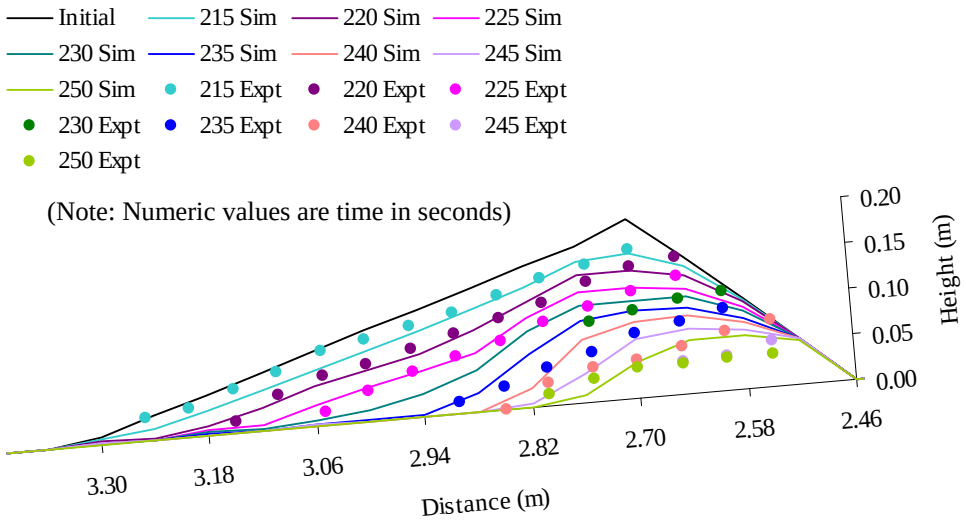

Figure 5.14 Comparison of dam surface erosion at incised channel (channel slope = 5^{o})

(Note: Numeric values are time in seconds)

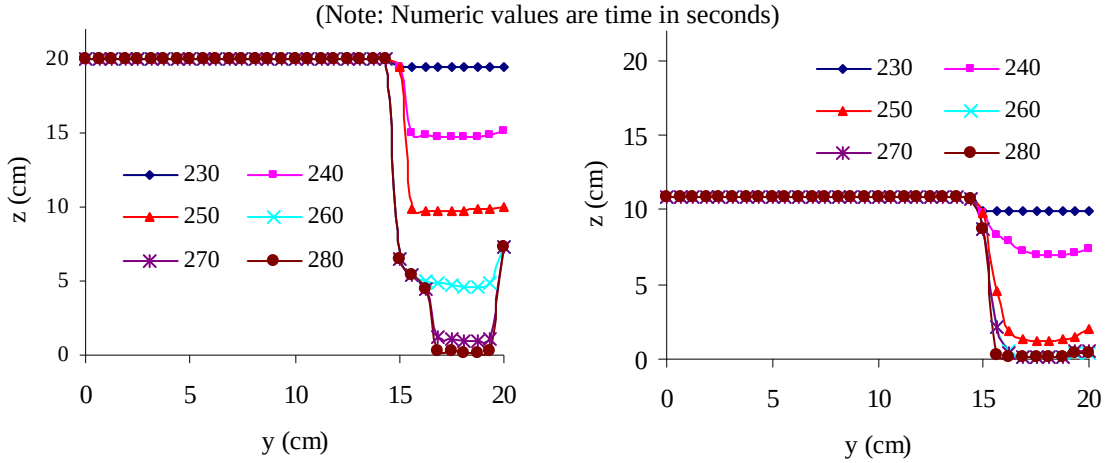

Channel slope = 17°

Channel slope = 17°

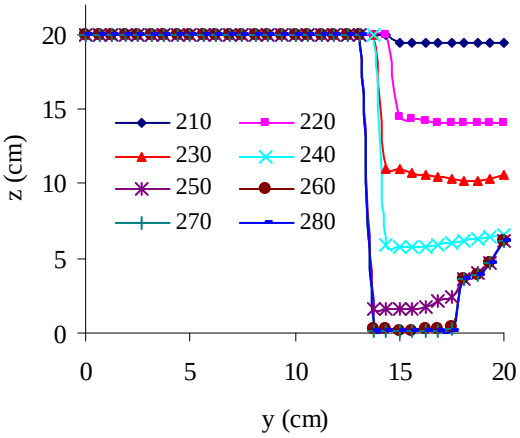

Channel slope = 10°

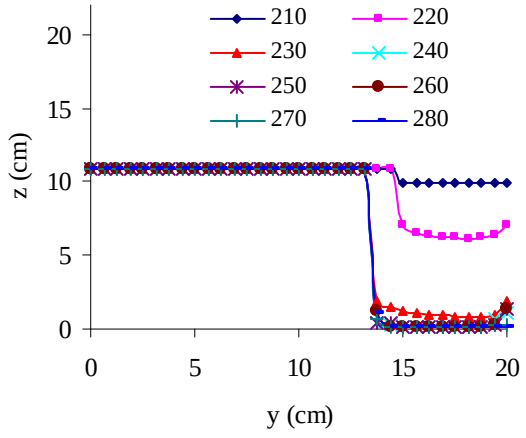

Channel slope = 10°

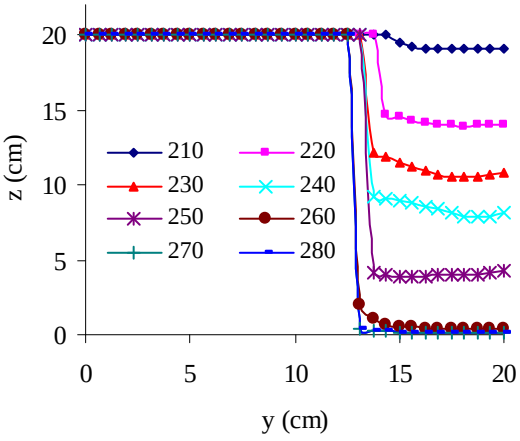

Channel slope = 5°

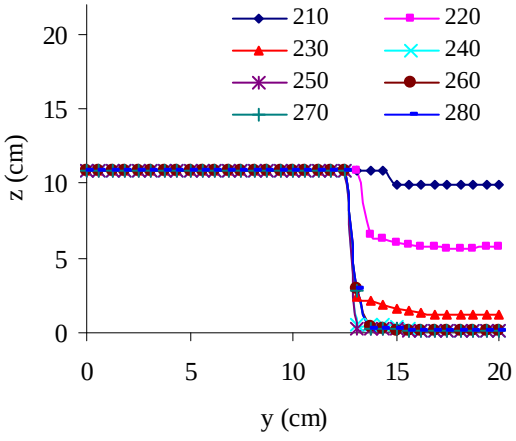

Channel slope = 5°

(a) Cross sectional shape of incised channel at the crest

(b) Cross sectional shape of incised channel at 30cm downstream from the crest

Figure 5.15 Cross sectional shape of incised channel at two sections

Summary

A combined numerical model (dam surface erosion and flow model + seepage flow model) is developed for simulation of outflow hydrograph due to landslide dam failure by overtopping. Many experiments were carried out in different channel slopes for overtopping with full channel width and partial channel width. The proposed model was tested for different experimental cases of landslide dam failure due to overtopping and reasonably reproduced the resulting outflow hydrographs. The simulated overtopping time and dam surface erosion at different time steps are in good agreement with experiments. The simulated breach width depends on inflow and reservoir volume. The incised channel is almost vertical for both simulation and experiments in small inflow discharge and small reservoir volume. In the case of larger inflow discharge and larger reservoir volume, slumping occurred at irregular time steps. The peak discharge is highly influenced by sliding of breached channel bank at crest. The predicted hydrograph can be used for flood disaster mitigation in the downstream. Further application of model is possible to other experiment/actual cases of landslide dam failure.

Chapter 6

Integrated Model to Predict Flood/Debris Flow Hydrograph

6.1 Introduction

The possibility of formation and failure of landslide dam in the mountainous area during heavy rainfall or earthquake events has been the focus of research since last two decades. The prediction of outflow hydrograph and flood routing is essential to mitigate possible losses and damages in the upstream and downstream of landslide dam and to evacuate people in a safe area when a flood event occurs. As already described in Chapter 2 the dam may fail by different failure modes. The peak discharges and shape of outflow hydrographs produced by different failure modes are different in terms of magnitude and shape of hydrographs. Almost all the existing models are just applicable to individual failure modes like, overtopping from full channel width, overtopping from partial channel breach and piping. If we can integrate principles of hydrology, hydraulics, sediment transport, soil mechanics, the geometry and material properties of the dam and the reservoir properties, we can predict failure mode and outflow hydrograph accordingly. In this context, an attempt has been made to incorporate integration of three separate models: (i) model of seepage flow analysis, (ii) model of slope stability and (iii) model of dam surface erosion and flow to predict the outflow hydrograph resulted from failure of landslide dam by overtopping and sudden sliding. The main advantage of an integrated model is that it can detect failure mode due to either overtopping or sliding based on initial and boundary conditions.

The model of the landslide dam failure to predict outflow hydrograph consists of three models. The seepage flow model calculates pore water pressure and moisture content inside the dam body. The model of slope stability calculates the factor of safety and the geometry of critical slip surface according to pore water pressure and moisture movement in the dam body. The model of dam surface erosion and flow calculates dam surface erosion due to overflowing water. General outline of proposed integrated model is shown in Figure 6.1.

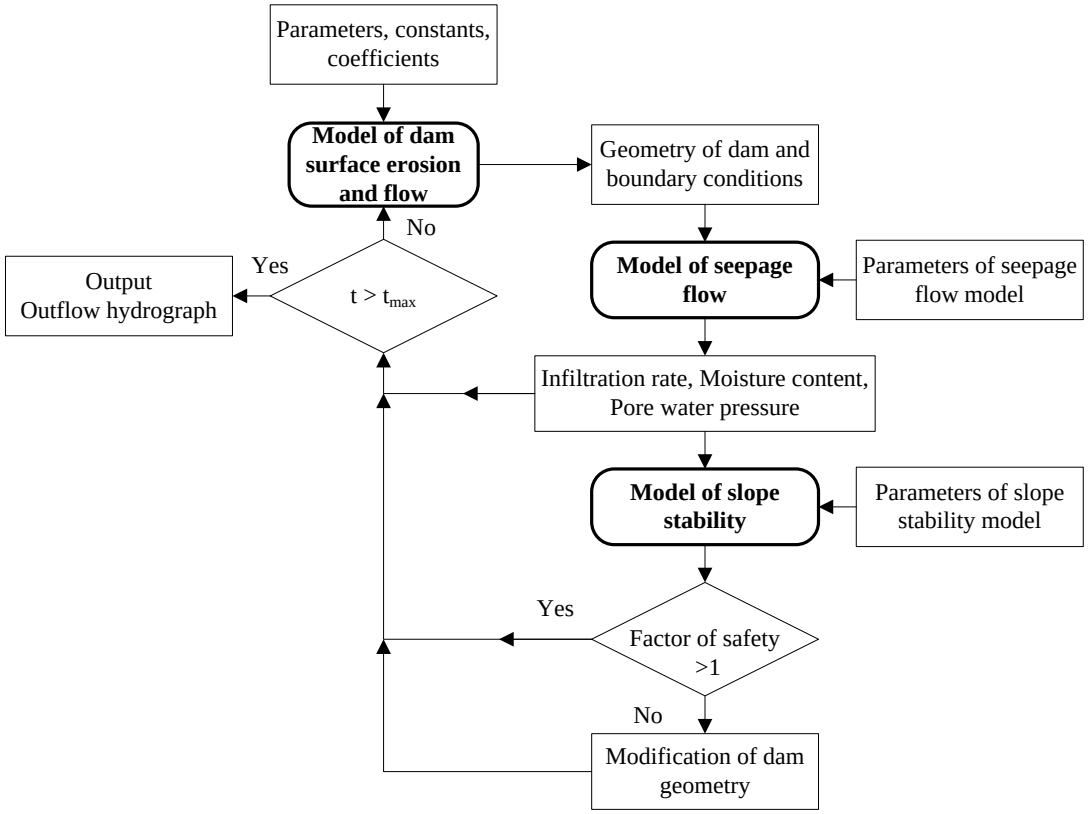

Figure 6.1 Model of landslide dam failure to predict flood/debris flow hydrograph

The linkage between seepage flow model and slope stability model and seepage flow model and dam surface erosion and flow model has been already discussed in Chapter 4 and Chapter 5 respectively. The linkage between slope stability model with dam surface erosion and flow model is briefly described here.

Linkage between slope stability model and dam surface erosion and flow model

In the specified time step we can check the stability of dam body with the help of parameters of slope stability model and input boundary conditions from seepage flow model (pore water pressure and moisture content of each grid cell of seepage flow model) and dam surface erosion and flow model (water depth and geometry of dam body). If factor of safety is less than 1 the new dam profile is determined by slope stability model and modified geometry is used for model of dam surface erosion and flow.

In case of sudden sliding failure, simplified assumption is made for initial transformation of the dam body after the slip failure. Figure 6.2 shows the simplified assumption of shape of deposition after sliding. There is some time lag between slip failure and movement of the slipped soil mass but in the model, the time necessary for such a deformation is assumed as nil. Based on many experiments, as shown in Figures 6.3, 6.4 and 6.5 for different channel slopes, the slipped mass is assumed to stop at the sliding surface where slope is less than the angle of repose and the shape of the slipped mass is assumed as trapezium. The height of trapezium is determined by equating the volume of the deposit with that of the slipped mass and making equal number of ordinates in the both stability model and model of dam surface and erosion. The erosion process by the overspilled water is analysed for the modified dam shape.

The erosive action of the overtopping flow removes material from the top part of the dam. The overtopped flow grows to debris flow by adding the eroded dam material to it, if the slope and length of dam body satisfy the critical condition for the occurrence of a debris flow.

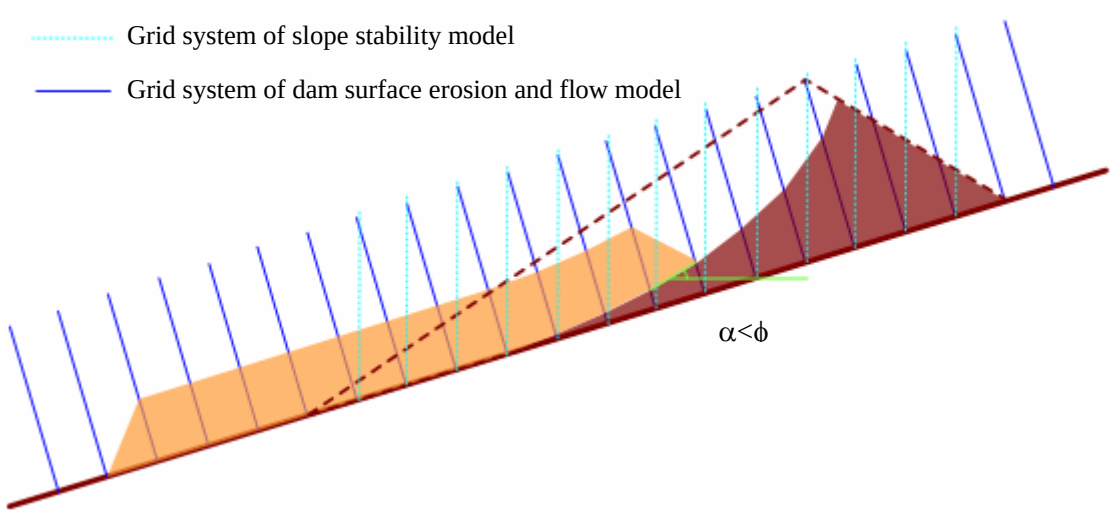

Figure 6.2 Simplified assumption of shape of deposition after sliding

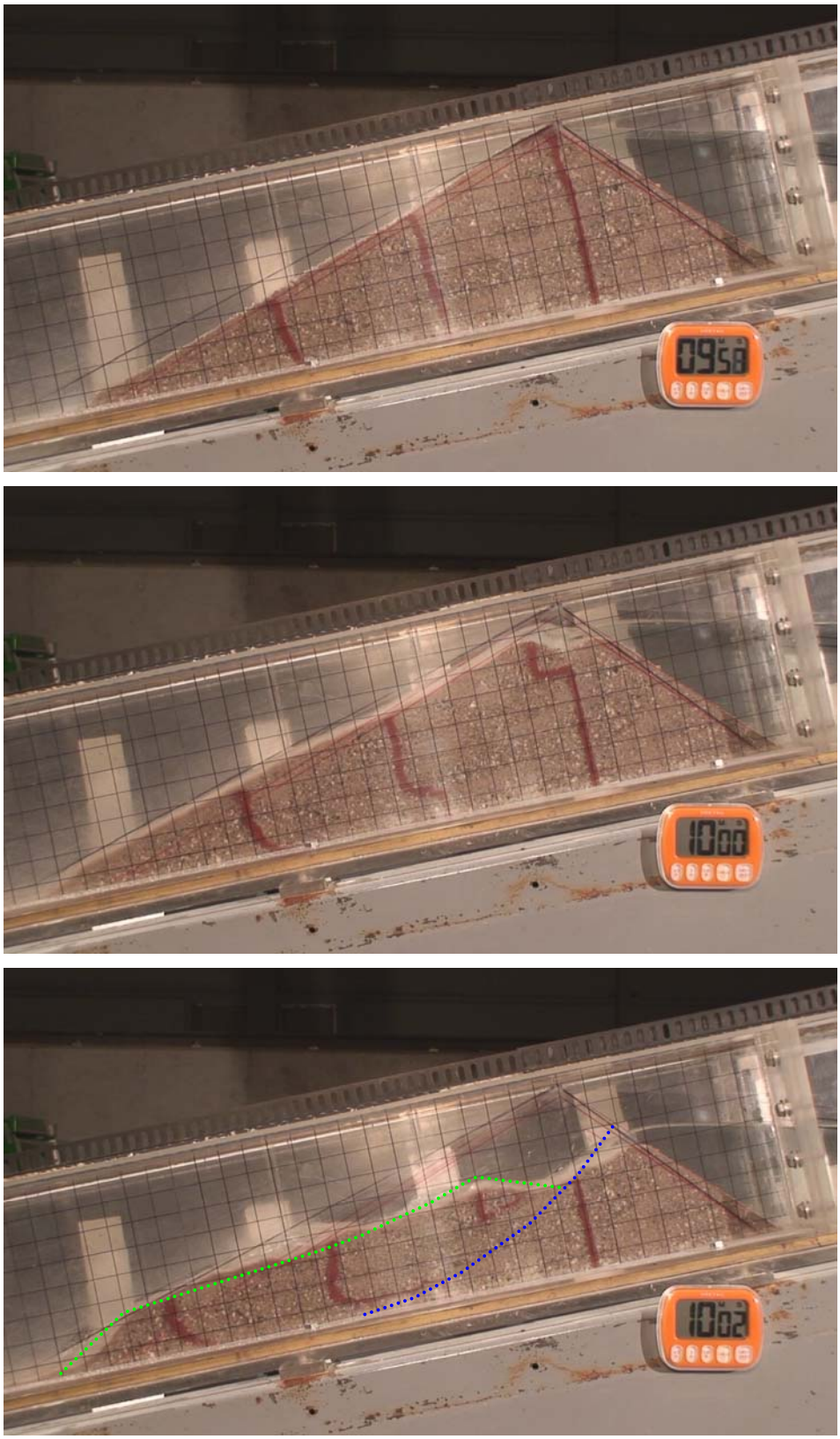

Figure 6.3 Shape of the dam body after deposition of slipped mass

(Flume slope = 13^{o})

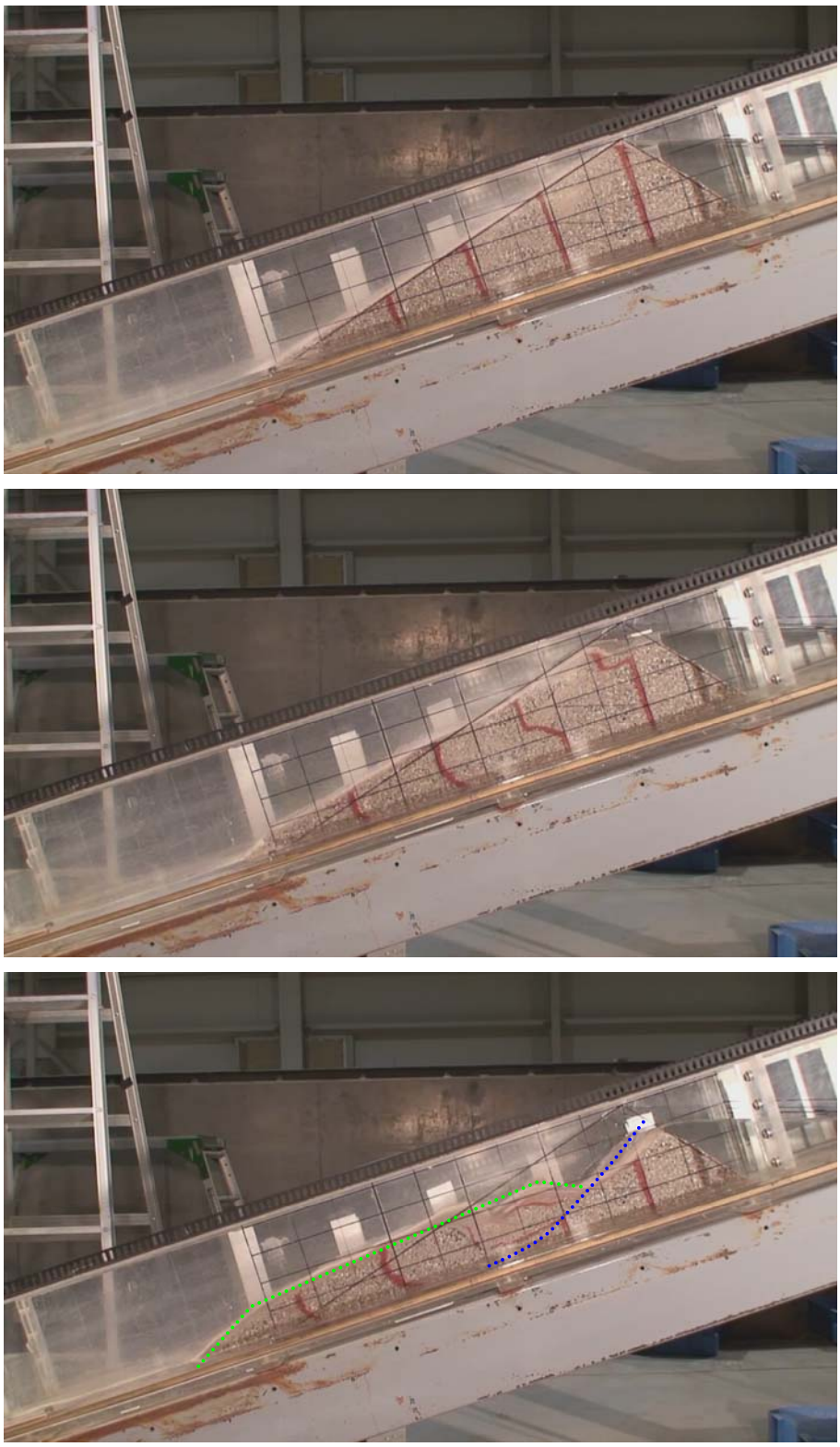

Figure 6.4 Shape of the dam body after deposition of slipped mass

(Flume slope = 17^{o})

Figure 6.5 Shape of the dam body after deposition of slipped mass (Flume slope = 20^{o})

6.2 Verification of model with experiments

6.2.1 Experimental study and conditions of calculation

The sediment, Mix 1-7 was used to prepare dam body. Different parameters of sediment mix including van Genuchten parameters are shown in table 2.1. The flume slope was 17 degree. Height of the dam and base length were 20cm and 84cm respectively. The experimental flume and arrangement of other accessories are shown in Figure 2.1.The shape of the dam body at different time step due to surface erosion after overtopping and the shape of slip surface during sliding were measured by analyses of video taken from the flume side. Water content reflectometers (WCRs) were used to measure the temporal variation of moisture content during seepage process. Load cell and servo type water gauge were used to measure sediment and total flow in the downstream end of the flume.

Inflow discharge of 30.5cm^3/sec was used. The initial moisture content of the dam body is 20% and saturated hydraulic permeability K_s is 0.0003m/sec. The parameters and the grid systems used in the calculation are $K_e = 0.11, K_{es} = 1,\ \delta_d = 0.05,\ c_* = 0.655,\ \sigma = 2.65$g/cm^3, d = 1mm, Δx = 60mm, Δy = 6.25mm and $\Delta t = 0.002$ sec.

6.2.2 Results and discussions

Steady discharge of 30.5cm^3/sec was supplied from the upstream part of the flume. The sudden sliding of the dam body was observed at 447sec in the experiment whereas in the simulation it was observed at 410sec. The simulated time was slightly earlier than the experimentally observed time that may be due to the assumption of immobile air phase in unsaturated flow and variation of saturated hydraulic conductivity due to non uniform mixing of sediments and possible variation in degree of compaction. The correction factor used in Janbu's simplified method to account for the effect of the interslice shear forces is not considered in this study. However, the range of correction factor for non-cohesive soil is small. Figure 6.6 shows the comparison of simulated and experimental slip surface. The geometry of predicted critical slip surface was similar to that observed in the experiment.

For the same experimental conditions, moisture content in the dam body was measured by using WCRs. Figure 6.7 shows the simulated and experimental results of moisture profile at WCR-4, WCR-5, WCR-6, WCR-8, and WCR-9 which are in good agreement.

The simulated result of overtopping erosion of deformed dam body after sliding is shown in Figure 6.8. Figure 6.9 shows the simulated and experimental results of outflow hydrograph. There is some time lag between failure of dam and movement of the slipped soil mass but in the model, the time necessary for such a deformation is assumed as nil so the simulated peak is earlier than experimental peak. Peak discharge depends on the shape of the dam body assumed after sliding and parameters of erosion and deposition velocity.

The movement of moisture in the dam body measured by using WCRs, critical slip surface observed in the experiment and predicted outflow hydrograph are close to the result of numerical simulation.

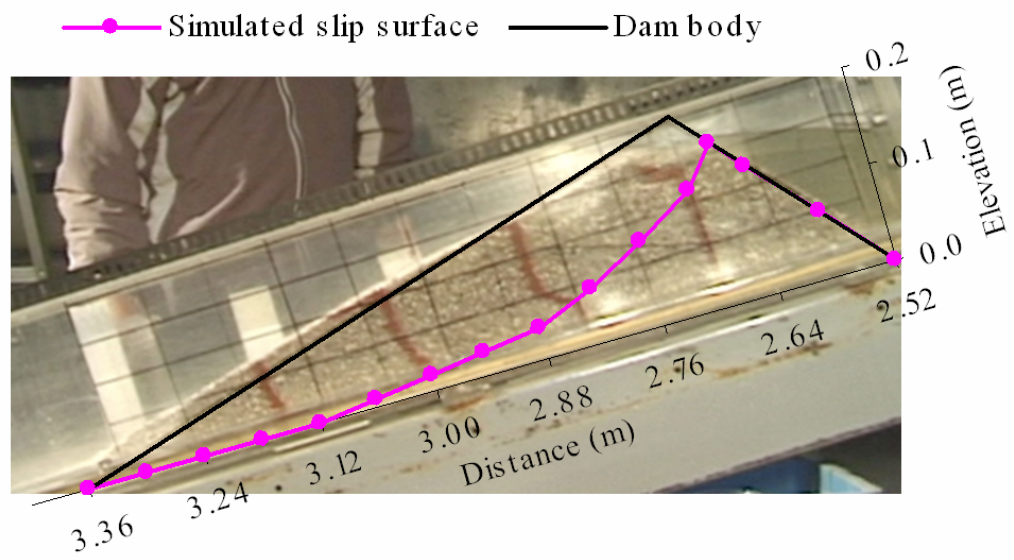

Figure 6.6 Comparison of simulated and experimental slip surface

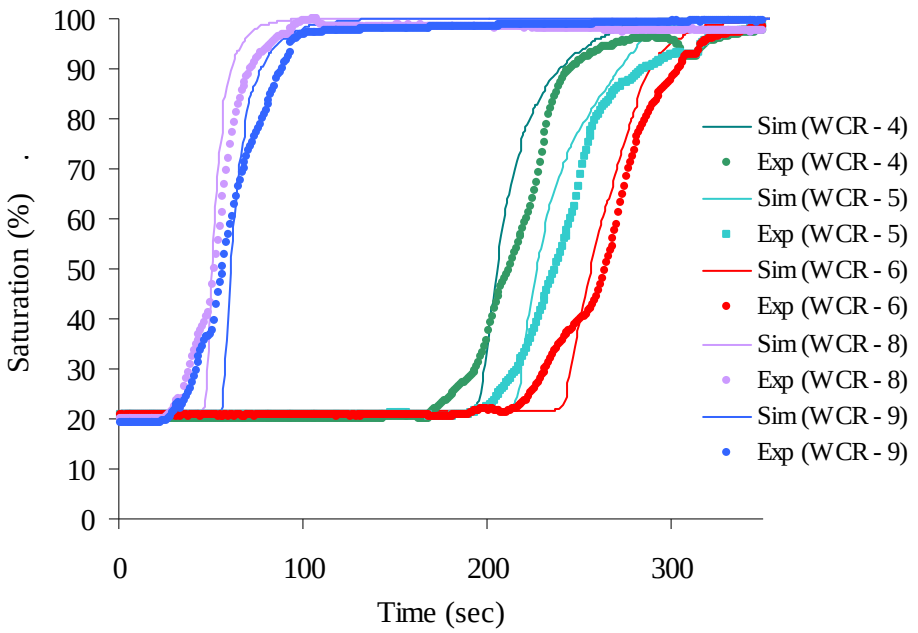

Figure 6.7 Simulated and experimental results of water content profile for different WCRs

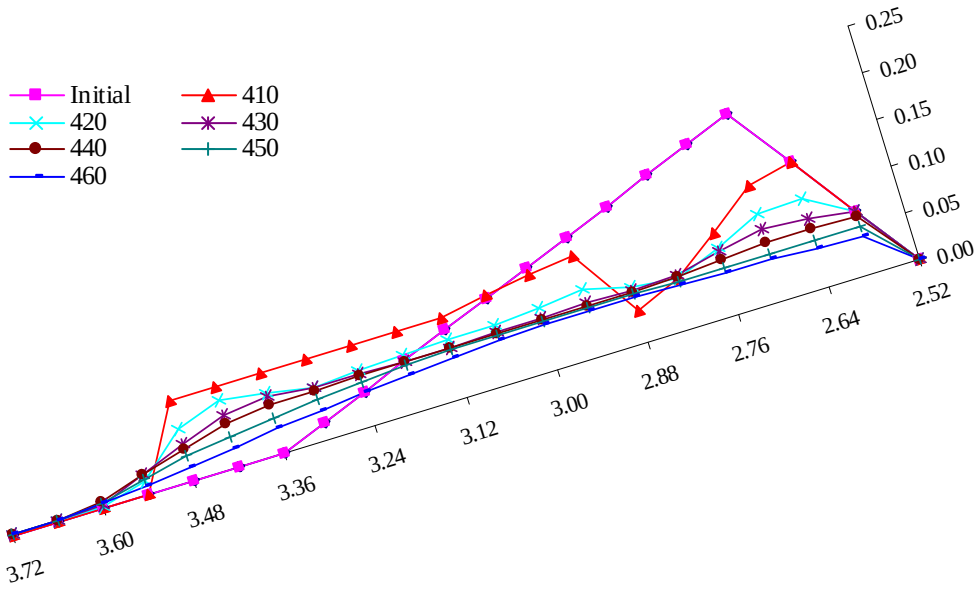

Figure 6.8 Overtopping erosion of deformed dam body after sliding

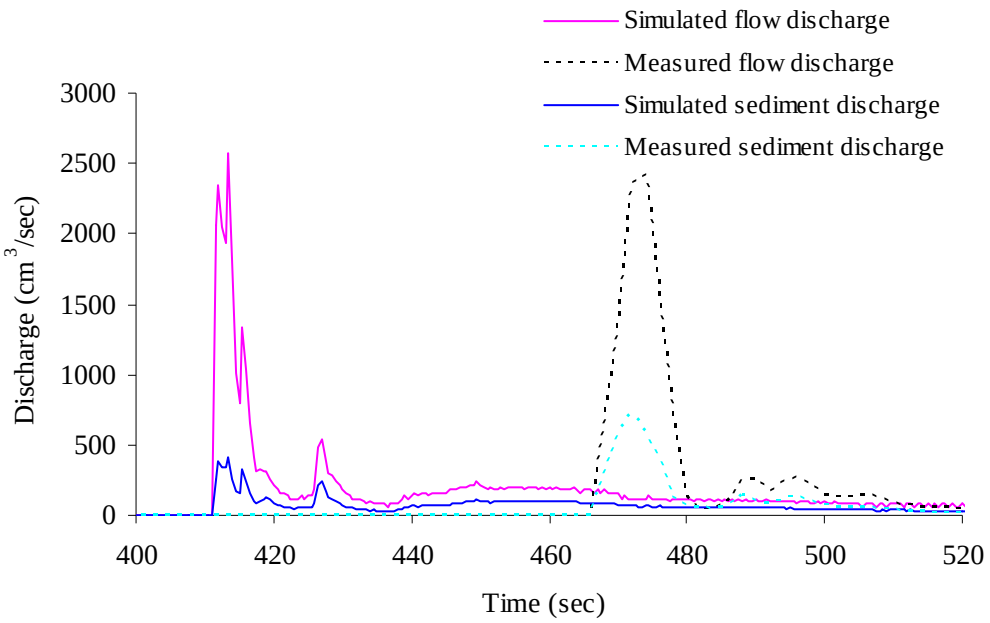

Figure 6.9 Outflow hydrograph

6.3 Applicability of an integrated model for actual landslide dam failure

The integrated or individual models can be used for the simulation of landslide dam failure to predict slope failure and outflow hydrograph. The model is validated with different experimental cases for small landslide dam, so it is applicable for actual landslide dam and we don't need to consider scale effect. However, the size and geometry of the dam body and reservoir used in the experiments are small and simple compare to actual cases. The main data required for the simulation of landslide dam are incoming flow discharge, dam geometry, reservoir topography, dam material properties. However such data for historical landslide dam failure are not available to validate the model. Some studies (Ponce and Tsivoglou, 1981; Fread, 1988b) attempted to simulate outflow hydrograph for Mantaro landslide dam, Peru that occurred in 1974 but the estimated actual peak discharge itself is different according to different researchers. It is difficult to measure peak discharge during the passage of a peak flood. An estimate of peak discharge can be obtained indirectly by using a slope area method. The estimated peak discharge is affected by Manning's n-value of the reach. However, for debris flow, an accurate determination of Manning's n-value in the field is precluded by several factors that affect flow resistance. In the context of data scarcity of actual landslide dam failure, the model can be also used to analyse hypothetical case of landslide dam failure for sensitivity

analysis of different parameters.

The experimental studies are focused on homogenous and cohesionless soil. The variation of sediment properties in the space such as saturated hydraulic conductivity, van Genuchten parameters can be measured by both field and laboratory experiments. Such a space dependent parameters can be used in the model. The erosion process in cohesive material is different so further modification in the model is essential to make model applicable for cohesive material.

6.4 Landslide dam and Hazard management

Landslide dams are fairly frequent phenomena in mountainous regions. Once landslide dams are formed, the dam's outbursts can cause heavy damage. Therefore, appropriate counter measures must be taken quickly. Although the initial event is local, it causes dramatic consequences upon failure at a large distance downstream. This study will briefly describe the recommended response method after formation of a landslide dam for the mitigation of upstream and downstream flood hazard. By implementing good management of the crisis, the evacuation of the persons in the upstream reservoir area and in the downstream valley is possible before failure of the landslide dam. Many researchers have discussed about different countermeasures taken in the past and recent landslide dam events such as Schuster and Costa (1986), Sassa (1999), Korup (2002 and 2005), Bonnard (2005), Hancox et al. (2005), Risley et al. (2006), Marui and Yoshimatus (2007), Becker et al. (2007). Past experiences from these events are useful for the management of landslide dam-break floods to reduce loss of life and properties from future events.

Recently, on 10th June, 2008, China successfully drained out one of the biggest quake lake, Tangjiashan, that was formed by 12th May earthquake. Both structural and non-structural measures were adopted for the potential hazard management. Preparation of downstream evacuation plan based on three different scenarios of floods, evacuation of more than 250,000 people, installation of video monitoring system at quake lake and downstream, construction of 475 meter long channel, firing of missiles and use of dynamite to deepen and clear channel, blasting of floating objects in water drained to prevent obstruction of water flow, precautions for the safety of structures in the downstream etc. are the significant measures adopted to achieve decisive victory in reducing water level of Tangjiashan lake.

Figure 6.10 The Cycle of Disaster Management (after Wilhite and Svoboda, 2000)

Recent predictions of climate change suggest that many part of world will experience a higher frequency of extreme rainfall events and increase in the number and intensity of typhoons and hurricanes will produce a rising danger of landslides in future. So, the formation and failure of landslide dam in the mountains area will be also increased by global climate change. Mitigating the impact of risks associated with landslide dam failure requires the use of all components of the cycle of disaster management (Figure 6.10), rather than only the crisis management portion of this cycle. Preparedness, mitigation, and prediction/early warning actions (i.e., risk management) are essential to reduce the potential hazards before failure of landslide dam. Impact assessment, response, recovery and reconstruction activities should follow after failure of landslide to return the affected area to its pre-disaster state.

6.4.1 Before formation of landslide dam

Scenario based hazard assessments are beneficial for development of emergency response plans prior to occurrence of landslide dam. Identification of areas that are most susceptible to dam-break flooding will help to mitigate the hazard of future landslide dams. The preventive human action was essential to mitigate the consequences of the potential or effective dam breaches for the protection of populations and infrastructures in the downstream. Based on landslide hazard map, detail study of potential dangerous landslide which may cause landslide dam is necessary. Detail modeling of the formation of the landslide dam, failure and the analysis of the flow

conditions in the downstream helps to identify areas of risk and prioritize their mitigation and response efforts. A good example of these preventive actions is given by Sechilienne landslide in the valley of Romanche river (France). As the monitoring results after some years induced to think that the potential rockfall volume could be larger than expected, a gallery was built so as to allow a partial diversion of the river flow in case of the formation of a landslide dam. Finally a detailed modelling of the formation of the dam, studied by two different dynamic approaches has allowed the determination of the dam height in several scenarios and thus the analysis of the flow conditions downstream (Bonnard, 2005).

Korup (2005) assessed geomorphic hazard from a landslide dam-break flood on the basis of conditional probabilities for the alpine South Westland region of New Zealand, where formation and failure of landslide dams is frequent. Clerici and Perego (2000) analyzed the recent evolution of the Corniglio landslide (Northern Italy) with the help of GIS in order to predict the most likely mechanisms of future evolution and simulated reactivation to assess the probability of blockage formation and dam stability. This type of study is necessary in potential landslide prone area before the formation of landslide dam. GIS-based modeling of virtual landslide dam is a simple and cost-effective approach to approximate site-specific landslide dam and lake dimensions, reservoir infill times, and scaled magnitude of potential outburst floods.

Jakob and Jordan (2001) proposed geomorphic approach to estimate design floods in mountain streams. Peak discharge produced by different geomorphic processes such as debris flows, landslide dam failures, glacial outburst floods and snow avalanches in the watershed can significantly exceed the design floods estimated by traditional methods. Use of geomorphic approach to estimate design floods for water resources and engineering projects including downstream flood hazard management is necessary to reduce the potential hazards from unexpected catastrophic floods.

6.4.2 After formation of landslide dam

After a heavy rainfall or strong earthquakes, the mountain areas should be immediately patrolled to see whether landslide dams were formed. If landslide dams are found, an urgent warning should be announced to those living downstream to evacuate to safety zones. Urgent and permanent measures for occurrences of landslide dams must be taken. The preventive human actions are essential to mitigate the consequences of the potential or effective dam breaches.

Accurate prediction of peak flow discharge is necessary to decide appropriate measures, including evacuation (Mizuyama, 2006). Figure 6.11 presents the recommended countermeasures that should be taken in the event that a landslide dam is formed. Predicted failure time will guide the countermeasures to be adopted however it depends on many other factors like potential hazards in the upstream and downstream, resources availability, site accessibility, risk from continued seismic activity, rainfall etc.

Collection of information

Topographic information on new landslide dam can be determined by using a laser profiling technique (Sato et al., 2007). Remote sensing data like, ASTER, SRTM, IKONOS can be also used to investigate landslide geometry and the morphology of the adjacent drainage works (Trommler et al., 2008). Digital topographic map can be used to determine landslide dammed lake volume, upstream and downstream hazard assessment.

It is possible to predict probable time of failure by overtopping with knowledge of river discharge, predicted rainfall, seepage through the dam and topography upstream from the dam. Most probable failure mechanism can be identified based on the information of shape of the dam body and geotechnical assessment of landslide dam material.

Non-structural measures

Empirical regression relations that linked the lake and dam characteristics to peak flow provides quick estimate of the potential maximum size of the dam-break flood (see details in Chapter 5). Triangular hydrograph that can be routed downstream is possible to derive from predicted peak discharge and knowledge of volume of storage that may release from the reservoir and time for volume of storage to release (Hagen, 1996).

Physically based numerical model or physical laboratory model test is possible if probable failure time is longer and required data are available. Estimated outflow hydrograph can be used to predict potential inundated area by using flow routing model. One dimensional (Fread, 2000) or two dimensional models (Takahashi et al., 2001) can be used to predict downstream hazards. Simple and quick GIS rule-based approach (Chen et al., 2004) can be also used to early warning and preliminary inundation hazard mapping. The uncertainties involved in flood hazard

assessment make it prudent to plan for a realistic worst case scenario, rather than some lesser event that could be exceeded because of some unforeseen circumstance (Hancox et al., 2005).

Risk assessments are the foundation for making decisions about the best means for managing a potential risk. Risk assessments provide informed options for risk management. Risk assessments are prospective analyses of the extent of a hazard, the exposure of people and property to that hazard, the likelihood of a damaging event and the likely resultant economic and societal consequences of that event.

Monitoring and warning systems

Parallel to the structural countermeasures to prevent the collapse of the landslide dam, installation of monitoring and observation systems are also essential for the better management of potential risk in the case of emergency. Monitoring system like water level gauge, debris flow sensor, monitoring camera around landslide dam and arrangement of information transfer system will help to make decision to evacuate the inhabitants of upstream reservoir area and downstream floodplain area in case of dam failure. These types of monitoring and warning systems were used in Higashi-Takezawa landslide dam and the Terano landslide dam (Marui and Yoshimatsu, 2007). Frequent monitoring of landslide dam by helicopter, installation of monitoring equipment such as a radio-linked water-level recorder and an arrangement of manual quick-call “telephone tree” system to contact all residents in an emergency were implemented before the failure of Mount Adams landslide dam in the Poerua River (Becker et al, 2007). Vibrating wire tiltmeters can be used to monitor stability of slope. Regular inspection of the dam and landslide area is necessary to check for seepage on the dam face or further falls of landslide debris which may block the natural spillway channel. If such landslide falls on the reservoir it may cause flooding in the upstream area (e.g. Monte Zandila rockslide in the Valtellina valley, Italy) and may cause overtopping due to wave generated by fall of landslide mass directly in the lake.

Structural measures

Landslide dam can be stabilized by structural measures that control discharge and thus prevent overtopping. Excavation of channel will reduce depth and volume of the lake and it also reduce the flooding in the upstream and potential hazard in the downstream. The simplest and most commonly used method has been construction of channeled spillways either across adjacent

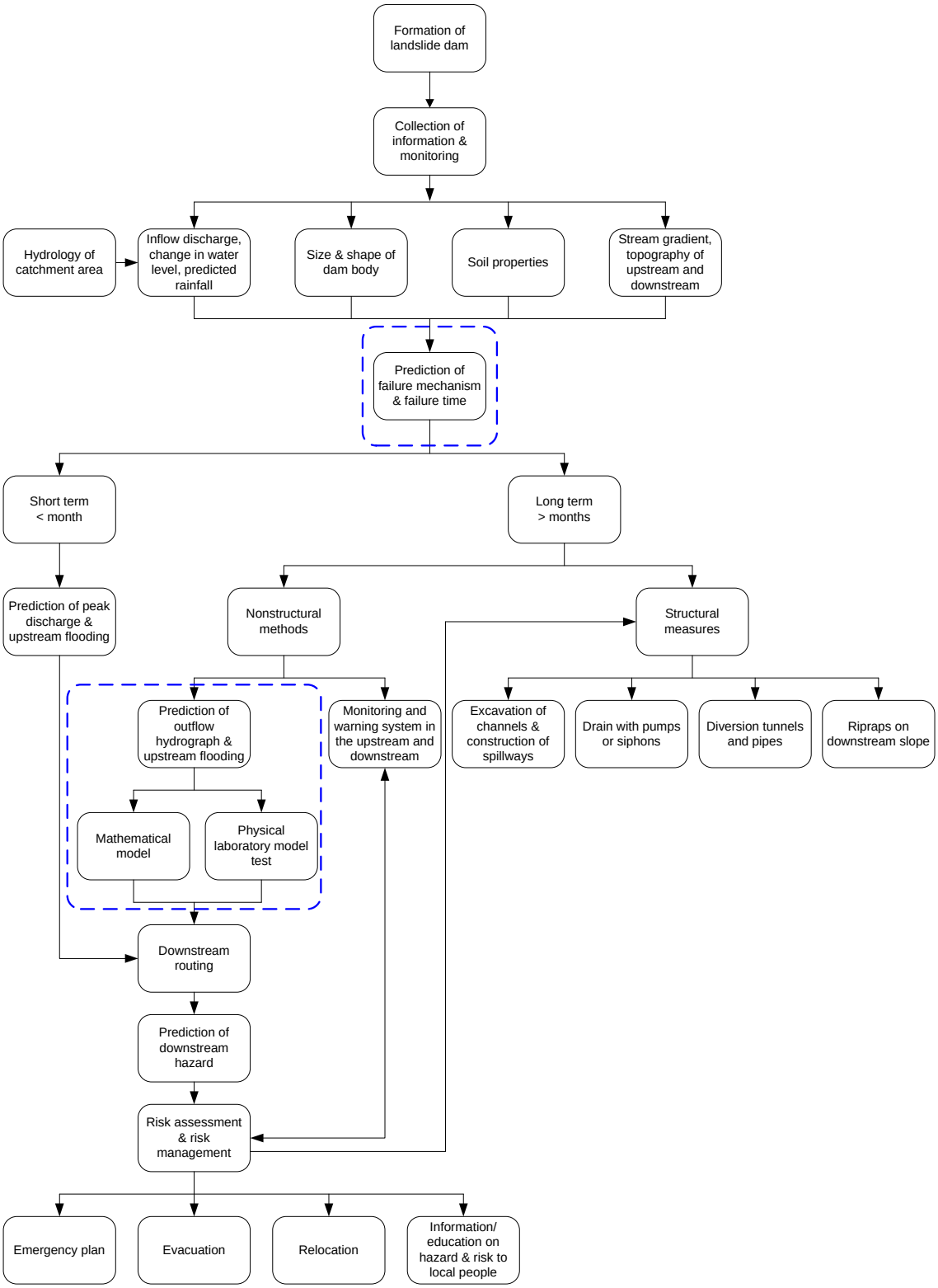

Figure 6.11 Countermeasures to be taken after the formation of landslide dam

bedrock abutments or over the landslide dam itself (Schuster and Costa, 1986, Becker et al., 2007). Spillways excavated across landslide dams are not always successful in preventing failure and flooding because they sometimes are enlarged rapidly by the high-velocity outlet flow. Other methods of structural measures are construction of diversion tunnel, use of pumps and siphons to pass part of river discharge to reduce the water level in the reservoir.

Structural measures have been attempted on many landslide dams in recent years as soon as possible after they formed. However, in some cases, overtopping has occurred before installation of satisfactory control measures.

The present study is focused on prediction of outflow hydrograph caused by landslide dam failure by both mathematical modeling and laboratory experiments. The predicted outflow hydrograph can be used for downstream flood routing, prediction of hazard and risk assessment. From Figure 6.11, it is clear that prediction of outflow hydrograph plays vital role in both non-structural and structural counter measures to cope with landslide dam failure.

Summary

An integrated model was developed for simulation of outflow hydrograph due to landslide dam failure by overtopping and sliding. The proposed model was tested for experimental case of landslide dam failure due to overtopping and sliding and reasonably reproduced the resulting hydrograph. The numerical simulation and experimental results of movement of moisture in the dam body, predicted critical slip surface and time to failure of the dam body are also in good agreement. Prediction of peak flow discharge and outflow hydrograph from failure of landslide dam is necessary to decide appropriate measures including evacuation. Possible counter measures after formation of landslide dam were discussed with reference to literature of previous case studies.

Chapter 7

Conclusions and Recommendations

The formation and failure of landslide dam are common geomorphic process in mountain regions all over the world. The major impacts of landslide dam include backwater ponding, catastrophic outburst floods and debris flows. Predicted flood/debris flow hydrograph caused by landslide dam failure can be used as an upstream boundary condition for subsequent flood routing to predict inundation area and hazard in the downstream to provide adequate safety measures in the event of landslide dam failure. Landslide dam failure is frequently studied as an earthen dam failure. Very few models are developed for landslide dam failure that can treat the flow as both sediment flow and debris flow. Most of the existing models are applicable to overtopping failure of landslide dam. In this context, an attempt was made to incorporate integration of three separate models to predict the outflow hydrograph resulted from failure of landslide dam by overtopping and sudden sliding. The seepage flow model calculates pore water pressure and moisture content inside the dam body. The model of slope stability calculates the factor of safety and the geometry of critical slip surface according to pore water pressure and moisture movement in the dam body. The model of dam surface erosion and flow calculates dam surface erosion due to overflowing water.

The key features of integrated model can be summarized as follows:

- Infiltration process is incorporated in an integrated model although this process is neglected in almost all available models.

- The model can predict time at which landslide dam may fail and also detect failure mode due to either overtopping or sliding based on initial and boundary conditions. Outflow hydrograph is calculated according to failure mode.

- The model can predict both total discharge and sediment discharge hydrograph. The model is capable to treat all types of flow based on sediment concentration.

7.1 Conclusions

The conclusions of this study are summarized as follows:

Comparison of peak discharge produced by landslide dam failure

The comparison of peak discharge with mean annual maximum instantaneous flood discharge for some events of natural dam failure in Nepal indicated that the peak discharge may be many times greater than any normal rainfall triggered flood.

Critical channel slope to predict failure mode

Critical channel slope for sediments, Mix 1-6 and Mix 1-7 are derived from flume experiments. For particular discharge and dam height we can determine critical channel slope. If the channel slope is close to critical channel slope the dam may fail by instantaneous slip failure. If channel slope is flatter than critical channel slope progressive failure may occur and if steeper then overtopping flow may occur.

Comparison of peak discharge for different failure modes

Set of flume experimental data was used to compare the peak discharge for different failure modes. Progressive failure produced maximum peak discharge compare to other failure modes. Based on data set of embankment dam compiled by Froehlich (1995), peak discharge produced by seepage or piping failure is higher compared to overtopping failure for higher dam factor.

Seepage flow model

Infiltration into variable saturated porous media is modeled by the Richards' equation. The pressure based Richards' equation discritized by finite differences technique is used in numerical simulation. The numerical simulation and experimental results of movement of moisture in the dam body are in good agreement for both 2D and 3D cases.

Transient slope stability model

Sudden failure of landslide dam was studied in experimental flume for constant head and steady discharge in the upstream reservoir. A high constant water level or gradual rise of water level in

the reservoir causes water to penetrate into the dam body and it increases mobilized shear stress and dam fails by sudden collapse when it becomes larger than resisting shear stress. Transient slope stability model combined with seepage flow model was developed. The factor of safety considers temporal variation of both pore water pressure and moisture content inside the dam body.

The numerical procedure used for the identification of critical noncircular slip surface with the minimum factor of safety is based on dynamic programming and the Janbu's simplified method. A 2D analysis is only valid for slopes which are long in the third dimension. However, failure of natural slopes and landslide dams confined in a narrow U- or V-shaped valley occurs in three dimensions. Therefore 3D approach is more appropriate to analyze such stability problems. The 3D slope stability analysis based on dynamic programming and random number generation incorporated with 3D simplified Janbu's method is also used to determine minimum factor of safety and the corresponding critical slip surface for landslide dam in the V-shaped valley. The 3D seepage flow model is also coupled with 3D slope stability model so the combined model is capable for transient slope stability analysis. Numerical simulations and flume experiments were performed to investigate the mechanism of landslide dam failure due to sliding for both 2D and 3D cases. The lateral slope of the flume bed was horizontal for 2D case and was inclined for 3D case. The numerical simulation and experimental results of predicted critical slip surface and time to failure of the dam body are in good agreement for both 2D and 3D cases.

Dam surface erosion and flow model

A combined numerical model is developed for simulation of outflow hydrograph due to landslide dam failure by overtopping. The proposed model is tested for different experimental cases of landslide dam failure due to full channel width and partial channel width overtopping. The results show the model is able to reasonably reproduce the resulting hydrograph. The simulated overtopping time and dam surface erosion at different time steps are also in good agreement with experiments.

The simulated breach width depends on inflow and reservoir volume. The incised channel is almost vertical for both simulation and experiments in small inflow discharge and small reservoir volume. In the case of larger inflow discharge and larger reservoir volume, slumping occurred at irregular time steps. The peak discharge is highly influenced by sliding of breached channel bank at crest.

Integrated model to predict outflow hydrograph

An integrated numerical model is developed for simulation of outflow hydrograph due to landslide dam failure by overtopping and sliding. The proposed model is tested for experimental case of landslide dam failure due to overtopping and sliding and the model reasonably reproduced the resulting hydrograph. The numerical simulation and experimental results of movement of moisture in the dam body, predicted critical slip surface and time to failure of the dam body are also in good agreement.

Prediction of outflow hydrograph to cope with landslide dam failure

Prediction of peak flow discharge and outflow hydrograph from failure of landslide dam is necessary to decide appropriate measures including evacuation. Prediction of outflow hydrograph plays vital role in both non-structural and structural counter measures to cope with landslide dam failure.

7.2 Recommendations for future researches

The study is focused on failure of landslide dam of non-cohesive material. The failure mechanism of landslide dam of cohesive material is different, so further study is essential for the application in such a dam. The model developed in this study is still in the preliminary stage of concept of integrated model and it has many limitations. Some limitations and recommendations to improve and make fully integrated model to predict failure modes and resulting flood is discussed here.

Application of ANN, GA to determine failure mode

The study attempted to determine criteria to predict failure modes. As explained in Chapter 2, failure mode depends on many factors and it is difficult to relate failure mode with few parameters. It is possible to use data mining techniques like Artificial Neural Network (ANN), Genetic Algorithm (GA) etc to determine failure mode based on number of input parameters by doing number of experiments in different sediment size with different sediment properties and dam shape.

Use of rigorous method of slope stability analysis

In this model slope stability analyses was carried out by Janbu's simplified method. This method is based on the assumption that the interslice forces are horizontal. This method may violate moment equilibrium for the soil mass as a whole. Although assumptions are required in all methods to make the problem statically determinate and to obtain a balance between the number of equations and the number of unknowns that are solved for, methods that satisfy all conditions of equilibrium e.g., Janbu's rigorous analysis, Morgenstern and Price's method, and Spencer's method can be used for more accurate result.

Modeling of movement of slipped mass

In sudden sliding failure, simplified assumption is made for initial transformation of the dam body after the slip failure. Based on many experiments the slipped mass is assumed to stop at the sliding surface where slope is less than angle of repose and the shape of the slipped mass is assumed as trapezium. However to model actual failure process we have to consider both movement of slipped soil mass and erosion by overspilled water at each time step. The applicability of sled model (Sassa, 1999); Discontinuous Deformation Analysis (DDA) etc should be explored in future.

Stability of breached channel bank

The enlargement of breached channel is modeled as erosion of side wall due to shear stress of flowing water. However slumping of side slope of breached channel occurs at irregular time steps and is depending on condition of flow and material of the dam body. During breach formation, breach enlargement proceeded rapidly below the water surface in the breach channel. Above the water level there was some apparent cohesion added by water content and adhesion so the side wall is very steep and undermines the slope. So, further improvement of model is necessary to incorporate this phenomenon. Breached channel bank stability model with capability to predict timing and dimensions of bank failure along breach channel is required to couple with integrated model.

Progressive failure

Few examples of landslide dam failure by seepage are discussed in Chapter 1. Peak discharge produced by progressive failure is higher compared to other types of failure. Further

experimental and numerical study is necessary to include progressive failure of landslide dam due to seepage in integrated model of landslide dam failure.

Landslide-generated waves overtopping floods

Landslide dam may also fail by landslide-generated waves overtopping. This phenomenon can also be incorporate in the integrated model to predict outflow hydrograph. Extensive laboratory experiments are essential to study such triggering event and failure mechanism.

Probabilistic approach

The developed models are deterministic. There are many uncertainties in soil properties of dam materials such as hydraulic conductivity, angle of friction, cohesion etc. So, probabilistic approach is necessary to take into account different uncertainties.

Prediction of flood risk in the downstream

The predicted flood/debris flow hydrograph can be used as a boundary condition for downstream flood routing. 1D or 2D flood routing model with the capability to model sediment transport can be used to predict downstream hazard and its mitigation. Proper location of refuges and evacuation routes can be shown in the hazard map to evacuate local residents in a safe and proper manner in the event of landslide dam failure.

References:

Adhikari, D. P. and Koshimizu, S.: Debris flow disaster at Larcha,upper Bhotekoshi Valley, Central Nepal, *Island Arc*, Vol. 14, pp. 410-423, 2005.

Arai, K. and Tagayo, K.: Determination of noncircular slip surface giving the minimum factor of safety in slope stability analysis, *Soils and Foundations*, Vol. 25(1), pp.43-51, 1985.

Ashida, K.: Case study on the choking of river channel due to landslide-Totsugawa disasters in 1889, Prediction and countermeasures of secondary disaster, 2, *Zennkoku Bousai Kyoukai*, pp. 37-45, 1987. (in Japanese)

Assouline, S., Tessier, D. and Bruand, A.: A conceptual model of the soil water retention curve, *Water Resour. Res.,* Vol. 34, pp223–231, 1998.

Awal, R., Nakagawa, H., Kawaike, K., Baba, Y. and Zhang, H.: Numerical approach to predict flood/debris flow hydrograph due to landslide dam failure, *Proceedings of the First NEA-JC Seminar on "Current and Future Technologies"*, 2007. (in CD ROM)

Awal, R., Nakagawa, H., Baba, Y. and Sharma, R. H.: Numerical and experimental study on landslide dam failure by sliding, *Annual Journal of Hydraulic Engineering*, JSCE, Vol.51, pp.7-12, 2007.

Awal, R., Nakagawa, H., Kawaike, K., Baba, Y. and Zhang, H.: An integrated approach to predict outflow hydrograph due to landslide dam failure by overtopping and sliding, *Annual Journal of Hydraulic Engineering*, JSCE, Vol. 52, pp.151-156, 2008.

Baker, R.: Determination of the critical slip surface in slope stability computations, *International Journal for Numerical and Analytical Methods in Geomechanics*, Vol.4, pp.333-359, 1980.

Baligh, M. M. and Azzouz, A. S.: End effects on stability of cohesive slopes, *Geotech. Engrg. Div.,* ASCE, Vol.101, GT11, pp.1105-1117, 1975.

Bechteler, W. and Broich, K.: Effects in dam-break modeling*, Proc. 24th IAHR Congress,* Madrid, Spain, pp.A189-A200, 1991.

Becker, J. S., Johnston, D. M., Paton, D., Hancox, G. T., Davies, T. R., McSaveney, M. J. and Manville, V. R.: Response to Landslide Dam Failure Emergencies: Issues Resulting from the October 1999 Mount Adams Landslide and Dam-Break Flood in the Poerua River, Westland, New Zealand, *Natural Hazards Review*, Vol.8 (2), pp. 35-42, 2007.

Bellman, R.: Dynamic programming, Princeton University Press, *Princeton*, N.J, 1957.

Bishop, A. W.: The use of slip circles in the stability analysis of earth slopes, *Geotechniqu*e, Vol. 5(1), pp.7–17, 1955.

Bonnard, Ch.: Technical and human Aspects of Historic Rockslide Dammed Lakes and Landslide Dam Breaches, in *Security of Natural and Artificial Rockslide Dams* (K. Abdrakhmatov et al., Eds), NATO Advanced Research Workshop Publication, Bishkek, Kyrgyzstan, Published by the Italian Society of Engineering Geology, 2005.

Boutrup, E. and Lovell, C. W.: Searching techniques in slope stability analysis, *Engineering Geology*, Vol.16, pp.51-61, 1980.

Brandt, A., Bresler, E., Diner, N., Ben-Asher, L., Heller, J. and Goldman, D.: Infiltration from a trickle source: 1. Mathematical models, *Soil Sci. Soc. Am. Proc*., Vol.35, pp.675-689, 1971.

Brito, C. C., Pereira, J. H. F., Gitirana, G. F. N. Jr., and Fredlund, D. G.: Transient stability analysis of a collapsible dam using dynamic programming combined with finite element stress fields, *IXth Int. Symp. on Landslides*, Vol.2, pp.1079–1084, 2004.

Broich, K.: Mathematical modeling of dambreak erosion caused by overtopping, *Proceedings of the 2nd CADAM Workshop*, Munich, October 1998.

Brown, R.J. and Rogers, D.C.: BRDAM users manual, *Water and Power Resources Services*, U.S. Department of the Interior, Denver, Colorado, USA, 1981.

Brooks, R.H., and Corey, A.T.: Hydraulic properties of porous media, Colorado State Univ., *Hydrology Paper No. 3*, pp.27 , 1964.

Campbell, G.S.: A simple method for determining unsaturated conductivity from moisture retention data. *Soil Sci.,* Vol. 117, pp311–314, 1974.

Campbell Scientific, Inc.: CS616 and CS625 Water content reflectometers, *Instruction Manual*, 2004.

Canuti P, Casagli N, Ermini L.: Inventory of landslide dams in the Northern Apennine as a model for induced flood hazard forecasting. In *Managing Hydro-geological Disasters in a Vulnerate Environment*, Andah K (ed.), CNR-GNDCI Publication 1900, CNR-GNDCI-UNESCO (IHP): Perugia; pp.189-202, 1998.

Carson, B.: Erosion and sedimentation process in the Nepalese Himalaya, *ICIMOD occasional paper no.1*, ICIMOD, 1985.

Casagli N, Ermini L.: Geomorphic analysis of landslide dams in the Northern Apennine, *Transactions of the Japanese Geomorphological Union*, Vol. 20(3), pp. 219-249, 1999.

Cencetti, C., Fredduzzi, F., Marchesini, I., Naccini, M. and Tacconi, P.: Some considerations about the simulation of breach channel erosion on landslide dams, *Computational Geosciences*, Vol.10, pp.201–219, 2006.

Celestino, T. B. and Duncan, J. M.: Simpliefied search for noncircular slip surfaces, Proc. 10th Int. Conf. *Soil Mech. Found. Engng.*, Stockholm, Vol.3, pp.238-250, 1981.

Celia, M.A., Bouloutas, E.T. and Zarba, R.L.: A general mass-conservative numerical solution of the unsaturated flow equation, *Water Resour. Res*., Vol.26, pp.1483-1496, 1990.

Chen, C.-Y., Chen, T.-C., Yu, F.-C. and Hung, F.-Y.: A landslide dam breach induced debris flow – a case study on downstream hazard areas delineation, *Environmental Geology*, Vol. 47, pp. 91-101, 2004.

Chen, Q., Zhang, L.M., and Zhu, F.Q.: Effects of material stratification on the seepage field in a rockfill dam, In *Proceedings of the 2nd Chinese National Symposium on Unsaturated Soils*, Hangzhou, China, 23–24 April 2005, Chinese Soil Mechanics and Geotechnical Engineering Society, Beijing, China, pp.508–515, 2005.

Chen, Q. and Zhang, L.M.: Three-dimensional analysis of water infiltration into the Gouhou rockfill dam using saturated-unsaturated seepage theory, *Canadian Geotechnical Journal*, Vol.43, pp.449-461, 2006.

Chen, R. H. and Chameau, J. L.: Three-dimensional limit equilibrium analysis of slopes, *Geotechnique*, Vol.33(1), pp.31-40, 1983.

Chhetri Poudyal, M. B. and Bhattarai, D.: Mitigation and management of floods in Nepal, 2001

Clement, T. P., Wise, W. R. and Molz, F. J.: A physically based, two-dimensional, finite-difference algorithm for modeling variably saturated flow, *Journal of Hydrology*, Vol. 161, pp. 71-90, 1994.

Clerici, A. and Perego, S.: Simulation of the Parma River blockage by the Corniglio landslide (Northern Italy), *Geomorphology*, Vol.33, pp.1–23, 2000.

Coleman, S.E., Andrews, D.P. and Webby, M.G.: Overtopping breaching of noncohesive homogeneous embankments, *Journal of Hydraulic Engineering*, Vol. 128(9), pp.829-838, 2002.

Cooley, R.L.: Some new procedures for numerical solution of variably saturated flow problems, *Water Resour. Res*., Vol.19, pp.1271-1285, 1983.

Costa, J. E.: Floods from dam failures, *U.S. Geological Survey, Open-File Rep. No. 85-560*, Denver, 54, 1985.

Costa, J.E. and Schuster, R.L.: The formation and failure of natural dams, *Geological Society of America Bulletin 100*, pp.1054–106, 1988.

Costa J.E., Schuster R.L.: Documented historical landslide dams from around the world, *US Geological Survey Open File Report*, pp.91–239, 1991.

Cristofano, E. A.: Method of computing erosion rate for failure of earthfill dams, *Bureau of Reclamation*, Denver, Colorado, USA, 1965.

Dane, J.H. and Mathis, F.H.: An adaptive finite difference scheme for the one-dimensional water flow equation*, Soil Sci. Soc. Am. J.,* Vol.45, pp.1048-1054, 1981.

David C. Froehlich: Peak Outflow from Breached Embankment Dam, *J. Water Resour. Plng. and Mgmt.*, Vol 121(1), pp. 90-97, 1995.

Davies,T.R., Manville, V., Kunz, M. and Donadini, L.: Modeling Landslide Dambreak Flood Magnitudes: Case Study*, Journal of Hydraulic Engineering*, Vol. 133(7), pp. 713-720, 2007

Day, P.R. and Luthin, J.N.: A numerical solution of the differential equation of flow for a vertical drainage problem, *Soil Sci. Soc. Am. Proc*., Vol.20, pp.443-446, 1956.

De Looff, H., Steetzel, H.J. and Kraak, A.W.: Breach growth: experiments and modeling, *Proc. 25th Int. Conf. Coastal Engineering, Orlando*, USA, pp.2746-2755, 1997.

Dhital, M. R.: Landslide investigation and mitigation in Nepal, Abstracts: 17th Himalaya-Karakorum-Tibet Workshop, India*, Journal of Southeast Asian Earth Sciences* , Volume 20, Issue 4, Supplement 1, pp 9, April 2002.

Dixit, A.: Floods and Vulnerability: Need to Rethink Flood Management, In Mirza, M.M.; Dixit, A; Nishat, A. (eds) Flood Problem and Management in South Asia reprinted from *Natural Hazard*, Vol. 28, pp.155-179, 2003.

Duncan, J. M.: State-of-the-art static stability and deformation analysis, Stability and Performance of Slopes and Embankments: II, *Geotechnical Special Publication 31, ASCE*, Reston, VA, pp.222–266, 1992.

Duncan, J. M.: Landslides: Investigation and Mitigation, Transportation Research Board, *National Research Council,* National Academy Press, Washington, DC, pp.337–371, 1996a.

Duncan, J. M.: State of the art: limit equilibrium and finite element analysis of slopes, ASCE*, Journal of Geotechnical Engineering*, Vol.122(7), pp.577–596, 1996b.

Duncan, J. M. and Wright, S. G.: Soil Strength and Slope Stability, *John Wiley & Sons*, Hoboken, N.J., 2005.

Dunning, S. A., Rosser, N. J., Petley, D. N. and Massey, C. R.: Formation and failure of the Tsatichhu landslide dam, *Landslides*, Vol. 3, pp.107-113, 2006.

Ermini, L. and Casagli, N.: Prediction of the behaviour of landslide dams using a geomorphological dimensionless index, *Earth Surface Processes and Landforms*, Vol.28, pp.31-47, 2003.

Evans, S. G.: The maximum discharge of outburst floods caused by the breaching of man-made and natural dams, *Can. Geotech. J.,* Vol.23(4), pp.385–387, 1986.

Fread, D.L.: The NWS DAMBRK: The NWS dam-break flood forecasting model, Office of Hydrology, *National Weather Service*, Silver Spring, Maryland, USA, 1984.

Fread, D.L.: The NWS DAMBRK model: theoretical and background/user documentation, *National Weather Service (NWS)* Report, NOAA, Silver Spring, Maryland, USA, 1988a.

Fread, D.L.: BREACH: an erosion model for earthen dam failures, *National Weather Service (NWS) Report*, NOAA, Silver Spring, Maryland, USA, 1988b.

Fredlund, D. G., Morgenstern, N. R. And Widger, R. A.: Shear strength of unsaturated soils, *Canadian Geotechnical Journal*, Vol.15(3), pp.313-321, 1978.

Fredlund, D.G.: Analytical methods for slope stability analysis: state-of-the-art. In Proceedings of the 4th International Symposium on Landslides, Toronto, Sept. 16-21, *Canadian Geotechnical Society*, Toronto, pp. 229-250, 1984.

Fredlund, D.G., and Krahn, J.: Comparison of slope stability methods of analysis, *Canadian Geotechnical Journal*, Vol.14, pp.429-439, 1997.

Freeze, R.A.: The mechanism of natural groundwater recharge and discharge 1. One-dimensional, vertical, unsteady, unsaturated flow above a recharging and discharging groundwater flow system, *Water Resour. Res.,* Vol.5, pp. 153-171, 1969.

Freeze, R.A.: Three dimensional transient, saturated unsaturated flow in a groundwater basin, *Water Resour. Res.,* Vol.7, pp.347-366, 1971a.

Freeze, R.A.: Influence of the unsaturated flow domain on seepage through earth dams, *Water Resour. Res.,* Vol.7, pp.929-941, 1971b.

Freeze, R. A.: Mathematical models of hillslope hydrology, in Kirkby, M. J., ed., *Hillslope Hydrology*, John Wiley, pp. 177-225, 1976.

Froehlich, D. C.: Peak outflow from breached embankment dam, *J. Water Resour. Plan. Manage. Div.,* Am. Soc. Civ. Eng., Vol. 121(1), pp. 90–97, 1995.

Fujita, Y. and Tamura, T.: Enlargement of breaches in flood levees on alluvial plains, *Journal of Natural Disaster Science*, Vol.9(1), pp.37-60, 1987.

Gens, A., Hutchinson, J.N. and Cavounidis, S.: Three dimensional analysis of slides in cohesive soils, *Geotechnique*, Vol. 38(1), pp.1-23, 1988.

Giger, M. W. and Krizek, R. J.: Stability analysis of vertical cut with variable corner angle, *Soils and Foundations*, Vol.15(2), pp.63-71, 1975.

Gitirana, de F.N.G. Jr., Fredlund, D.G.: Analysis of Transient Embankment Stability Using the Dynamic Programming Method, *Proceedings of the 56th Canadian Geotechnical Conference*, Winnipeg, Manitoba, Vol.1, pp.807-814, 2003.

Giuseppetti, G. and Molinaro, P.: A mathematical model of the erosion of an embankment dam by overtopping, *Proc. Int. Symp, Analytical Evaluation of Dam Related Safety Problems*, Copenhagen, Denmark, pp.329-341, 1989.

Glazyrin, G. Ye., and Reyzvikh, V. N.: Computation of the flow hydrograph for the breach of landslide lakes, *Soviet Hydrology,* Selected Papers, No.5, pp.492-496, 1968.

Greco, V.R.: Efficient Monte-Carlo technique for locating critical slip surface, *Journal of Geotechnical Engineering*, ASCE, Vol.122(7), pp.517–525, 1996.

Gupta, C.S., Bruch, J.C., Jr., and Comincioli, V.: Three-dimensional unsteady seepage through an earth dam with accretion, *Engineering Computations* (Swansea, Wales), Vol.3(1), pp.2–10, 1986.

Hagen, V. K.: Re-evaluation of design floods and dam safety, *Proc., 14th Congress of Int. Commission on Large Dams*, International Commission on Large Dams, Paris, 1982.

Hagen, V. K.: Discussion: Peak outflow from breached embankment dam, *Journal of Water Resources Planning and Management*, Vol.122, pp.314-316, 1996.

Hahn, W., Hanson, G.J. and Cook, K.R.: Breach morphology observations of embankment overtopping tests, *Proc. 2000 Joint Conf. Water Resources Engineering and Water Resources Planning and Management*, Minneapolis, USA, 2000. (CD-ROM)

Hancox, G.T., McSaveney, M.J., Manville, V. and Davies, T.R.H.: The October 1999 Mt Adams rock avalanche and subsequent landslide dam-break flood and effects in Poerua River, Westland, New Zealand, *New Zealand Journal of Geology and Geophysics*, Vol.48, pp.683-705, 2005.

Havnø, K., Van Kalken, T. and Olesen, K.: A modeling package for dam break simulation, *Proc. Int. Symp, Analytical Evaluation of Dam Related Safety Problems*, Copenhagen, Denmark, pp.387-397, 1989.

Haverkamp, R., M. Vauclin, J. Touma, P.J. Wierenga, and G. Vachaud.: A comparison of numerical simulation models for one dimensional infiltration, *Soil Sci. Soc. Am. J*., Vol. 41, pp285–294, 1977.

Haverkamp, R. and Vauclin, M.: A comparative study of three forms of the Richards' equation used for predicting one-dimensional infiltration in unsaturated soil. *Soil Sci. Soc. Am. J*., Vol.45, pp.13-20, 1981.

Hermanns, R.: All Clear for Allpacoma Landslide Dam, *MAP:GAC Newsletter*, Vol.5, No.1, 2005.

Höeg K., Lövoll, A. and Vaskinn K.A.: Stability and breaching of embankment dams: field tests on 6 m high dams, *International Journal on Hydropower and Dams*, Vol.11(1), pp.88-92, 2004.

Hovland, H. J.: Three-dimensional slope stability analysis method, *Geotech. Eng. Div.*, ASCE, Vol.130, GT9, pp.971-986, 1977.

Hungr, O., Salgado, F.M. and Byrne, P.M.: Evaluation of a three-dimensional method of slope stability analysis, *Canadian Geotechnical Journal*, Vol. 26, pp.679-686, 1989.

Huusein Malkawi, A. I., Hassan, W. F. And Sarma, S. K.: Global search method for locating general slip surface using Monte Carlo techniques, *Journal of Geotechnical and Geoenvironmental Engineering*, Vol.127(8), pp. 688-698, 2001

Huyakorn, P.S., Thomas, S.D. and Thompson, B.M.: Techniques for making finite elements competitive in modeling flow in variably saturated media, *Water Resour. Res.,* Vol.20, pp.1099- 1115, 1984.

Huyakorn, P.S., Springer, E.P., Guvanasen, V. and Wadsworth, T.D.: A three dimensional finite element model for simulating water flow in variably saturated porous media, *Water Resour. Res.,* Vol.22, pp.1790-1808, 1986.

Ito, K.: Zenkoji Earthquake -- disaster of landslide and flood, *Chiri,* Vol.28-4, pp.45-54, 1983. (in Japanese)

Ito, N.: Study on river embankment failure caused by overtopping, Master's Thesis, *Department of Civil and Earth Resources Engineering*, Kyoto University, 2007.

Jackob, J. and Jordan, P.: Design flood estimates in mountain streams – the need for a geomorphic approach, *Can. J. Civ. Eng*., Vol.28, pp.425-439, 2001.

Janbu, N.: Application of composite slip surface for stability analysis, *Proceedings of the European Conference on Stability of Earth Slopes*, Stockholm, Vol. 3, pp. 43–49, 1954a.

Janbu, N.: Stability Analysis of Slopes with Dimensionless Parameters, Harvard Soil Mechanics Series 46, *Harvard University Press*, Cambridge MA, 1954b.

Janbu, N.: Slope stability computations, Soil Mechanics and Foundation Engineering Report, *The Technical University of Norway*, Trondheim, 1968.

Janbu, N.: Slope stability computations, in *Embankment - Dam Engineering: Casagrande Volume*, R. C. Hirschfeld and S. J. Pouros, Eds., Wiley, Hoboken, NJ, pp. 47–86, 1973.

Janbu, N., Bjerrum, L. and Kjaernsli, B.: Veiledning ved lφsning av fundamenterings oppgaver (in Norwegian with English summary: Soil mechanics applied to some engineering problems), *Norwegian Geotechnical Institute*, Publ. No. 16, 1956.

Japanese Ministry of Construction: Data Book on Natural Dams, River Planning Section, *Chobu Constriction Bureau*, 1987.

Jiang, J.-C., Baker, R. and Yamagami, T.: The effect of strength envelope nonlinearity on slope stability computations, *Can. Geotech. J.*, Vol.40(2), pp.308-325, 2003.

Jiang, J.-C. and Yamagami, T.: Determination of the sliding direction in 3D slope stability analysis, *Proc. 44th Symp. of the Jap. Geotech. Society*, pp.193-200, 1999 (in Japanese).

Jiang, J.-C. and Yamagami, T.: Three-dimensional slope stability analysis using an extended Spencer method, *Soils and Foundation*, Vol.44(4), pp.127-135, 2004.

Johnson, F. A. and Illes, P.: A classification of dam failures, *International Water Power and Dam Construction*, pp.43-45, 1976.

Kato, Y., Miyano, T. and Mizuyama, T.: Outburst of a small landslide dam on the Imokawa River (prompt report), *Journal of the Japan Society of Erosion Control Engineering*, Vol.57(6), 2005.

Khanal, N. R.: Assessment of Natural Hazards in Nepal, Unpublished report submitted to the Research Division, *Tribhuvan University*, Kirtipur, Kathmandu, Nepal, 1996.

Kirkland, M.R.: Algorithms for solving Richards' equation for variably saturated soils. Ph.D. Thesis, *Department of Mechanical Engineering*, New Mexico State University, Las Cruces, 1991.

Kirkpatrick, G. W.: Evaluation guidelines for spillway adequacy, The evaluation of dam safety, *Engineering Foundation Conf.*, ASCE, New York, pp.395–414, 1977.

Korup, O.: Recent research on landslide dams – a literature review with special attention to New Zealand, *Progress in Physical Geography*, Col.26, pp.206-235, 2002.

Korup, O.: Geomorphometric characteristics of New Zealand landslide dams, *Engineering Geology*, Vol.73, pp.13-35, 2004.

Korup, O.: Geomorphic hazard assessment of landslide dams in South Westland, New Zealand: fundamental problems and approaches, *Geomorphology*, Vol.66(1-4), pp.167-188, 2005.

Kosugi, K.: Three-parameter lognormal distribution model for soil water retention, *Water Resour. Res.* Vol.30, pp891–901, 1994.

Lam, L., Fredlund, D.G., and Barbour, S.L.: Transient seepage model for saturated–unsaturated soil systems: a geotechnical engineering approach, *Canadian Geotechnical Journal*, Vol.24, pp.565– 580, 1987.

Lam, L. and Fredlund D. G.: A general limit equilibrium model for three-dimensional slope stability analysis, *Can. Geotech. J.,* Vol.30, pp.905-919, 1993.

Liao, W.M. and Chou, H.T.: Debris flows generated by seepage failure of landslide dams. Debris-Flow Hazards Mitigation: Mechanics, Prediction, and Assessment, *Rickenmann & Chen*, pp.315-325, 2003.

Loukola, E. and Huokuna, M.: A numerical erosion model for embankment dams failure and its use for risk assessment, *Proc. CADAM (EU Concerted Action on Dam Break Modelling) Munich meeting*, Munich, Germany, 1998.

MacDonald, T. C. and Langridge-Monopolis, J.: Breaching characteristics of dam failures, *J. Hydraul. Eng*., Vol.110 (5), pp.567–586, 1984.

Machida, H.: Rapid erosional development of mountain slopes and valleys caused by large landslides in Japan, *Geographical Reports of Tokyo Metropolitan University* 1, pp.1-72, 1966.

Marui, H. and Yoshimatsu, H.: Landslide dams formed by the 2004 Mid-Nigata Prefecture earthquake in Japan, in *Progress in landslide science*, edited by Sass et al., pp285-293, 2007.

Manville, V.: Techniques for evaluating the size of potential dambreak floods from natural dams, Science Rep. No. 2001/28, *Institute of Geological and Nuclear Sciences*, Wellington, New Zealand, pp.72, 2001.

Meadowcroft, I.C, Morris, M.W., Allsop, N.W.H. and McConnell, K.: Tollesbury managed set back experiment: breach design and construction, and embankment failure experiment, *HR Wallingford Report TR 5*, Wallingford, UK, 1996.

Mizuyama, T.: Countermeasures to cope with landslide dams – prediction of the outburst discharge, *Proc. of 6th Japan-Taiwan Join Seminar on Natural Disaster Mitigation*, 2006 (in CD ROM).

Moench, M. and Dixit, A.: "Adaptive Capacity and Livelihood Resilience – Adaptive Strategies for Responding to Floods and Droughts in South Asia", *Institute for Social and Environmental Transition*, pp. 83, 2004.

Mohamed, M.A.A., Samuels, P.G. and Morris, M.W.: Improving the accuracy of prediction of breach formation through embankment dams and flood embankments. In: Bousmar & Zech (Eds), *River Flow 2002*, Swets & Zeitlinger, Lisse, the Netherlands, pp.663-673, 2002.

Mohamed, M.A.A., Morris, M., Hanson, G.J. and Lakhal, K.: Breach formation: laboratory and numerical modeling of breach formation, *Proc. Dam Safety 2004*, ASDSO Phoenix, Arizona, USA, 2004. (CD-ROM)

Mora, S., Madrigal, C., Estrada, J. and Schuster, R.: The 1992 Rio Toro landslide dam, Costa Rica, *Landslide News*, Vol. 7, pp.19-21, 1993.

Morgenstern, N. R., and Price, V. E.: The analysis of the stability of general slip surfaces, *Geotechnique*, Vol.15(1), pp.79–93, 1965.

Morgenstern, N. R.: The evaluation of slope stability - a 25 years perspective, *In Stability and Performance of Slopes and Embankments*, Geotechnical Special Publication 31, ASCE, New York, Vol. 1, pp.1-26, 1992.

Mori, T.: Study on prediction of flood discharge and response when natural dam bursts, PhD dissertation, *Kyoto University*, 2007, pp.115.

Morris, M.: CADAM Concerted action on dambreak modeling, Final Report, Report SR 571, *H. R. Wallingford*, UK, 2000.

Morris, M. and Hassan, M.: Breach formation through embankment dams & flood defense embankments: a state of the art review, *Impact Project Workshop*, H. R. Wallingford, UK, 2002.

Nguyen, V. U.: Determination of critical slope failure surfaces, *Journal of Geotechnical Engineering*, ASCE, Vol. 111(2) pp.238-250, 1985.

Narasimhan, T.N. and Witherspoon, P.A.: An integrated finite difference method for analyzing fluid flow in porous media, *Water Resour. Res.,* Vol.12(1), pp.57-64, 1976.

Neuman, S.P.: Saturated-unsaturated seepage by finite elements. *J. Hydraul. Div. ASCE*, Vol.99 (HYl2), pp.2233-2250, 1973.

Ng, C.W.W., Wang, B., and Tung, Y.K.: Three-dimensional numerical investigations of groundwater responses in an unsaturated slope subjected to various rainfall patterns, *Canadian Geotechnical Journal*, Vol.38, pp.1049–1062, 2001.

Ng, K.L.A., and Small, J.C.: Simulation of dams constructed with unsaturated fills during construction and impounding, In *Unsaturated soils*, Edited by E.E. Alonso and P. Delage, A.A. Balkema, Rotterdam, The Netherlands, pp.281–286, 1995.

O'Connor, J.E., and Costa, J.E.: The world's largest floods, past and present—their causes and magnitudes, *U.S. Geological Survey Circular 1254*, pp.13, 2004.

Pan Shuibo and Loukola, E.: Chinese-Finnish cooperative research work on dam break hydrodynamics, *National Board of Waters and the Environment*, Helsinki, Finland, 1993.

Pereira, J. H. F., and Fredlund, D. G.: Numerical analysis of the post-filling performance of small collapsing earth dams, *XIth Pan- American Conf. on Soil Mechanics and Geotechnical Engineering*, Vol. 3, pp.1129–1140, 1999.

Peviani, M.A.: Simulation of earth-dams breaking processes by means of a morphological numerical model, *Proc. CADAM (EU Concerted Action on Dam Break Modelling) Zaragoza meeting, Zaragoza*, Spain, pp.381-397, 1999.

Pham, H. T. V. and Fredlund, D. G.: The application of dynamic programming to slope stability analysis, *Canadian Geotechnical Journal*, Vol.32, pp.233–246, 1995.

Ponce, V.M. and Tsivoglou, A.J.: Modeling gradual dam breaches, *Journal of Hydraulic Division*, Vol.107(7), pp.829-838, 1981.

Powledge, G.R. and Dodge, R.A.: Overtopping of small dams − an alterative for dam safety. In: Waldrop, W.R. (Ed.), Hydraulics and Hydrology in the Small Computer Age, *Proceedings of Specialty Conference*, New York, ASCE, pp.1071-1076, 1985.

Ramamurthy, T., Narayan, C.G.P. and Bhatkar, V.P., Variational method for slope stability analysis, In *Proceedings of the 9th International Conference on Soli Mechanics and Foundation Engineering*, Tokyo, Vol.3, pp.139-142, 1977.

Revilla, J., and Castillo, E.: The calculus of variations applied to stability of slopes, *Géotechnique*, Vol.27(1), pp. 1–11, 1977.

Richards, L. A.: Capillary Conduction of Liquids through Porous Mediums, *Physics*, Vol.1, pp.318-333, 1931.

Risley, J., Walder, J. and Denlinger, R.: Usoi dam wave overtopping and flood routing in the Bartang and Panj Rivers, Tajikistan, *U.S. Geological Survey Water-Resources Investigatins Report 03-4004*, pp.28, 2006.

Rozov, A.L.: Modeling of washout of dams, *Journal of Hydraulic Research*, Vol.41(6), pp.565-577, 2003.

Rubin, J.: Theoretical analysis of two-dimensional, transient flow of water in unsaturated and partly saturated soils, *Soil Sci. Soc. Am. Proc*., Vol.32, pp.607-615, 1968.

Russo, D., Zaidel, J., and Laufer, A.: Numerical analysis of flow and transport in a three-dimensional partially saturated heterogeneous soil, *Water Resources Research*, Vol.34(6), pp.1451–1468, 1998.

Sankar, K.: Landslides in Burhi Gandaki at Labu Bensi, *Journal of Nepal Engineers' Association*, pp.47-49, 1969.

Sassa, K.: Landslides of the World, *Kyoto University Press*, pp.413, 1999.

Sato, H. P., Yagi, H., Koarai, M., Iwahashi, J. and Sekiguchi, T.: Airborne LIDAR Data Measurement and Landform Classification Mapping in Tomari-no-tai Landslide Area, Shirakami Mountains, Japan, *Progress in Landslide Science*, pp.237-249, 2007.

Satofuka, Y., Yoshino, K., Mizuyama, T., Ogawa, K., Uchikawa, U. and Mori, T.: Prediction of floods caused by landslide dam collapse, *Annual J. of Hydraulic Engineering*, JSCE, Vol.51, pp.901-906, 2007 (in Japanese).

Schuster, R.L., and Costa, J.E.: A perspective on landslide dams, in Schuster, R.L., ed., Landslide Dams: Processes, Risk, and Mitigation: *ASCE Geotechnical Special Publication No. 3*, pp.1-20, 1986.

Schustr, R. L.: Outburst debris flows from failure of natural dams, *Proceedings 2nd International Conference on Debris flow Hazard Mitigation*, Taipeh, pp.29-42, 2000.

Schuster, R.L., and Highland, L.M.: Socioeconomic and Environmental Impacts of Landslides in the Western Hemisphere, *U.S. Geological Survey Open-File Report 01-0276*, 2001.

Sharma, R. H. and Nakagawa, H.: Predicting timing and location of rainfall triggering shallow landslides, *Annual J. of Hydraulic Engineering*, JSCE, Vol.49, pp.43-48, 2005.

Shrestha, A. B. and Shrestha, M. L.: Glacial Lake Outburst Floods and Other Flash Floods in Nepal – Country Report, *International Workshop on Managing Flash Floods and Sustainable Development in the Himalayas,* China., 2005.

Siegel, R. A., Kovacs, W. D. And Lovell, C. W.: Random surface generation in stability analysis, ASCE, *J. Geotech. Eng. Div*., Vol.107, GT7, pp.996-1002, 1981.

Singh, V.P. and Scarlatos, P.D.: Analysis of gradual earth-dam failure, *Journal of Hydraulic Engineering*, Vol.114(1), pp.21-42, 1988.

Singh, V.P.: Dam breach modeling technology, *Water Science and Technology Library*, Volume 17, Kluwer Academic Publishers, 1996.

Spencer, E.: A method of analysis of the stability of embankments assuming parallel inter-slice forces, *Geotechnique*, Vol.17(1), pp.11–26, 1967.

Staiano, T., Rinaldi, M. and Paris, E.: Seepage and stability analysis of embankments during flood events, *XXIX IAHR Congress Proceedings*, Beijing, China, pp.16-21, 2001

Swanson, F. J., Ouyagi, N. and Tominaga, M.: Landslide dams in Japan, in Schuster, R. L., ed., Landslide Dams: Process, Risk and Mitigation: *ASCE Geotechnical Special Publication*, No.3, pp.131-145, 1986.

Tabata, S., Ikeshima, T., Inoue, K. and Mizuyama, T.: Study on prediction of peak discharge in floods caused by landslide dam failure, *Jour. of JSECE*, Vol.54, No.4, pp.73-76, 2001. (in Japanese)

Tabata, S., Mizuyama, T. and Inoue, K.: Landslide dams and disasters, *Kokon-shoin*, pp.205, 2002.

Takahashi, T.: High velocity flow in steep erodible channels, *Proc. IAHR Congress*, Lausanne, pp.42-53, 1987.

Takahashi T.: Debris flow, Monograph Series of IAHR, *Balkema*, pp.1-165, 1991.

Takahashi, T. and Kuang, S.F.: Hydrograph prediction of debris flow due to failure of landslide dam, *Annuals, Disas. Prev. Res. Inst.*, Kyoto Univ., No.31 B-2, pp.601-615, 1988. (In Japanese with English abstract)

Takahashi T. and Nakagawa, H.: Flood/debris flow hydrograph due to collapse of a natural dam by overtopping, *Journal of Hydroscience and Hydraulic Engineering*, JSCE, Vol.12, No.2, pp.41-49, 1994.

Takahashi, T., Chigira, M., Nakagawa, H., Onda, Y., Maki, N., Aguirre-Pe, J. and Jáuregui, E.: Flood and sediment disasters caused by the 1999 heavy rainfall in Venezuela, *Research Report of Natural Disasters*, pp.1-141, 2001.

Takei, A.: Aritagawa disasters in 1953, Prediction and countermeasures of secondary disaster, 2, *Zennkoku Bousai Kyoukai*, pp. 47-71, 1987. (in Japanese)

Tingsanchali, T. and Chinnarasri, C.: Numerical modeling of dam failure due to flow overtopping, *Hydrological Sciences Journal*, Vol. 46(1), pp.113-130, 2001.

Trommler, N.; Huggel, C.; Korup, O. and Schneider, J. F.: Assessing post-failure geomorphic impact of an earthquake-triggered landslide dam, Jhelum River, Pakistan, *Geophysical Research Abstracts*, Vol. 10, EGU2008-A-00622, 2008.

Tsutsumi, D., Fujita, M. and Hayashi, Y.: Numerical simulation on a landslide due to Typhoon 0514 in Taketa City, Oita Prefecture, *Annual J. of Hydraulic Engineering*, JSCE, Vol.51, pp.931-936, 2007.

Ugai, K.: Three-dimensional stability analysis of vertical cohesive slopes, *Soils and Foundation*, Vol.25(3), pp.41-48, 1985.

Ugai, K.: Three-dimensional slope stability analysis by simplified Janbu method, *Journal of Japan landslide Society*, Vol.24(3), pp.8-14, 1987 (In Japanese).

Ugai, K.: Three-dimensional slope stability analysis by slice methods, In *Proceedings of the 6th International Conference on Numerical Methods in Geomechanics,* Innsbruck, Austria, Vol.2, pp.1369-1374, 1988.

Ugai, K. and Hosobori, K.: Extension of simplified Bishop method, simplified Janbu method and Spencer method to three dimensions, *Proc. Japanese Society of Civil Engineers,* No. 394/III-9, pp.21-26, 1988 (in Japanese).

U.S. Army Corps of Engineers, User's Manual HEC-1, Flood hydrograph package (Computer Program 723-X6-L2010), *Hydrologic Engineering Center*, Davis, California, 1981.

USACE: Engineering and Design - Drainage and Erosion Control Mobilization Construction, Engineer Manual, Department of the Army, *US Army Corps of Engineers (USACE)*, Washington, D.C., 1984.

van Genuchten, M.Th.: A closed-form equation for predicting the hydraulic conductivity of unsaturated soils, *Soil Sci. Soc. Am. J*., Vol.44, pp892–898, 1980.

Visser, P.J., Vrijling, J.K. and Verhagen, H.J.: A field experiment on breach growth in sand-dikes, *Proc. 22nd Int. Conf. Coastal Engineering*, Delft, the Netherlands, pp.2087-2100, 1991.

Visser, P.J.: Breach growth in sand-dikes, PhD thesis, *Delft University of Technology*, Delft, the Netherlands, 1998.

Walder, J. S., and O'Connor, J. E.: Methods for predicting peak discharge of floods caused by failure of natural and constructed earth dams, *Water Resour. Res*., Vol.33(10), pp.12, 1997.

Wang, Z.G. and Bowles, D.S.: Three-dimensional non-cohesive earthen dam breach model. Part 1: theory and methodology, *Advances in Water Resources*, Vol. 29, pp.1528-1545, 2006.

Wahl, T. L.: Prediction of embankment dam breach parameters, *Dam Safety Research Report*, U.S. Department of the Interior, Bureau of Reclamation, Dam Safety Office, 1998.

Wahl, T. L.: Uncertainty of Predictions of Embankment Dam Breach Parameters, *J. Hydr. Engrg*., Vol.130(5), pp. 389-397, May 2004

WECS: Erosion and sedimentation in the Nepal Himalaya, *Kefford Press*, Singapore, 1987.

Weidinger, J. T., and Ibetsberger, H. J.: Landslide dams of Tal, Latamarang, Ghatta Khola, Ringmo, and Darbhang in the Nepal Himalayas and related hazards, *Journal of Nepal Geological Society*, Vol.22, pp.371-380, 2000.

Weidinger, J.T.: Landslide dams in the high mountains of India, Nepal and China – stability and life span of their dammed lakes*, Italian Journal of Engineering Geology and Environment*, Special Issue I, pp. 67-80, 2006.

Wetmore, J.N. and Fread, D.L.: The NWS simplified dam-break flood forecasting model, *National Weather Service Report*, NOAA, Silver Spring, Maryland, USA, 1991.

Wilhite, D. A. and Svoboda, M. D.: Drought early warning systems in the context of drought preparedness and mitigation, Early Warning Systems for Drought Preparedness and Drought Management, *Proceedings of an Expert Group Meeting in Lisbon*, Portugal, 2000.

Wilkinson, P. L., Brooks, S. M. and Anderson, M. G.: Design and application of an automated non-circular slip surface search within a combined hydrology and stability model (CHASM), *Hydrological Processes*, Vol. 14, pp. 2003-2017, 2000.

Wilkinson, P. L., Anderson, M. G. and Lloyd, D. M.: An integrated hydrological model for rain-induced landslide prediction, *Earth Surface Processes and landforms*,Vol.27, pp. 1285-1297, 2002.

Wishart, J. S.: Overtopping breaching of rock-avalanche dams, Master of Engineering, Thesis, *University of Canterbury*, 2007.

Whisler, F.D. and Watson, K.K.: One-dimensional gravity drainage of uniform columns of porous materials, *J. Hydrol.*, Vol.6, pp.277-296, 1968.

Xie, H.Q., He, J.D., Zhang, J.H., and Xie, J.Q.: 3D seepage flow characteristics in the right bank of the Zipingpu project, *Journal of Sichuan University (Engineering Science Edition)*, Chengdu, China, Vol.33(6), pp.10–13, 2001.

Xing, Z.: Three-dimensional stability analysis of concave slopes in plan view, *Geotech. Eng. Div., ASCE*, Vol. 114, GT6, pp.658-671, 1988.

Yamagami, T. and Ueta, Y.: Noncircular slip surface analysis of the stability of slopes: An application of dynamic programming to the Janbu method, *Journal of Japan Landslide Society*, Vol. 22(4), pp.8-16, 1986.

Yamagami, T. and Ueta, Y.: Search for noncircular slip surfaces by the Morgenstern-Price Method, In *Proceedings of the 6th International Conference on Numerical Methods in Geomechanics*, Innsbruck, pp.1335-1340, 1988.

Yamagami, T. and Jiang, J.-C.: A search for the critical slip surface in three-dimensional slope stability analysis, *Soils and Foundations*, Vol.37(3), pp.1-16, 1997.

Zhu, D.-Y.: A method for locating critical slip surfaces in slope stability anaysis, *Can. Geotech J.*, Vol.38, pp.328-337, 2001.

Zhu, Y.: Breach Growth in Clay-Dikes, PhD thesis, *Delft University of Technology*, Delft, the Netherlands, 2006.

Zou, J.-Z., Williams, D.J., and Xiong, W.-L.: Search for critical slip surfaces based on finite element method, *Canadian Geotechnical Journal*, Vol.32, pp.233–246, 1995.

List of Figures

List of Tables

Curriculum Vitae

Name Ripendra AWAL

Citizenship Nepal

Birth 1973 November 25, Bhaktapur, Nepal

Ph.D. Student (2005 - 2008)
Department of Civil and Earth Resources Engineering
Kyoto University, Kyoto, Japan

M. Sc. in Water Resources Engineering (2002 - 2003)
Department of Civil Engineering, Institute of Engineering
Tribhuvan University, Kathmandu, Nepal

B.E. in Civil Engineering (1993 - 1997)
Department of Civil Engineering, Institute of Engineering
Tribhuvan University, Kathmandu, Nepal

Papers based on the Thesis

Awal, R., Nakagawa, H., Kawaike, K., Baba, Y. and Zhang, H.: Experimental study on prediction of failure mode of landslide dams, *Fourth International Conference on Scour and Erosion (ICSE-4)*, November 2008. (Accepted)

Awal, R., Nakagawa, H., Kawaike, K., Baba, Y. and Zhang, H.: Transient slope stability analysis of landslide dam failure, *The Eighth International Conference on Hydro-Science and Engineering (ICHE)*, September 2008. (Accepted)

Nakagawa, H., Awal, R., Kawaike, K., Baba, Y. and Zhang, H.: Prediction of natural dam failure and resultant flood/debris flow discharge, *Japan-Brazil Memorial Symposium on Science and Technology*, Brazil, June 2008.

Awal, R., Nakagawa, H., Kawaike, K., Baba, Y. and Zhang, H.: Prediction of flood/debris flow hydrograph due to landslide dam failure by overtopping and sliding, *Annuals of the Disaster Prevention Research Institute*, Kyoto University, No.51B, April 2008. (in print)

Awal, R., Nakagawa, H., Kawaike, K., Baba, Y. and Zhang, H.: An integrated approach to predict outflow hydrograph due to landslide dam failure by overtopping and sliding, *Annual J. of Hydraulic Engineering, JSCE*, Vol. 52, pp. 151-156, February 2008.

Awal, R., Nakagawa, H., Kawaike, K., Baba, Y. and Zhang, H.: Numerical approach to predict flood/debris flow hydrograph due to landslide dam failure, *Proceedings of the First NEA-JC Seminar on "Current and Future Technologies"*, October 2007 (in CD ROM).

Awal, R., Nakagawa, H., Kawaike, K. and Baba, Y.: Prediction of outflow hydrograph due to landslide dam failure, *Proceedings of the 26th Annual Meeting of the Japan Society for Natural Disaster Science*, pp.19-20, September 2007.

Awal, R., Nakagawa, H., Baba, Y., Sharma, R. H. and Ito, N.: Study on landslide dam failure by sliding, *Annuals of the Disaster Prevention Research Institute*, Kyoto University, No.50B, pp.653-660, April 2007.

Awal, R., Nakagawa, H., Baba, Y. and Sharma, R. H.: Numerical and experimental study on landslide dam failure by sliding, *Annual J. of Hydraulic Engineering*, JSCE, Vol. 51, pp.7-12, February 2007.